DEVELOPMENT OF A PREDICTIVE MUSCULOSKELETAL HYBRID MODEL BASED ON MAXIMUM WEIGHT LIFTING TASK

By

RAHID ZAMAN

Bachelor of Science in Mechanical Engineering
Military Institute of Science and Technology
Dhaka, Bangladesh
2014

Master of Science in Mechanical Engineering
University of Alaska Fairbanks
Fairbanks, Alaska
2018

Submitted to the Faculty of the
Graduate College of the
Oklahoma State University
in partial fulfillment of
the requirements for
the Degree of
DOCTOR OF PHILOSOPHY
May, 2022

DEVELOPMENT OF A PREDICTIVE

MUSCULOSKELETAL HYBRID MODEL BASED ON

MAXIMUM WEIGHT LIFTING TASK

Dissertation Approved:

Dr. Yujiang Xiang

Dissertation Adviser

Dr. Jerome Hausselle

Dr. Shuodao Wang

Dr. Guoliang Fan

ACKNOWLEDGEMENTS

First of all, I am thankful to Almighty Allah for bringing me up to this point. I always feel blessed by Him for giving me an amazing advisor like Dr. Yujiang Xiang. Dr. Xiang is an inspiration in my life. He was always with me by my side during the ups and downs of my academic and personal life. I would like to thank Dr. Jerome Hausselle and Dr. Shuodao Wang for their valuable guidance and serving on the committee. I would like to thank Dr. Guoliang Fan also for agreeing to serve on my committee and guide me in my research. I would also like to thank Dr. James Yang, Ritwik Rakshit, and Jazmin Cruz from Texas Tech University for providing experimental data.

I am also thankful to National Science Foundation (NSF) for funding this project. The funding award number for this project is 1849279.

I must thank all of my colleagues in Dr. Xiang's lab and the staff of the Mechanical and Aerospace Engineering department and Graduate School for helping me with documentation.

Finally, I would like to thank my parents (G M Azizur Rahman and Mrs. Shamsunnahar) and my wife Rowshon Ara Mannan Munny for always being with me and sacrificing a lot just for me. I would also like to thank my elder brother (G M Shahid uz Zaman Sumon), mother-in-law (Mahmuda Akhter Hena), and late father-in-law (MD Abdul Mannan) for their support.

It is a beautiful journey with all of you guys! I am indeed blessed!

Name: RAHID ZAMAN

Date of Degree: MAY, 2022

Title of Study: DEVELOPMENT OF A PREDICTIVE MUSCULOSKELETAL HYBRID MODEL BASED ON MAXIMUM WEIGHT LIFTING TASK

Major Field: MECHANICAL AND AEROSPACE ENGINEERING

Abstract: Manual material handling (MMH), particularly lifting, is one of the main reasons for work-related joint and back injuries. Injuries associated with MMH play a significant role in the economy. Therefore, it is necessary to determine subject-specific maximum lifting weight and explain why these lifting-related injuries occur. However, it is challenging to determine the maximum lifting weight by experiments as it is a time-consuming process and risky for the participants. Computational biomechanical models can reveal the insight of human lifting motion and help us to find the reasons behind lifting-related injuries. Musculoskeletal models are complicated and computationally heavy, making them infeasible for real-time application. Skeletal models are computationally efficient but lack muscle physiology in their formulations. This makes it unable to assess musculoskeletal injuries. A novel hybrid model is introduced in this study to predict maximum lifting weight and lifting motion and to evaluate musculoskeletal injury for that lifting motion. The hybrid predictive model consists of a predictive skeletal module and an Opensim musculoskeletal module to balance the computational speed and physiological accuracy. The skeletal models predict joint torques, joint angle profiles, center of pressure (COP), and ground reaction forces (GRFs) for both symmetric and asymmetric liftings. The predicted joint angles, GRFs and COP are inputted into OpenSim musculoskeletal module to estimate muscle activations and joint reaction forces. The hybrid predictive models are used to analyze joint torques, muscle activations, and lumbar spine joint reaction forces for both symmetric and asymmetric lifting tasks to prevent musculoskeletal injuries. The developed hybrid model is also able to predict maximum lifting weight by using subject-specific dynamic joint strength and assess associated injury risks. The proposed hybrid model is both computationally efficient and generic, and it can be readily applied to other motions as well. The hybrid predictive musculoskeletal model has wide applications for workers' injury prevention to reduce the risk of musculoskeletal disorders.

TABLE OF CONTENTS

Chapter Page

Chapter Page

LIST OF TABLES

Table Page

LIST OF FIGURES

Figure Page

Figure Page

CHAPTER I

INTRODUCTION

1.1 Motivation

Manual material handling (MMH), particularly lifting, is one of the main reasons for work-related joint and back injuries. Injuries associated with MMH play a significant role in the economy. Therefore, it is necessary to determine subject-specific maximum lifting weight, and explain why these lifting-related injuries occur. However, it is challenging to determine the maximum lifting weight by experiments, as it is hazardous and risky for the participants. Also, experimental-data-based injury analysis is not feasible in the industrial environment, as it is time-consuming and requires large space, expensive equipment, and trained personnel. Computational biomechanical models can reveal the insight of human lifting motion and help us to find the reasons behind lifting-related injuries. Musculoskeletal models are complicated and computationally heavy which make it infeasible for real-time application. Skeletal models are computationally efficient, but lack muscle physiology in their formulations. This makes it unable to assess musculoskeletal injuries. A novel hybrid model is introduced in this study to predict maximum lifting weight and lifting motion, and to assess musculoskeletal injuries for that lifting motion. The hybrid model consists of a predictive skeletal module and an injury

assessing musculoskeletal module in OpenSim to reduce analytical complexity and to maintain a balance between computational speed and physiological accuracy. The hybrid model aims to help us to predict maximum weight lifting motion and to assess injuries for different types of workplace lifting motions.

The primary goal of this study is to develop a computational ergonomic tool to predict maximum lifting weight and lifting motion, and to assess musculoskeletal injuries for manual material handling, including symmetric lifting and asymmetric lifting.

1.2 Objectives

The general objective of this research is to develop a computational biomechanical tool, which can predict maximum lifting weight, lifting motion, joint torques, muscle activations, joint reaction forces, and potential musculoskeletal injuries. The general objective can be detailed into four aspects.

The first objective is to develop an optimization formulation which can predict maximum lifting weight and lifting motion. For this purpose, we develop a multi-objective optimization (MOO) based formulation considering dynamic joint strength.

The second objective is to develop an efficient model to predict the symmetric maximum weight lifting using the proposed MOO formulation. Considering the computation speed, we will employ a 10-degrees-of-freedom (DOF) two-dimensional (2D) skeletal model for symmetric lifting.

The third objective is to develop a model for asymmetric lifting, which has the capability to predict the asymmetric maximum lifting weight and motion. Considering the movement of the

human body during asymmetric lifting and the differences of ground reactions forces (GRFs) on both sides of the sagittal plane, we will employ a 40-DOF three-dimensional (3D) skeletal model.

The fourth objective is to develop a novel hybrid predictive model to assess potential musculoskeletal injuries during maximum weight lifting. For this purpose, we will integrate the skeletal models with an OpenSim musculoskeletal model. We will use the prediction results from the skeletal models as the inputs into the OpenSim musculoskeletal model to analyze muscle activations and joint reaction forces. The combined package is called the hybrid predictive model, which can predict maximum lifting weight and motion, and assess potential musculoskeletal injuries for different lifting weights.

Finally, we will demonstrate the hybrid predictive model as a computational ergonomic tool to evaluate potential lower back injuries during symmetric and asymmetric lifting tasks.

1.3 Background

Lifting is one of the main reasons for work-related joint and back injuries (Freburger et al., 2009), which is the most common reason for seeking medical care for civilians (Childs et al., 2014) and the military (Cohen et al., 2010). According to the Bureau of Labor Statistics, in 2018, overexertion and bodily reaction were the top reasons for missed workdays (U.S. Bureau of Labor Statistics, 2018). The same source also reported that the most affected sectors are agriculture, mining, construction, manufacturing, wholesale trade, and retail trade industries. Most of the jobs in these industries are related to manual material handling (MMH). According to this statistic, retail trade is the most affected sector, and in this sector 36 percent of the days

away from work (DAFW) result from sprains, strains, and tears. 17 percent of these cases are related to low back injuries (LBI). The financial impact of LBI and work-related musculoskeletal disorders (WMSDs) is cross-sectoral because it affects the workers' productivity and increases the cost to health care and social support systems (Hartvigsen et al., 2018). A study on a large sample of workers' compensation claims shows that about 32% of all claims and 36% of compensation costs are related to MMH (Dempsey and Hashemi, 1999). In the United States, the economic impact of MMH-related injuries such as LBI and WMSDs is more than $100 billion per year, considering the direct and indirect costs (Katz, 2006). The direct cost of MMH injuries was over $13 billion in 2016 in the USA (Liberty Mutual Insurance, 2019). Therefore, it is essential to identify the risk factors associated with WMSDs and LBI to find a practical ergonomic solution.

There are mainly two types of lifting techniques used in workplaces. One is squat lifting, and the other is stoop lifting. The most common advised lifting technique is squat lifting or leg lifting for heavy objects, in which the back remains as straight as possible, and the knees are flexed (Garg and Moore, 1992, Van Dieen et al., 1999). In addition, there are mainly two types of squat liftings based on the carrying box locations: symmetric lifting and asymmetric lifting.

To analyze the lifting motion, we can either collect data experimentally or predict motion kinematics and kinetics using computational tools. Some injury-assessment techniques are entirely dependent on experimental or clinical data. Some are invasive (Bergmann et al., 2014, Wilke et al., 2001) and others are non-invasive (Ausavanonkulporn et al., 2019, Bazrgari et al., 2007, Beaucage-Gauvreau et al., 2019, Kim and Zhang, 2017, Kingma et al., 2006, Kingma et al., 2016). Measuring in-vivo joint reaction forces requires invasive surgery (Bergmann et al., 2014, Wilke et al., 2001). Muscle activations, motion kinematics, and kinetics can be

measured by non-invasive experiments using motion capture, electromyography (EMG), and force plates. However, experimental data acquisition requires huge space, expensive equipment, and highly skilled people, which are not feasible for many industries. Also, experimental procedures for maximum lifting weight are very risky and hazardous for a subject. Moreover, a subject's physiological and psychological barriers make the experimental approach infeasible to find out the true maximum lifting weight. Considering all these facts, the computational biomechanical model becomes attractive to find the maximum lifting weight and the optimal motion. Computational biomechanical modeling is not a mature discipline yet. However, it is becoming popular day by day because of its safety and repeatability in a virtual environment.

1.3.1 Computational biomechanical models

Computational biomechanical models or simulation-based biomechanical models have shown a way in advancing knowledge of lifting biomechanics. It has also become an important tool for assessing injury risks during lifting. There are mainly two types of simulation models for predicting symmetric and asymmetric liftings: (i) skeletal model and (ii) musculoskeletal model.

(i) Skeletal model

Skeleton-model-based simulation is computationally efficient as it does not include muscle physiology in its formulation. It is the simplest version of a human model, which works mainly based on joint strength. On the way towards developing a computational skeletal model, the joint strength of the model is an important factor. There are mainly two types of joint strength models: static joint strength and dynamic joint strength. The static joint strength is constant

and independent of time, joint angle, and angular velocity. Dysart and Woldstad (1996) used the static joint strength for posture prediction. The use of the static joint strength in simulation simplifies the computation, but it does not reflect a biological joint properly. Biological joints are fundamentally different from robotic joints, as their strengths change with joint angle, angular velocity, and time.

On the other hand, the dynamic joint strength is a function of joint angle and angular velocity (Azghani et al., 2009, Frey-Law et al., 2012, Hussain and Frey-Law, 2016, Looft, 2014). Dynamic joint strength is required to predict the maximum lifting weight in the optimization formulation. In Gundogdu et al. (2005), a 2D dynamic-joint-strength-based model was presented to predict the optimal lifting motion using a genetic algorithm. Another 2D human model was proposed to predict the symmetric maximum weight lifting motion based on the dynamic joint strength (Xiang et al., 2019, Xiang et al., 2021). In Sreenivasa et al. (2018), a 12-DOF 2D model was used to study the influence of hip and lumbar flexibility during lifting motion considering the dynamic joint strength.

Different researchers used different types of skeletal models. Based on the dimension of a model, we can classify the models into two categories: 2D model and 3D model.

Over the past decades, many researchers have been working on human biomechanical modeling. However, only a few researchers have worked on lifting motion prediction. A summary of the literature on 2D computational models for lifting is given in Table 1.1. Initially, researchers worked on the 2D model, as it has fewer DOFs and is computationally efficient. However, all the DOFs of a 2D model are constrained in the sagittal plane of a human body. For example, based on the NIOSH (National Institute of Occupational Safety and Health)

lifting equation, a static and 2D biomechanical model was proposed to estimate the strength needed for a specific MMH task (Waters and Garg, 2010). In another study, a 5-link sagittal model was used to predict the optimal lifting motion using space-time optimization (Chang et al., 2001). Lin et al. (1999) introduced a 5-DOF 2D model to predict the lifting motion based on the static joint strength. Song et al. (2016) proposed a MOO-based 2D model which can predict symmetric lifting motion. These models were based on the static joint strength and cannot predict maximum lifting weight and motion. Xiang et al. (2020) proposed a 10-DOF lifting model based on the dynamic joint strength. 2D models can predict symmetric lifting motions only. It cannot predict asymmetric lifting motions, as all DOFs are in the sagittal plane.

Table 1.1 Literature on skeletal biomechanical models for human lifting

2D Skeletal Models					
Reference	**Motion/ posture**	**DOFs**	**Joint strength**	**Objective functions**	**Algorithm**
Song et al. (2016)	Motion prediction	5 DOFs	Static	Min torque square + max motion smoothness	Sequential quadratic programming
Waters and Garg (2010)	Strength estimation of MMH task	-	Static	-	NIOSH lifting equation
Chang et al. (2001)	Lifting prediction	5 DOFs	Static	Min the sum of torque squares	Sequential quadratic programming
Lin et al. (1999)	Lifting motion	5 DOFs	Static	Min the effort	Generalized reduced gradient (GRG) based GRG2 software
Gundogdu et al. (2005)	Lifting motion	5 DOFs	Dynamic	Min joint torque	Genetic algorithm
Sreenivasa et al. (2018)	Lifting motion	12 DOFs	Dynamic	Min total muscle torques and hamstring muscle forces	Direct shooting method using MUSCOD-II software
Xiang et al. (2021)	Lifting motion	10 DOFs	Dynamic	Min dynamic effort + max box weight	Sequential quadratic programming
3D Skeletal Models					
Ma et al. (2009)	Posture prediction	3D skeleton with 28 DOFs	Static	Min fatigue + min discomfort	Sequential quadratic programming
Marler et al. (2011)	Posture prediction	3D skeleton with 113 DOFs	Static	Min maximum torque + min joint angle	Sequential quadratic programming
Xiang et al. (2010)	Motion prediction	3D skeleton with 55 DOFs	Static	Min torque square + max stability	Sequential quadratic programming
Zaman et al. (2020, 2021a, b)	Motion prediction	3D skeleton with 40 DOFs	Dynamic	Min dynamic effort + max box weight	Sequential quadratic programming

In contrast, a 3D model can give more insights into lifting motion and predict both symmetric and asymmetric lifting motions. Even in a study, it is shown that the 3D model can predict the symmetric lifting better than the 2D model, as a 3D model can capture the changes of GRFs during symmetric lifting (Zaman et al., 2020c). Researchers used different types of 3D models to analyze lifting tasks. A 113-DOF 3D skeletal model was used to analyze box lifting tasks (Marler et al., 2011). In another study, a 28-DOF 3D skeletal model was used to simulate lifting tasks (Ma et al., 2009). In both studies, static joint strengths were used to predict the lifting postures. In another study, a 55-DOF model was used to predict lifting motion based on the static joint strength (Xiang et al., 2010). As a result, the model cannot predict the maximum lifting weight and lifting motion accurately. Based on the dynamic joint strength, Zaman et al. (2020, 2020b) proposed a 40-DOF 3D skeletal model to predict the maximum lifting weight and motion for symmetric and asymmetric lifting motions. A summary of 3D computational models for lifting is given in Table 1.1.

As skeletal models do not provide any information about muscle and tendon, it is difficult to find out potential musculoskeletal injuries based on skeletal models. But, musculoskeletal injuries are very common in heavy weight lifting. Musculoskeletal models can be used to assess muscle and tendon injuries during heavy weight lifting.

(ii) Musculoskeletal models

Muscle-driven dynamic simulations can give us the estimation of muscle and joint forces, which are difficult to obtain from experiments or predictive skeletal models. It also helps us to study the cause-and-effect for various muscle and joint physiological properties, which is vital in injury assessment. Anybody (Anybody technology) and LifeMod are closed source software. SIMM and OpenSim are open-source software.

Table 1.2: Literature on musculoskeletal biomechanical models for human lifting

Without predictive capability					
Reference	**Motion/ Posture**	**DOFs**	**Joint strength**	**Objective functions**	**Algorithm**
Mirakhorlo et al. (2013)	Lifting motion with given trajectories	Full body (rigid body has 55 joints, each arm has 118 muscles, each leg has 35 muscles and trunk has 158 muscles)	Static	Min the maximum muscle force to analyze the effects of stance width for different lifting techniques	Min-max optimizer of Anybody software
Blache et al. (2015a)	Lifting motion with given trajectories	22 DOFs Upper body model with 57 muscle-tendon units	Static	Min the muscle activations to analyze the effects of height and load on shoulder muscle work	Static optimization tool of OpenSim software
Stambolian et al. (2016)	Lifting motion with given trajectories	55 DOFs Full body model with over 1000 muscles	Static	Min trunk muscle activities to evaluate lower back for careful box lifting	Polynomial solver (a Dynamic optimization methodology) of Anybody software
Ghiasi et al. (2016)	Given posture with muscle force prediction	6 DOFs Lumbar spine model	Static	Min muscle stress + max spine stability to investigate the trunk muscle activities during lifting	Vector evaluated particle swarm optimization (VESPO) and Nondominated sorting genetic algorithm (NSGA)
With predictive capability					
Dembia et al. (2019)	Squat-to-stand motion prediction	Skeletal torso and musculoskeletal leg with 9 muscles	Static	Min the combination of the sum of squared excitation and the duration of the motion	Direct collocation

Zaman et al. (2019)	Motion prediction	10 DOFs skeletal model, 30 DOFs musculoskeletal model with 324 musculotendon actuators	Dynamic	Max box weight	Static optimization tool of OpenSim software

Determining a suitable tradeoff between the complexity of a model and the computational speed of the simulation is an important consideration in developing a computational biomechanical model. A summary of musculoskeletal models used for lifting motion by different researchers is given in Table 1.2. Mirakhorlo et al. (2013) used a full-body musculoskeletal model in Anybody software to evaluate the impact of stance width on muscle activation patterns and spinal loading during various lifting techniques like the squat, stoop, and semi-squat liftings. The model did not have the predictive capability, and the trajectories were defined to generate the lifting motion. Blache et al. (2015a) used an upper-body musculoskeletal model in the OpenSim to study the effect of load height and weight on shoulder muscles while lifting a load from waist to shoulder and eye height. The model did not have the predictive capability, and inverse kinematics was used to obtain the joint angles from markers' positions. In another study, the level of co-activation was used to evaluate the effects of lifting height, weight, and phase on the superficial shoulder muscles (Blache et al., 2015b). A 3D musculoskeletal trunk model was introduced to investigate the trunk muscles during lifting (Ghiasi et al., 2016). However, this model only had 6 DOFs and was a simplified version of the human trunk. The lifting posture was given to predict the muscle forces. Stambolian et al. (2016) used a full-body model in the Anybody software to analyze lower back muscles for careful box placement. Although these musculoskeletal models can reveal a great deal of

information about muscle force, activation, and lumbar spine stress, these musculoskeletal models do not have the capability to predict lifting motion.

On the other hand, predictive musculoskeletal models can predict changes for various physiological quantities such as muscle forces, activations, muscle moment arms, and joint reaction forces without any invasive experiments. Recently, muscle-driven dynamic simulations have made much progress in estimating muscle and joint forces for walking (Dembia et al., 2019) and jumping (Porsa et al., 2016). However, predictive musculoskeletal models for lifting are rare. This type of model can help to identify the effect of environmental parameters (external load, location, size of the box, etc.) and body kinematics (stance width) on physiological quantities. It also helps to study the causal relationship of various muscle and joint physiological properties, which is essential for injury assessment.

1.3.2 Prediction formulation and algorithm

The accuracy and efficiency of a biomechanical model largely depend on the prediction formulation and algorithm. Compared to experimental methods, predictive methods are more powerful in cause-and-effect studies. The predictive simulation methods available in literature can be roughly divided into five categories:

(i) Forward-dynamics simulations

In forward dynamics motion prediction, forces or torques applied to the model are used as the design variables and inputs in the equations of motion (EOM) to generate the kinematics of the motion. Integration of differential EOM over time is needed to get all the kinematics. Popular integrators to solve forward dynamics problems are Runge-Kutta, Matlab ode45, Euler method, and backward differential formula (BDF). It needs to optimize the initial conditions

to predict the motion, which is computationally demanding. Anderson and Pandy (1999) used a forward dynamics approach to simulate a maximum height vertical jump motion.

(ii) Inverse-dynamics simulations

In inverse dynamics simulations, joint angles are used as the design variables and inputs to the EOM to find the net joint moments. Inverse dynamics was successfully implemented to predict both symmetric (Xiang et al., 2011, Zaman et al., 2020) and asymmetric lifting motions (Zaman et al., 2021a).

(iii) Collocation methods

Direct collocation is a powerful nonlinear optimization technique in which both the controls and the states are parameterized using piecewise continuous polynomials. Direct collocation was used to solve the muscle redundancy problem in De Groote et al. (2016). This method was also used to solve the optimal control problem for a family of different cost functions which were used to predict human gait (Ackermann and Van den Bogert, 2010).

(iv) Control-based methods

Control based method can generate the dynamic simulation efficiently. For example, by employing feedforward and feedback control, computed muscle control (CMC) was used to calculate muscle excitations which drive the forward dynamic simulation to track the experimental data (Thelen and Anderson, 2006). This reduces the computational time significantly.

(v) Mixed-formulation methods

Inverse-muscular forward-skeletal dynamics (Shourijeh et al., 2014) or forward-muscular inverse-skeletal dynamics (Lloyd and Besier, 2003, Olney and Winter, 1985, Shourijeh et al.,

2016) have been applied with different optimization or optimal control strategies for musculoskeletal simulations.

1.3.3 MOO for lifting prediction

Optimization-based approach is an effective way to solve a redundant system. As the multi-link human model is a highly redundant system, the optimization-based approach is a preferred tool to find the optimal lifting motion. It is used to obtain the best result by minimizing or maximizing the objective functions considering the given constraints. However, for optimization-based approaches, defining the objective functions plays a vital role in predicting the lifting motion accurately. A 3D skeletal model was used with four objective functions, which had the functionality to analyze the lifting motion for each objective function separately (Xiang et al., 2012a). In another study, a 3D biomechanical model was proposed, where lumbar forces were considered as the objective function to study the effect of lumbar torque limit during lifting (Xiang et al., 2008).

Combining multiple objective functions may give better prediction results, where we need to maximize some objective functions and minimize other objective functions. In this case, MOO is used, which is also known as vector optimization or Pareto optimization. In Xiang et al. (2021), MOO was employed to minimize the joint torque and maximize the box weight in human lifting simulation. In another study, it showed that the MOO approach results in an 18.9% reduction in the overall root mean square (RMS) errors for the predicted joint angles when compared to the single objective optimization-based lifting motion prediction (Song et al., 2016). MOO was incorporated in a 3D model to predict the lifting motion more accurately (Xiang et al., 2010, 2012b).

1.4 Contributions

The musculoskeletal model is a complicated system that makes the direct prediction slow and computationally heavy. Some skeletal models can predict lifting motion, as discussed in section 1.3, but do not have the capability to predict the maximum lifting weight. In this study, we will first use skeletal models to predict the maximum lifting weight and motion considering the dynamic joint strength. Both symmetric and asymmetric lifting motions will be predicted. Then we will integrate the skeletal models with the OpenSim musculoskeletal model by inputting the predicted joint angle and GRF profiles into the OpenSim. Introducing the predictive capability into a full-body musculoskeletal model is a novel approach. The integrated model is called the hybrid predictive model. Using this novel hybrid model, we will be able to predict maximum lifting weight and lifting motion, and to assess injuries for lifting different weights without inheriting musculoskeletal complexity.

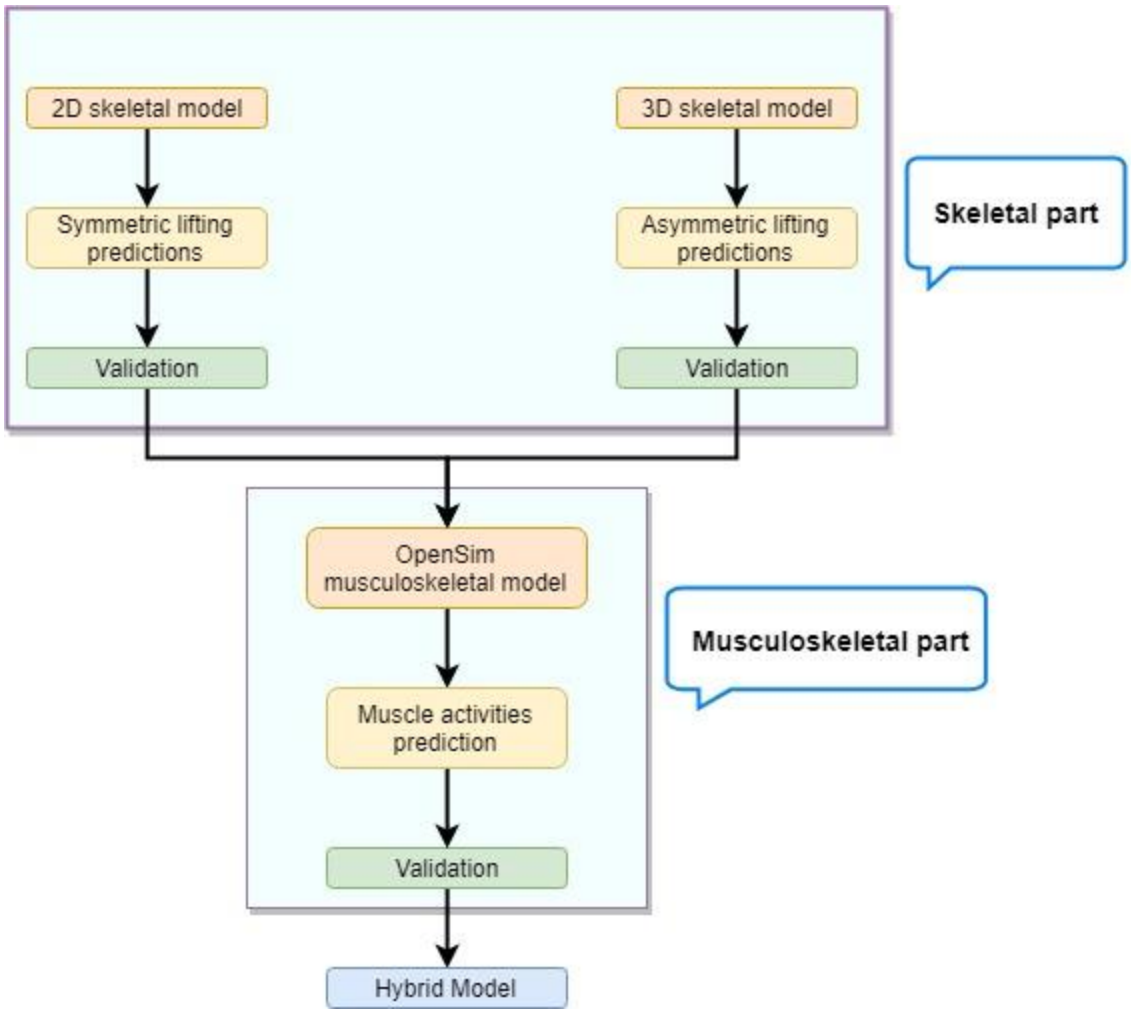

Figure 1.1: Flowchart of the hybrid model development procedure

To develop the hybrid model, at first, a 2D and a 3D skeletal models will be developed to predict symmetric and asymmetric maximum weight lifting motions, respectively, as shown in Figure 1.1. The 2D skeletal model has 10 DOFs, and the 3D skeletal model has 40 DOFs. The skeletal models are used to predict the maximum lifting weight governed by the dynamic joint torque limits which are functions of joint angle and angular velocity. MOO is employed in the formulation to predict the lifting weight and motion more accurately. A systematic procedure to choose the best coefficients for MOO is also presented.

Then, the skeletal models are integrated with the OpenSim musculoskeletal model to develop the novel hybrid model. The hybrid model can predict the maximum lifting weight, motion, and joint torques for symmetric and asymmetric liftings. The musculoskeletal module of the hybrid model can estimate muscle activations and joint reaction forces. Based on the predicted joint torques, muscle activations, and joint reaction forces, the hybrid model can assess potential injuries for both symmetric and asymmetric liftings.

Finally, based on the hybrid model, an ergonomic tool will be developed and validated for lifting. This ergonomic tool can predict and evaluate various lifting-related injuries effectively and efficiently so as to protect workers in the workplace.

1.5 Overview of Thesis

In chapter 1, we will briefly discuss the state-of-art research for lifting motion prediction and simulations, including different models and optimization formulations.

In chapter 2, we will present the details of a 2D skeletal model, including anthropometric data and EOM. We will also present the MOO-based formulation considering the dynamic joint strength and the procedure to select the optimal weighting coefficients for MOO. Finally, the predicted maximum weight symmetric lifting motion will be validated with the experimental data.

In chapter 3, the development of a 40-DOF 3D skeletal model and MOO-based formulation will be presented for asymmetric maximum weight lifting prediction. The simulation results will be compared with the experimental data.

In chapter 4, a novel hybrid predictive model will be introduced to simulate symmetric lifting for different weights by integrating the 2D skeletal lifting motion prediction with the OpenSim. The predicted joint angles, GRFs, muscle activations /forces, and joint reaction forces will be validated using experimental and literature data. The hybrid model will be deployed for three-step injury analysis.

Finally, in chapter 5, the hybrid model will be deployed to predict asymmetric lifting motion and muscle activations. A systematic comparison will be presented between symmetric and asymmetric liftings for lower back related injury analysis.

CHAPTER II

TWO-DIMENSIONAL SKELETAL SYMMETRIC MAXIMUM WEIGHT LIFTING PREDICTION

2D models of the human body are widely used in biomechanics to simulate and analyze symmetric human movement, because of their simplicity and efficiency. As the left and right side joint angles are symmetric in 2D models, it requires fewer DOFs to design a 2D model. As a result, it demands less computational cost and gives a faster optimization solution than a 3D skeletal or a musculoskeletal model does. We employed dynamic joint strengths and MOO with a 2D model to predict the optimal skeletal symmetric lifting motion, which will be used as inputs for the OpenSim musculoskeletal module. The combined package will work as the hybrid predictive model, which includes skeletal symmetric maximum lifting motion prediction and musculoskeletal symmetric maximum lifting motion analysis. The OpenSim musculoskeletal part and the integrated hybrid model will be discussed in chapter 4.

The purposes of this chapter are: (1) to generate symmetric 2D predictive lifting motion inputs into the OpenSim for hybrid predictive model development, (2) to determine the best weighting coefficients of MOO for maximum weight lifting. We will discuss in detail

about the mechanism of the 2D model, including kinematics, dynamics, EOM, optimization formulations, and determination of the best weighting coefficients for MOO. The validation of this model will also be presented at the end of this chapter by comparing its results with experimental data. As the predicted results of the 2D model will be used as the inputs for the musculoskeletal module for symmetric lifting, the overall predictive performance of the hybrid predictive model largely depends on the accuracy of the 2D model's predictive mechanism.

2.1 Two-dimensional skeletal model

The 2D model, used to predict symmetric maximum weight lifting, has 10 DOFs: three global DOFs (q_1, q_2, q_3) and seven human body joints ($q_4, \dots, q_{10}$) as shown in Figure 2.1. The global DOFs include two translations and one rotation, which move the pelvis to the current position in inertial Cartesian coordinates, while each human body joint is represented by a single rotation in 2D. The total DOFs are defined as $\boldsymbol{q} = [q_1, \dots, q_{10}]^{\mathrm{T}}$. Besides the spine joint, since the model is symmetric in the sagittal plane, only one set of shoulder (q_5) elbow (q_6), hip (q_7), knee (q_8), ankle (q_9), and metatarsophalangeal (q_{10}) joints are modeled in this study, as shown in Table 2.1.

Table 2. 1: Joint angle symbols and names of 2D model

Symbol	**Coordinate name**	**Symbol**	**Coordinate name**
q_1	Global translation joint coordinate	q_6	Elbow joint coordinate
q_2	Global translation joint coordinate	q_7	Hip joint coordinate
q_3	Global rotation joint coordinate	q_8	Knee joint coordinate
q_4	Spine joint coordinate	q_9	Ankle joint coordinate
q_5	Arm joint coordinate	q_{10}	Metatarsophalangeal joint coordinate

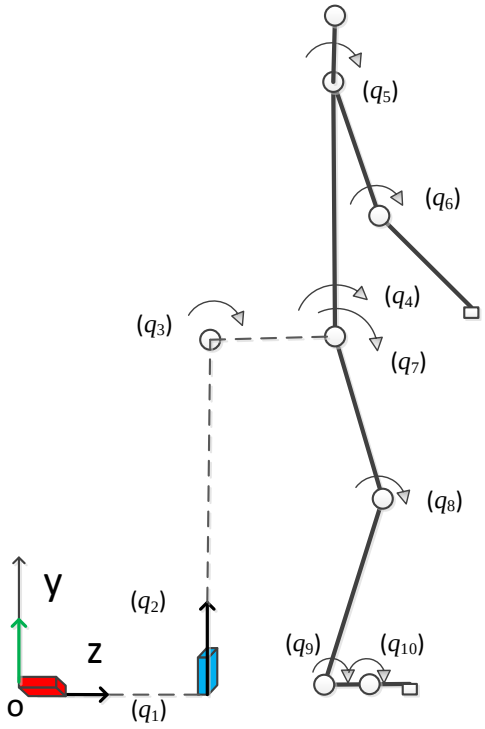

Figure 2.1: 2D skeletal human model

In addition, for these symmetric joints, the values of joint strength, link mass, and moment of inertia are doubled. The anthropometric data are given in Table 2.2. The data are generated from GEBOD^{TM} software with experimentally measured height, weight, and

stature data. The strength percentile is retrieved from symmetric maximum weight lifting (Xiang et al., 2019).

Table 2.2: Link length, mass, and moment of inertia of 2D model

Link name	Segment	Link length (m)	Link mass (kg)	Moment of inertia, I_{zz} ($kg \cdot m^2$)
Link 1 (L_1)	Sacrum to Shoulder	0.570	45.447	4.073
Link 2 (L_2)	Shoulder to Elbow	0.339	4.072	0.176
Link 3 (L_3)	Elbow to Wrist	0.311	3.877	0.135
Link 4 (L_4)	Pelvis, Hip to Knee	0.465	20.35	1.530
Link 5 (L_5)	Knee to Ankle	0.433	7.988	0.494
Link 6 (L_6)	Heel to Subtalar joint	0.090	1.7937	0.081
Link 7 (L_7)	Subtalar joint to Toe	0.100	0.1993	0.009

The major steps to develop a 2D skeletal model are: optimization formulations, 2D skeletal model setup, lifting prediction, and validation. The workflow of the 2D skeletal model development is shown in Figure 2.2.

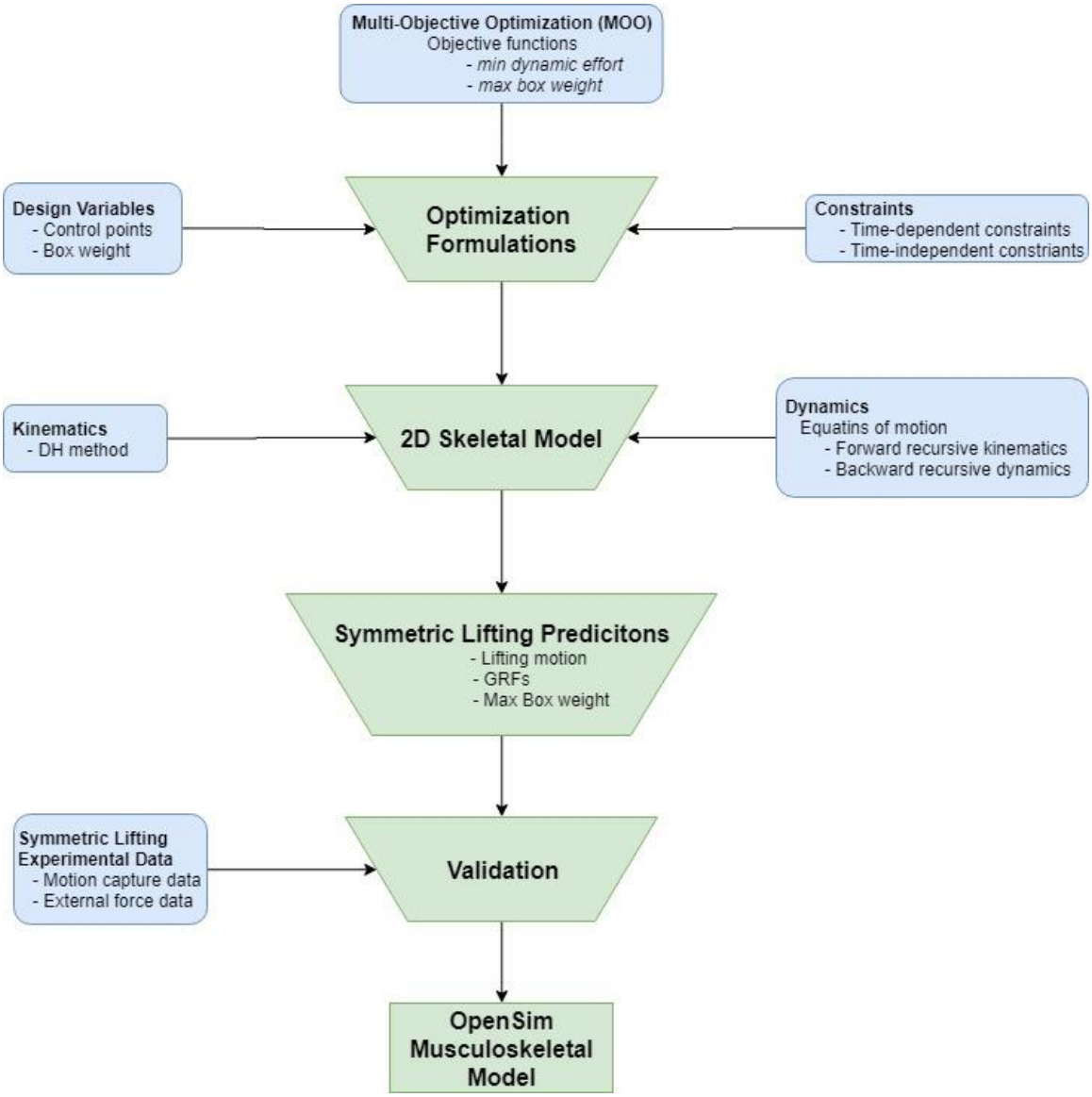

Figure 2.2: Development of the 2D skeletal model

2.2 Kinematics and dynamics

Denavit –Hartenberg method

Denavit and Hartenberg (1955) proposed a matrix-based method to systematically establish the translational and rotational relationships between adjacent links. This well-established method is called the DH method. The DH parameters are described in Table 2.3, where θ represents a rotation about the local z-axis, d represents the translational distance on the local z-axis, a represents the translational distance on the local x-axis, and α represents the rotation on the local x-axis. The motion sequence is θ, d, a, and α.

Table 2.3: DH table for a 2D human model

DOF	**θ**	**d**	**a**	**α**	**Segment**
q_1	π	0	0	$\pi/2$	global translation
q_2	$\pi/2$	L_1+L_2	0	$-\pi/2$	
q_3 (to spine)	0	0	0	0	global rotation
q_3(to leg)	0	0	0	0	
q_4	$-\pi/2$	0	L_1	0	spine
q_5	π	0	L_2	0	arm
q_6	0	0	L_3	0	
q_7	$\pi/2$	0	L_4	0	leg
q_8	0	0	L_5	0	
q_9	$-\pi/2$	0	L_6	0	
q_{10}	0	0	L_7	0	

Equations of motion

The general EOM of the 2D skeletal model can be expressed using the recursive Lagrangian formulation in matrix forms which contain forward recursive kinematics and backward recursive dynamics (Xiang et al., 2009b).

Forward recursive kinematics

$$\mathbf{A}_i = \mathbf{A}_{i-1}\mathbf{T}_i \tag{2.1}$$

$$\mathbf{B}_i = \dot{\mathbf{A}}_i = \mathbf{B}_{i-1}\mathbf{T}_i + \mathbf{A}_{i-1}\frac{\partial \mathbf{T}_i}{\partial q_i}\dot{q}_i \tag{2.2}$$

$$\mathbf{C}_i = \dot{\mathbf{B}}_i = \mathbf{C}_{i-1}\mathbf{T}_i + 2\mathbf{B}_{i-1}\frac{\partial \mathbf{T}_i}{\partial q_i}\dot{q}_i + \mathbf{A}_{i-1}\frac{\partial^2 \mathbf{T}_i}{\partial q_i^2}\dot{q}_i^2 + \mathbf{A}_{i-1}\frac{\partial \mathbf{T}_i}{\partial q_i}\ddot{q}_i \tag{2.3}$$

where q_i is the joint angle variable, $\mathbf{T}_i$ is the 4×4 DH link transformation matrix from the $(i-1)$th link frame to the ith link frame (Denavit and Hartenberg, 1955), $\mathbf{A}_i$, $\mathbf{B}_i$, $\mathbf{C}_i$ are the global recursive kinematics position, velocity, and acceleration matrices, respectively, and $\mathbf{A}_0 = [\mathbf{I}]$, $\mathbf{B}_0 = \mathbf{C}_0 = [\mathbf{0}]$.

After obtaining all the transformation matrices $\mathbf{A}_i$, $\mathbf{B}_i$, $\mathbf{C}_i$, the global position, velocity, and acceleration of a point in Cartesian coordinates can be calculated as

$$\overset{\mathrm{o}}{\boldsymbol{o}}\mathbf{r}_i = \mathbf{A}_i\mathbf{r}_i; \qquad \overset{\mathrm{o}}{\boldsymbol{o}}\dot{\mathbf{r}}_i = \mathbf{B}_i\mathbf{r}_i; \qquad \overset{\mathrm{o}}{\boldsymbol{o}}\ddot{\mathbf{r}}_i = \mathbf{C}_i\mathbf{r}_i \tag{2.4}$$

where $\mathbf{r}_i$ contains the augmented local coordinates of the point in the ith coordinate system.

Backward recursive dynamics (Xiang et al., 2009a)

$$\tau_i = \mathrm{tr}\left(\frac{\partial \mathbf{A}_{\mathrm{i}}}{\partial \mathrm{q_i}}\mathbf{D}_i\right) - \mathbf{g}^{\mathrm{T}}\frac{\partial \mathbf{A}_i}{\partial q_i}\mathbf{E}_i - \mathbf{f}_k^{\mathrm{T}}\frac{\partial \mathbf{A}_i}{\partial q_i}\mathbf{F}_i - \mathbf{G}_i^{\mathrm{T}}\mathbf{A}_{i-1}\mathbf{z}_0 \tag{2.5}$$

$$\mathbf{D}_i = \mathbf{I}_i\mathbf{C}_i^{\mathrm{T}} + \mathbf{T}_{i+1}\mathbf{D}_{i+1} \tag{2.6}$$

$$\mathbf{E}_i = m_i\mathbf{r}_i + \mathbf{T}_{i+1}\mathbf{E}_{i+1} \tag{2.7}$$

$$\mathbf{F}_i = \mathbf{r}_k\delta_{ik} + \mathbf{T}_{i+1}\mathbf{F}_{i+1} \tag{2.8}$$

$$\mathbf{G}_i = \mathbf{h}_k \delta_{ik} + \mathbf{G}_{i+1} \tag{2.9}$$

where $tr(\cdot)$ is the trace of a matrix, $\mathbf{I}_i$ is the inertia matrix for link i, $\mathbf{D}_i$ is the recursive inertia and Coriolis matrix, $\mathbf{E}_i$ is the recursive vector for the gravity torque calculation, $\mathbf{F}_i$ is the recursive vector for the external force-torque calculation, $\mathbf{G}_i$ is the recursive vector for the external moment torque calculation, $\mathbf{g}$ is the gravity vector, m_i is the mass of link i, $\mathbf{r}_i$ is the center of mass of link i, $\mathbf{f}_k = [0 \quad f_{ky} \quad f_{kz} \quad 0]^{\mathrm{T}}$ is the external force applied on link k, $\mathbf{r}_k$ is the position of the external force in the local frame k, $\mathbf{h}_k = [h_x \quad 0 \quad 0 \quad 0]^{\mathrm{T}}$ is the external moment applied on link k, $\mathbf{z}_0 = [0 \quad 0 \quad 1 \quad 0]^{\mathrm{T}}$ is for a revolute joint, $\mathbf{z}_0 = [0 \quad 0 \quad 0 \quad 0]^{\mathrm{T}}$ is for a prismatic joint, δ_{ik} is Kronecker delta, and the starting conditions are $\mathbf{D}_{n+1} = [\mathbf{0}]$, $\mathbf{E}_{n+1} = \mathbf{F}_{n+1} = \mathbf{G}_{n+1} = [\mathbf{0}]$.

2.3. Optimization formulations

The lifting task is formulated as a general nonlinear programming (NLP) problem: find the optimal design variables **x** to minimize a human performance measurement, $f(\mathbf{x})$, subject to physical constraints as follows:

$$\begin{aligned} &Find\text{: } \mathbf{x} \\ &To\text{: } \min f(\mathbf{x}) \\ &S.t. \quad h_i = 0, \qquad i = 1, \dots, l \\ &\qquad g_j \le 0, \qquad j = 1, \dots, k \end{aligned} \tag{2.10}$$

where, h_i are the equality constraints and g_j are the inequality constraints. Expressions for f, h_i and g_j are given in the following paragraphs. In this formulation, the box dimensions, initial and final positions of the box, and initial, intermediate, and final key joint values are obtained from the experiment.

Objective functions

The predicted motion largely depends on the objective function J which will be minimized during the optimization process. A MOO is utilized for the maximum weight lifting prediction by minimizing the dynamic effort and maximizing the lifting weight. The dynamic effort is defined as the time integral of squares of all joint torques (Xiang et al., 2011), and the maximizing box weight objective function is transformed into a minimizing negative logarithmic function of box weight. The MOO objective function is defined as (Xiang et al., 2021):

$$J = w_1 \mathrm{N}\left[\int_0^T \sum_{i=7}^{n} \left(\frac{\tau_i(\mathbf{x},t)}{\tau_i^U - \tau_i^L}\right)^2 dt\right] - w_2 \mathrm{N}[\log(W+10)] \tag{2.11}$$

where n is the number of DOF, τ_i^L and τ_i^U are the ith lower and upper dynamic joint torque limits, respectively, w_1 and w_2 are weighting coefficients for the two normalized objective functions, N[·] is the normalization function by dividing the function's maximum absolute value: for both dynamic effort function and negative logarithmic function of box weight, their maximum absolute values are achieved by purely maximizing box weight at $w_1 = 0$ and $w_2 = 1$ (Marler and Arora, 2004, 2005, Xiang et al., 2010).

Design variables

For the optimization problem, the time domain is discretized by using cubic B-spline functions. Thus, a joint angle profile q(t) is parameterized as follows:

$$q_i(t, \mathbf{s}, \mathbf{P}_i) = \sum_{j=0}^{m} N_j(t, \mathbf{s}) P_{ij}; \qquad 0 \le t \le T \tag{2.12}$$

where t is the time instant, $N_j(t, \mathbf{s})$ are the basis functions, $\mathbf{s}$ is the knot vector, and $P_{ij} = \{p_{i0}, \dots, p_{im}\}$ is the control points vector for the ith joint angle profile and $m + 1$ is the number of control points. The shape of the joint angle profile can thus be affected by changing the value of the control points. With this representation, the control points become the optimization variables. In this study, the box weight (W) is also the design variable, and the knot vector is specified and fixed in the optimization process. Five control points are used for each DOF. Thus, there are a total $5 \times n + 1(W) = 51$ optimization variables $\mathbf{x} = [\mathbf{P}_1^T \quad \cdots \quad \mathbf{P}_n^T \quad W]^T$ in the formulation. Then the joint angular velocity ($\dot{\mathbf{q}}$) and acceleration ($\ddot{\mathbf{q}}$) can be obtained from the first and second time derivatives of the B-spline discretization of the joint angle profile, respectively. Therefore, all joint state variables ($\mathbf{q}, \dot{\mathbf{q}}, \ddot{\mathbf{q}}$) are functions of B-spline control points ($\mathbf{P}$). Next, based on the joint state variables, the DH-based forward recursive kinematics (Eq. 2.4) is calculated for points of interest in the human model (foot ${}^{o}_{o}\mathbf{r}_{foot}$ and hand ${}^{o}_{o}\mathbf{r}_{hand}$). In addition, the joint torque $\boldsymbol{\tau}(\mathbf{x})$ is computed by plugging the joint state variables and box weight (external load) directly into EOM Eq. (2.5), and this is the inverse dynamics procedure.

Constraints

Two types of constraints are imposed on the lifting formulation: time-dependent constraints and time-independent constraints. Time-dependent constraints are imposed on uniform divided time points throughout the lifting motion. On the other hand, time-independent constraints are imposed on specific time points of the lifting motion.

The lifting optimization problem subjects to the following constraints:

(1) Time-dependent constraints:

(a) Joint angle limits constraints can be expressed as:

$$\mathbf{q}^L \leq \mathbf{q}(\mathbf{x}, t) \leq \mathbf{q}^U \tag{2.13}$$

where, $\mathbf{q}^L$ and $\mathbf{q}^U$ are lower and upper joint angle bounds.

(b) Dynamic joint strength is imposed in this study. Dynamic joint strength is a function of joint angle (q), angular velocity (v), strength percentile (z_{score}) and time (t). The lower and upper dynamic joint strengths are: $\tau_i^L = \tau_i^L(q_i, v_i, z_{score}, t)$ and $\tau_i^U = \tau_i^U(q_i, v_i, z_{score}, t)$ respectively. These two functions are logistic regression equations obtained from isometric and isokinetic strength tests using dynamometers (Frey-Law et al., 2012, Hussain and Frey-Law, 2016, Looft, 2014, Stockdale, 2011).

$$\tau_{peak\_U}^i = c_1 + c_2 \frac{4e^{-\frac{q_i - c_3}{c_4}}}{\left[1+e^{-\frac{q_i - c_3}{c_4}}\right]^2} + c_5 \frac{4e^{-\frac{v_i - c_6}{c_7}}}{\left[1+e^{-\frac{v_i - c_6}{c_7}}\right]^2} + c_8 \frac{4e^{-\frac{q_i - c_3}{c_4}}}{\left[1+e^{-\frac{q_i - c_3}{c_4}}\right]^2} \frac{4e^{-\frac{v_i - c_6}{c_7}}}{\left[1+e^{-\frac{v_i - c_6}{c_7}}\right]^2} \tag{2.14}$$

$$\tau_i^U = z_{score} * CV_U^i * \tau_{peak\_U}^i(q_i, v_i, t) + \tau_{peak\_U}^i(q_i, v_i, t) \tag{2.15}$$

$$\tau_i \leq \tau_i^U(q_i, v_i, z_{score}, t) \tag{2.16}$$

where $c_1 \sim c_8$ are regression coefficients, e is the exponential function, $\tau_{peak\_U}^i$ is the upper peak torque value for the ith joint in positive q_i direction as defined in Figure. 2.1, and CV_U^i is the upper coefficient covariance for the ith joint.

Similarly, for the lower dynamic joint torque limit:

$$\tau_{peak\_L}^{i} = d_1 + d_2 \frac{4e^{-\frac{q_i - d_3}{d_4}}}{\left[1+e^{-\frac{q_i - d_3}{d_4}}\right]^2} + d_5 \frac{4e^{-\frac{v_i - d_6}{d_7}}}{\left[1+e^{-\frac{v_i - d_6}{d_7}}\right]^2} + d_8 \frac{4e^{-\frac{q_i - d_3}{d_4}}}{\left[1+e^{-\frac{q_i - d_3}{d_4}}\right]^2} \frac{4e^{-\frac{v_i - d_6}{d_7}}}{\left[1+e^{-\frac{v_i - d_6}{d_7}}\right]^2} \quad (2.17)$$

$$\tau_i^L = z_{score} * CV_L^i * \tau_{peak\_L}^i(q_i, v_i, t) + \tau_{peak\_L}^i(q_i, v_i, t) \quad (2.18)$$

$$\tau_i \geq \tau_i^L(q_i, v_i, z_{score}, t) \quad (2.19)$$

where $d_1 \sim d_8$ are regression coefficients, e is the exponential function, $\tau_{peak\_L}^i$ is the lower peak torque value for the ith joint in negative q_i direction as defined in Figure. 2.1, and CV_L^i is the lower coefficient covariance for the ith joint. We modeled dynamic strengths for the ankle, knee, hip, lower spine joints with three DOFs, shoulder, elbow, and wrist joints, using experimental data from the literature (Frey-Law et al., 2012, Hussain and Frey-Law, 2016, Looft, 2014, Stockdale, 2011). In Eqs. (2.14-2.19), $\tau_{peak\_U}^i$, $\tau_{\text{peak\_L}}^i$, CV_U^i, and CV_L^i are statistical values obtained from experiments. The subject's strength percentile z_{score} is retrieved from an enumeration optimization process for symmetric maximum weight lifting based on experimental data (Xiang et al., 2019).

(c) Balance must be considered during the box lifting process. This is the zero-moment-point (ZMP) constraint,

$$^{o}_{o}\mathbf{r}_{ZMP}(\mathbf{x}, t) \in FSR \quad (2.20)$$

where $^{o}_{o}\mathbf{r}_{ZMP}$ is the calculated ZMP location (Xiang et al., 2010) , FSR represents foot support region (Vukobratović and Borovac, 2004, Xiang et al., 2009b).

(d) In addition, feet are fixed on level ground,

$$^{o}_{0}\mathbf{r}_{foot}(\mathbf{x}, t) = {}^{o}_{0}\mathbf{r}_{foot}^{E} \quad (2.21)$$

where ${}^{0}_{\mathbf{0}}\mathbf{r}_{foot}$ is the calculated global foot position from the 2D human model using Eq. (2.4), and ${}^{0}_{\boldsymbol{o}}\mathbf{r}^{E}_{foot}$ is the measured foot position from the experiment.

(2) Time-independent constraints:

(a) The initial and final box grasping locations are given based on experimental data:

$$ {}^{0}_{\mathbf{0}}\mathbf{r}_{hand}(\mathbf{x}, t) = {}^{0}_{\mathbf{0}}\mathbf{r}^{E}_{box}(t); \qquad t = 0, T \tag{2.22} $$

where ${}^{0}_{\mathbf{0}}\mathbf{r}_{hand}$ is the calculated global hand position using Eq. (2.4), and ${}^{0}_{\mathbf{0}}\mathbf{r}^{E}_{box}$ is the measured box handle position from experiment.

(b) The boundary and mid-time joint angle differences between the model and experiment are constrained in a small range $\varepsilon = 0.1$ rad at boundary and $\varepsilon = 0.15$ rad at mid-time, where q_i^E is the experimental joint angle for ith physical joint.

$$ \left| q_i(\mathbf{x}, t) - q_i^E(t) \right| \leq \varepsilon; \qquad i = 4, \dots, n\,; \quad t = 0, \frac{T}{2}, T \tag{2.23} $$

Where, n is the number of DOFs.

For the time-dependent constraints Eqs. (2.13-2.21), they are evaluated not only at the knot time point, but also at 2 additional time points between any two adjacent distinguished knots. For the time-independent constraints Eqs. (2.22, 2.23), they are evaluated only at the given specific time points. There is a total of 295 nonlinear constraints for the MOO lifting problem. The bounds for the design variables $\boldsymbol{x}$ are: $P_{ij} \in [-10\,, 10]$ rad and $W \in [0, 1000]$ N. The initial guesses are: $\mathbf{P} = \mathbf{0}$ and $W = 200$. The computation is close to real time.

2.4 Experimental data collection

Participants

The experimental protocol has been approved by the Institutional Review Board of the Texas Tech University, and all subjects signed the consent form. Thirteen male subjects aged 20 to 50 years old participated in the lab experiments (sex: male; age: 25.50 ± 7.22 years; height: 180.64 ± 5.15 cm; body mass: 82.34 ± 10.45 kg, where ± indicates standard deviation), and a squat lifting strategy was used for lifting experiments. Among these 13 subjects, 12 subjects were used for MOO simulation and 1 subject for MOO validation. The recruitment criterion is that subjects should be physically and mentally sound, able to perform the scripted task and not be on any medication that might hamper their performance for the box lifting task.

Experimental protocol

A Vicon Nexus motion capture system with five cameras (VICON, Oxford, UK) was used to collect kinematic data at 100 Hz. A plug-in-gait model with added iliac crests, giving 42 markers total, was used for the marker protocol (Cloutier et al., 2011). Two Kistler force plates (Kistler, Winterthur, Switzerland) were used to collect GRFs at 2000 Hz, and each foot was on one of the force plates. For each subject, the following anthropometrics were measured: height, weight, leg length, ankle width, knee width, wrist width, elbow width, shoulder offset, inter-ASIS distance, and waist circumference (Mital and Kromodihardjo, 1986, Schultz et al., 1982).

During the experiment, each participant was asked to psychophysically test their maximum weight-lifting capability through gradually adding the load until the subject requested to stop the increase. The real maximum weight lifting capacity was not adopted to avoid any injury during the experiment, i.e., the maximum weight in this study refers to the maximum weight that the participant can lift safely. Once the maximum lifting weight was obtained, the participant was ready to perform the lifting task. The subject was requested to lift a box (65 cm × 35 cm × 15 cm) forward, i.e., symmetric lifting, in three trials. Because the box did not have handles, it was placed on top of a weight disk about 2.54 cm on the floor so that the subject could fit their fingers under the box. The subject then lifted the box in the most comfortable and natural way and set it down on a 1-meter-tall table in front of them shown in Figure 2.3. After data collection, the data post-processing was conducted in the motion capture software Vicon Nexus.

Figure 2.3: 2D symmetric box lifting experiment

Data processing

The first step for data post-processing was marker labeling. Then the data were smoothed and converted into a C3D file. Finally, the C3D file was imported into Visual 3D (C-Motion, Inc., Germantown, MD, USA). Within Visual 3D, a skeletal model with fifteen segments based on the marker protocol used in the experiments was created to output coordinates and joint angles. The anthropometric measurements taken for each subject at the beginning of the experiment were used to create distinct and accurate skeletal models, allowing for more precise calculations.

The measured height and body mass for each subject at the beginning of the experiment were used to generate their body segments' lengths, centers of mass, and inertial properties through GEBOD^{TM}, a regression-based interactive utility (Cheng et al., 1994). Six joint angles (spine, shoulder, elbow, hip, knee, and ankle), the box weight obtained from the experiments for each individual subject, and the generated anthropometric data were used to obtain the strength percentile (z_{score}) for each subject (Xiang et al., 2019). Finally, the proposed 2D symmetric MOO inverse dynamics motion simulation was used to predict motions, GRFs, and maximum box weights.

2.5 Total error for MOO weighting coefficients

In section 2.3, two weighting coefficients are defined where $w_1 + w_2 = 1$. For each subject, 21 Pareto cases (0 to 20) are established, where the first case has $w_1 = 0.0$ for dynamic effort and $w_2 = 1.0$ for box weight. The remaining cases are created by increasing w_1 by 0.05 and decreasing w_2 by 0.05 until the final case set $w_1 = 1.0$ and $w_2 = 0.0$. A

Pareto optimal analysis, in conjunction with the total error (E_{Total}) analysis, is performed to determine the best case (weighting coefficients) for each subject. The experimental joint angle profiles, GRF profiles, and box weight are compared to the simulation data for all 21 cases. In this study, total error for each case is defined as

$$E_{Total} = \frac{RMSE_q}{RMSE_{qmax}} + \frac{RMSE_{vGRF}}{RMSE_{vGRFmax}} + \frac{RMSE_{hGRF}}{RMSE_{hGRFmax}} + \frac{E_W}{E_{Wmax}} \tag{2.24}$$

where $RMSE_q$ is the total root-mean-square error (RMSE) for the six major joint angle profiles (spine, shoulder, elbow, hip, knee, and ankle), $RMSE_{vGRF}$ is the RMSE for the vertical GRF profile, $RMSE_{hGRF}$ is the RMSE for the horizontal GRF profile, and E_W is the error for the box weight prediction. Note that joint angle and GRF profiles are vectors, and box weight is a scalar. The total error E_{Total} is normalized by dividing each error by their respective maximum error found among the 21 cases for that specific subject. After identifying the total error for all cases for each of the 12 subjects, an average total error is calculated for each case across all subjects. The Pareto case with the lowest average total error is chosen as the optimal values for the two weighting coefficients.

2.6 Validation

After identifying the best MOO weighting coefficients for the lifting model through total error analysis, another experimental subject is compared to the respective simulation results with and without MOO. The error of the predicted box weight and RMSE of each individual joint, vertical GRF, and horizontal GRF profiles, are calculated. In addition, Pearson coefficients for each individual joint angle and GRF profiles are calculated.

2.7 Results

Maximum weight lifting MOO for 12 subjects

As mentioned in section 2.3, both objective functions are appropriately normalized so that they have the same absolute magnitudes in the range $[0, 1]$. The MOO problem is depicted in the criterion space, where the two axes represent two objective functions, as shown in Figure 2.4. For example, the normalized joint torque square and normalized negative logarithmic function of box weight are plotted for Subject #3. The Pareto optimal curve is plotted in the criterion space by evaluating the objective functions for 21 cases in Eq. (2.12) by systematically varying weighting coefficients. The blue dots represent the Pareto optimal solution for each case. Similarly, for other subjects, Pareto optimal curves are plotted by evaluating the objective functions for 21 cases in criterion space, as shown in Figure 2.4.

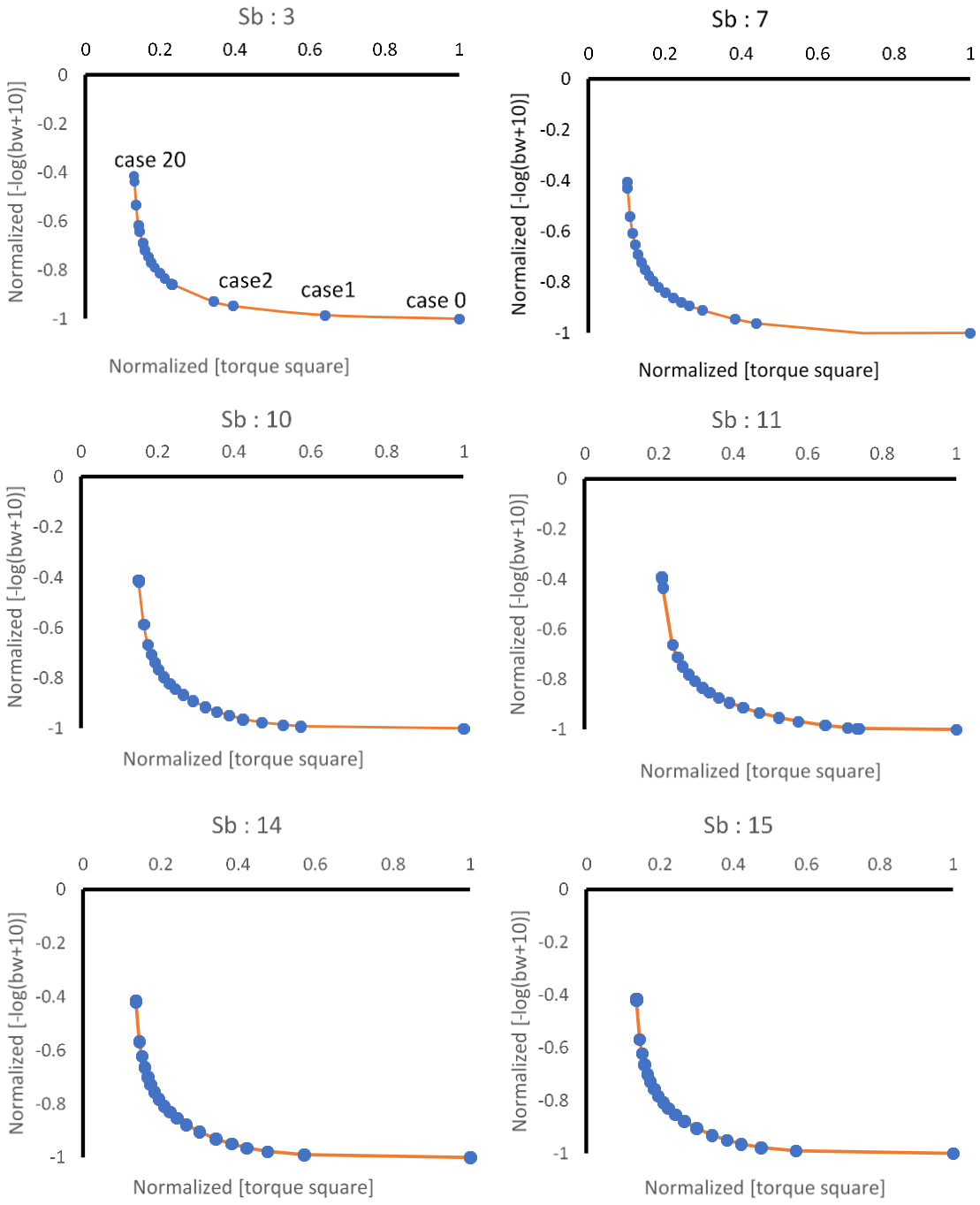
Sb : 3
Normalized [-log(bw+10)]
Normalized [torque square]
case 20
case2
case1
case 0
Sb : 7
Normalized [-log(bw+10)]
Normalized [torque square]
Sb : 10
Normalized [-log(bw+10)]
Normalized [torque square]
Sb : 11
Normalized [-log(bw+10)]
Normalized [torque square]
Sb : 14
Normalized [-log(bw+10)]
Normalized [torque square]
Sb : 15
Normalized [-log(bw+10)]
Normalized [torque square]

(Continued)

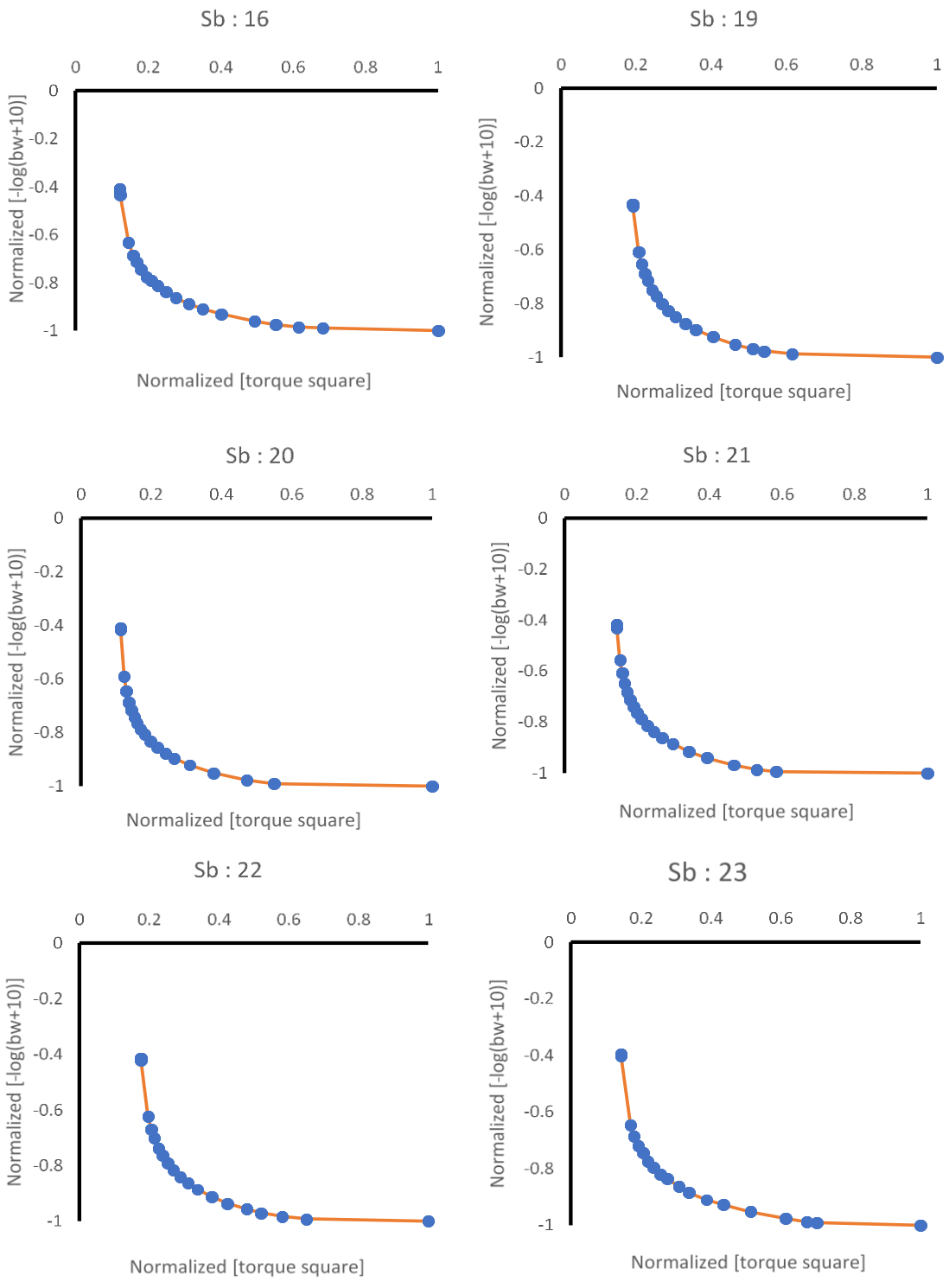

Figure 2.4: Pareto optimal curves for 12 subjects (sb: subject)

The best MOO weighting coefficients for maximum weight lifting

After calculation of the average total error for all Pareto cases of 12 subjects, Pareto case 3, where $w_1 = 0.15$ and $w_2 = 0.85$, has the lowest average total error with a value of 2.621. Pareto case 20 had the highest average total error of 3.337. As shown in Figure 2.5, the further away from case 3, the higher the average total error value would rise. Next, the maximum weight lifting motions of a subject (Subject #2) are simulated using the proposed MOO approach with the best weighting coefficients obtained from the 12 subjects' simulation pool. The results of MOO are compared with the simulation using single maximum weight objective function. The RMSE and Pearson coefficients for simulation with MOO and without MOO are presented in Tables 2.4 and 2.5, respectively. A visual comparison between the experimental data and their respective simulations can be seen in Figure 2.7.

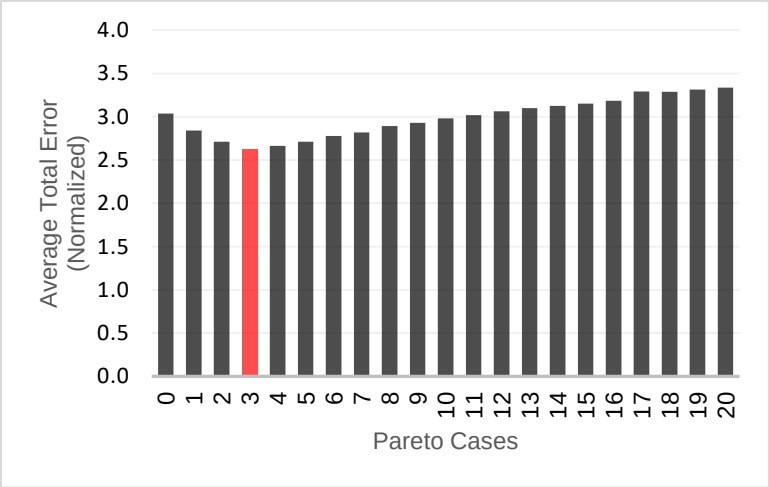

Figure 2.5: Average total error (normalized) for each Pareto case

Table 2.4: Error results for simulation with MOO and without MOO

	Subject #2	
	w/ MOO	w/o MOO
RMSE Spine	11.497	17.268
RMSE Shoulder	10.424	10.143
RMSE Elbow	7.167	13.039
RMSE Hip	6.276	7.600
RMSE Knee	9.743	7.254
RMSE Ankle	8.244	2.703
RMSE Q	53.350	58.007
RMSE Vertical GRF	121.864	122.050
RMSE Horizontal GRF	48.976	59.470
Error W	8.536	24.303

Where RMSE Q is the RMSE sum of spine, shoulder, elbow, hip, knee, and ankle joints.

Table 2.5: Pearson coefficient (r-values) results for simulation with MOO and without MOO

	Subject #2	
	w/ MOO	w/o MOO
Spine	0.928	0.593
Shoulder	0.980	0.957
Elbow	0.986	0.709
Hip	0.990	0.989
Knee	0.988	0.995
Ankle	0.914	0.990
Vertical GRF	0.334	0.268

The weighted sum method of MOO is used to aggregate the two objective functions. 12 subjects' lifting motions are simulated, and each one has 21 cases so that there are total 12×21 = 252 simulations. Next, the overall average total error for each case is calculated across the 12 subjects, and the case with the minimal error gives the best Pareto optimal weighting coefficients. In this study, the identified best weighting coefficients are 0.15 for dynamic effort and 0.85 for box weight, as shown in Figure 2.4. It is seen that the box

weight has a larger effect than the dynamic effort objective function. This is quite reasonable because the goal of the simulation is to maximize the lifting weight.

In Figure 2.4, the smooth Pareto optimal curves are generated for all 12 subjects. These smooth curves indicate that the numerical performance is stable for the proposed MOO approach. It is noted that the Pareto optimal solutions between case 0 (0.0, 1.0) and case 2 (0.1, 0.9) are almost on a horizontal straight line, where the dynamic effort changes substantially, but the box weight remains almost at a constant value (maximum). Similarly, the optimal solutions between the case 20 (1.0, 0.0) and case 18 (0.9, 0.1) are located on a steep vertical line where the box weight changes substantially, but the dynamic effort does not change much. The Pareto optimal curve represents the trade-off between the two objectives. For the maximum weight lifting simulation, it is advantageous to choose cases close to the horizontal flat portion of the Pareto optimal curve, where the maximum box weight is achieved with less dynamic effort. For example, relative to case 2, case 1 represents a substantial increase in effort for just a small improvement in box weight. Thus, case 2 is preferred over case 1 (Gunantara, 2018, Marler and Arora, 2004, Xiang et al., 2010). Note that w = (0.15, 0.85) corresponding to case 3 is identified as the best weighting coefficients to aggregate two objective functions.

The suggested weighting coefficients (0.15, 0.85) from the 12 subjects pool are used to simulate the maximum weight lifting motions for a subject (Subject #2). Table 2.4 shows that the subject has smaller RMSE Q values (total kinematics error) with MOO than those without MOO. Similarly, for the predicted box weight, MOO gives smaller error than the simulation without MOO. For GRFs, the subject has a smaller error by using the MOO method. This might be due to the inaccuracy of the GRF simulation in the model, e.g., the

initial lifting acceleration that exists in experiments is not incorporated in the optimization formulation in section 2.2. Based on the results from Table 2.4, it demonstrates that using MOO generally results in smaller simulation errors.

The Pearson coefficient results show that using MOO has a stronger correlation between simulation and experiment than without MOO. The r-values are larger using MOO except for the knee and ankle joints. The Pearson coefficients (r-values) show that the proposed MOO is an effective approach for simulating maximum weight lifting motion compared to the single objective optimization approach.

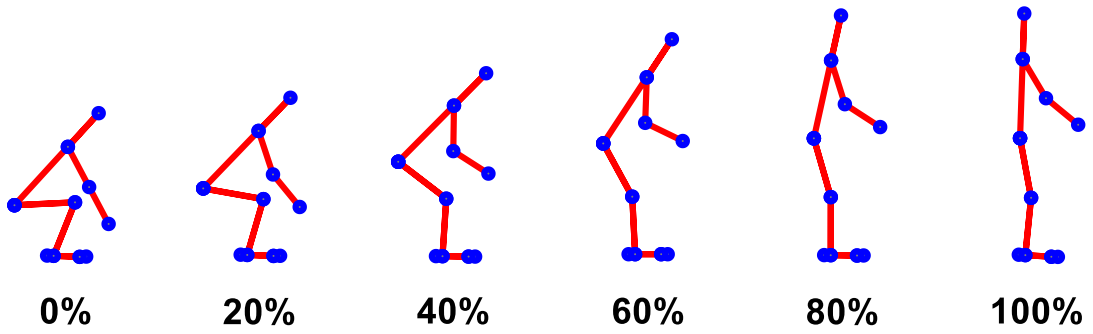

Figure 2.6: Snapshots of predicted symmetric lifting motion using 2D model

Figure 2.6 shows the predicted symmetric lifting motion using the 2D model and the best MOO coefficients. It took 3.34 seconds of CPU time for a desktop computer with an Intel (R) Xeon (R) E-2186G CPU @ 3.80GHz to solve the nonlinear optimization problem using SNOPT. The optimal lifting weight was 238.48 N, whereas the experimental maximum lifting weight was 233.73N.

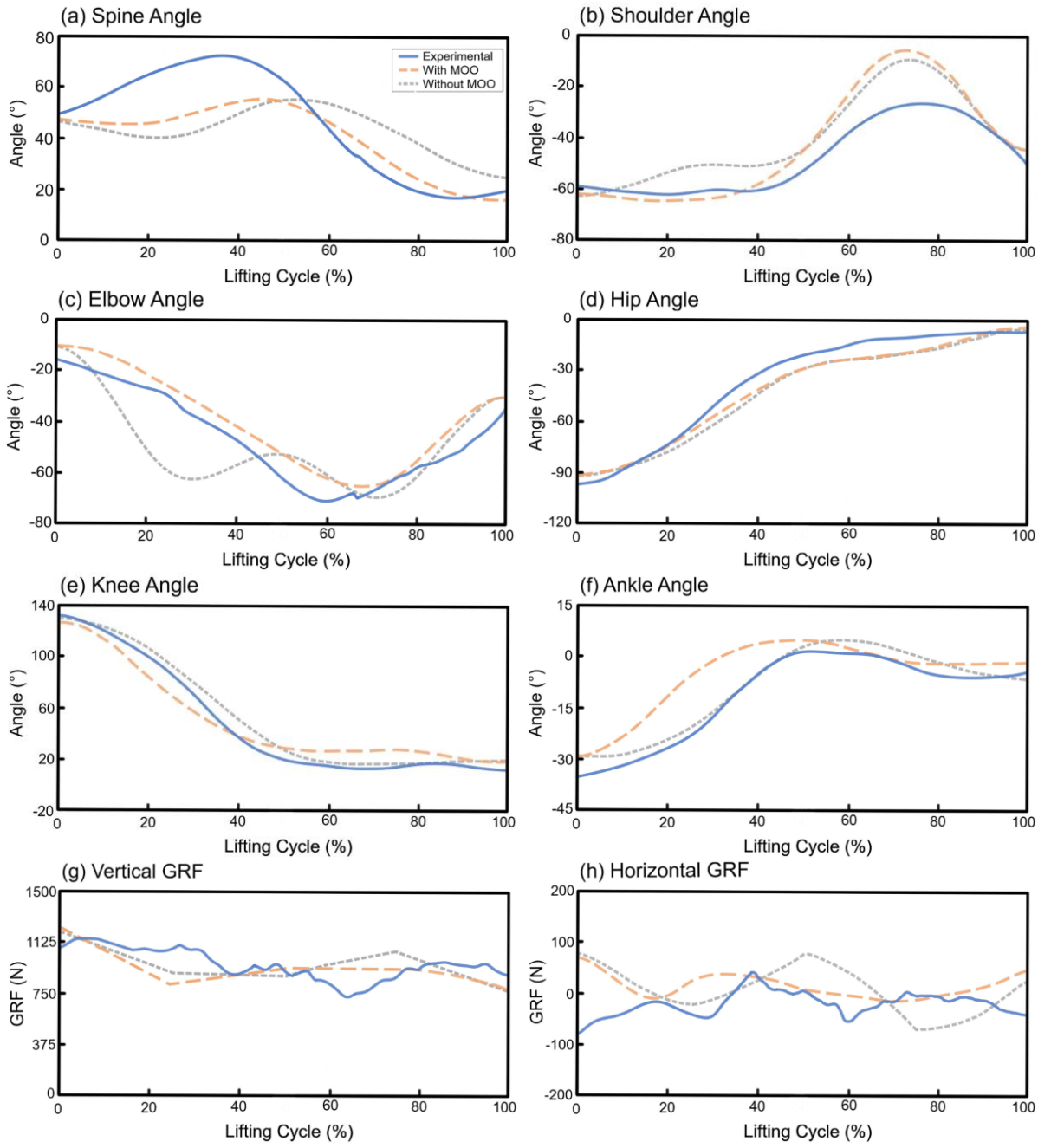

Figure 2.7: Joint angle and GRF profiles validation for Subject #2

Figures 2.7 compares the joint angle and GRF profiles between simulation and experiment. In Figure 2.7, it is apparent that using MOO gives more accurate simulation results than without using MOO except for the ankle joint. Overall, MOO has a smaller total kinematics RMSE value, as seen in Table 2.4 (RMSE Q).

2.8 Summary

This chapter presents a 2D skeletal model with MOO method that predicts a subject-specific maximum symmetric lifting weight and lifting motion while considering the subject's dynamic joint strength. The prediction is achieved by using aggregated objective functions and identified weighting coefficients for maximum weight lifting simulation. It has been demonstrated that the MOO approach generates more accurate simulations compared to the cases without MOO. The best MOO coefficients were used to predict the maximum lifting weight and motion. The MOO-based predicted joint angles and GRFs agree well with the experimental data except for some minor discrepancies.

There are some limitations in the study. First, a 2D model is used for symmetric lifting motion simulation. Considering the computational speed, simplicity of the model, and realistic results after validation, we demonstrate that the 2D model works well for symmetric lifting. Second, there are potential inaccuracies in the dynamic joint strength database from the literature. Third, three postures from the experiment are imposed as constraints in Eq. (2.23) at the initial time, mid-time, and final time. Based on the study (Xiang et al., 2010b), these experimental constraints are necessary to produce more accurate simulations for complicated whole-body lifting motions.

Despite having some limitations, the 2D human skeletal model is capable enough to predict the symmetric maximum lifting weight and lifting motion. However, a 3D model needs to be used to predict asymmetric lifting motion, because of the differences of motion and GRFs on both sides of the sagittal plane, as discussed in chapter 1. In addition, the validated MOO coefficients in this chapter will be used to predict asymmetric maximum lifting weight and lifting motion, which will be discussed in chapter 3.

CHAPTER III

THREE-DIMENSIONAL SKELETAL ASYMMETRIC MAXIMUM WEIGHT LIFTING PREDICTION

As the left and right side joint angles of the human body are considered symmetric in a 2D model, only symmetric motion can be simulated using the 2D model. For asymmetric lifting, we need a model which can capture all the changes on both sides of the human body during an asymmetric lifting task. A 3D musculoskeletal system would be the best model to capture all the human dynamics, but it is a complicated system. As we mentioned in chapter 1, considering the computational speed, it is unrealistic to directly use a musculoskeletal model for maximum weight lifting prediction. A dynamic-joint-strength-based 3D skeletal model can balance the computational cost and the accuracy of asymmetric lifting motion prediction. The prediction results generated from the 3D skeletal model will be inserted into the OpenSim musculoskeletal model to analyze muscle activities for lifting motion. The combined package is called hybrid predictive model for asymmetric lifting prediction, which can help us to assess injury risk for maximum weight asymmetric lifting task.

The purposes of this chapter are: 1) to develop a 3D skeletal model which can simulate and capture asymmetric lifting properties, 2) to generate asymmetric 3D predictive lifting inputs for the OpenSim musculoskeletal model to develop a hybrid model, 3) to validate the 3D skeletal model by comparing the simulation results with experimental data.

Like the hybrid model for symmetric lifting as discussed in chapter 2, the predicted results of the 3D model will be used as the inputs for the OpenSim musculoskeletal model for asymmetric lifting. So, the overall performance of the hybrid predictive model for asymmetric lifting prediction largely depends on the accuracy of the 3D model's predictive results.

3.1 Three-dimensional skeletal model

A 3D human skeletal model is used for predicting asymmetric maximum weight lifting motion. The model has 40 DOFs which are represented as $\mathbf{q} = [z_1\ z_2\ z_3\ \ldots\ldots z_{40}]$ in DH representations (Denavit and Hartenberg, 1955) as shown in Figure 3.1. The joint angle names and symbols are given in Table 3.1. The model consists of one virtual branch and five physical branches. The virtual branch contains six DOFs, among which three are global translations $[z_1\ z_2\ z_3]$ and the other three are global rotations $[z_4\ z_5\ z_6]$. The global translations move the model from the origin to the current location in the Cartesian coordinate system, and the center of global rotations is at the pelvis. The physical branch includes the spine, right arm, left arm, right leg, and left leg. The spine contains two joints, and each joint has three DOFs ($[z_7\ z_8\ z_9]$, $[z_{10}\ z_{11}\ z_{12}]$). The arms and legs are considered symmetric with respect to the sagittal plane of the spatial model. Each arm consists of three parts: upper arm, forearm, and hand. There are seven DOFs for each arm: three for the

shoulder, two for the elbow, and two for the wrist. Each leg consists of a thigh, a shank, a rearfoot, and a forefoot. There are seven DOFs for each leg: three for the hip, one for the knee, two for the ankle, and one for the metatarsal joint at the forefoot.

Table 3.1: Joint angle symbols and names of 3D model

Symbol	**Coordinate name**	**Symbol**	**Coordinate name**
z_1- z_3	Global translation joint coordinates	z_{18}- z_{19} z_{25}- z_{26}	Wrist joint coordinates (Right and Left)
z_4- z_6	Global rotation joint coordinates	z_{27}- z_{29} z_{34}- z_{36}	Hip joint coordinates (Right and Left)
z_7- z_{12}	Spine joint coordinates	z_{30} z_{37}	Knee joint coordinates (Right and Left)
z_{13}- z_{15} z_{20}- z_{22}	Shoulder joint coordinates (Right and Left)	z_{31}- z_{32} z_{38}- z_{39}	Ankle joint coordinates (Right and Left)
z_{16}- z_{17} z_{23}- z_{24}	Elbow joint coordinates (Right and Left)	z_{33} z_{40}	Subtalar joint coordinates (Right and Left)

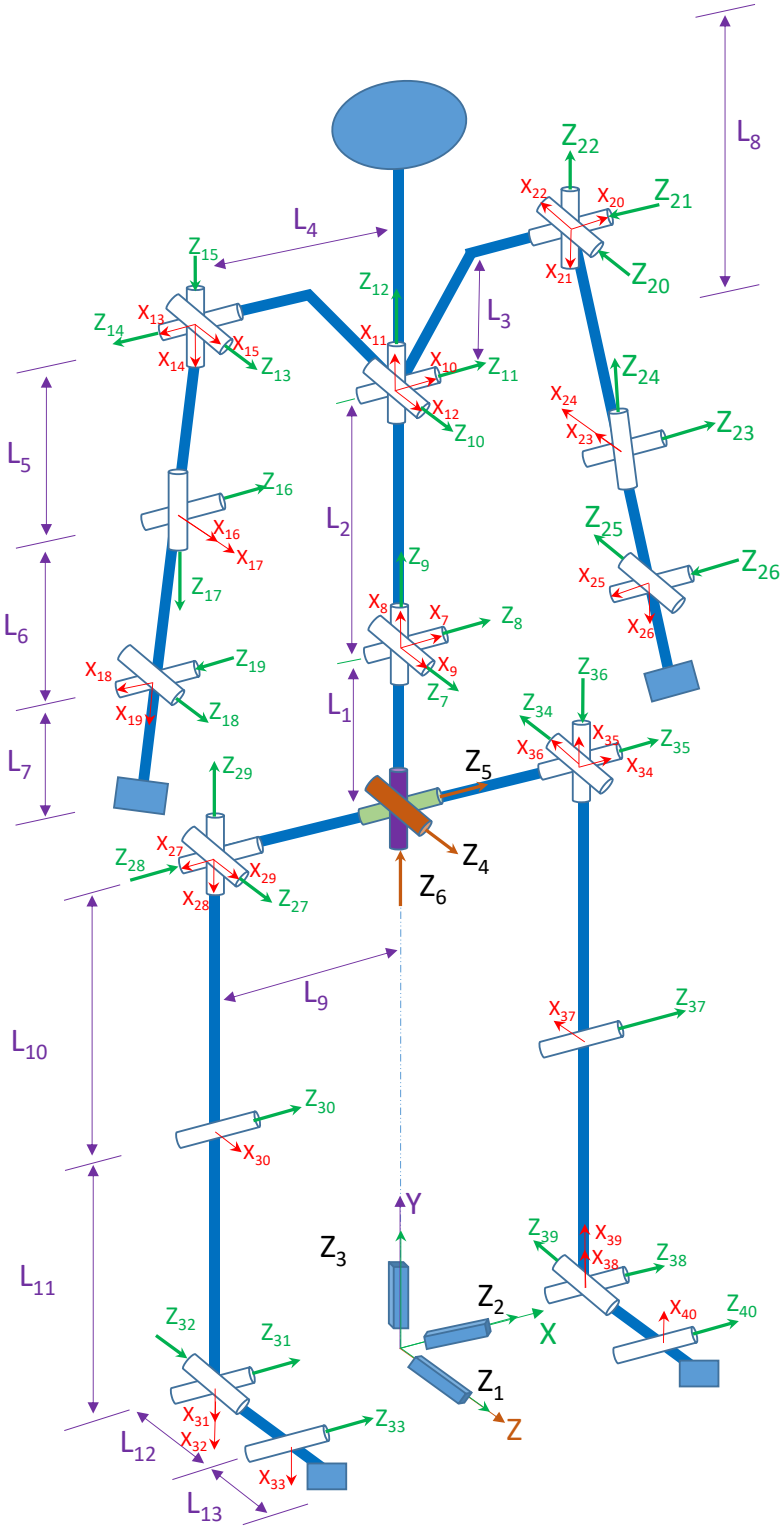

Figure 3.1: 3D skeletal model with 40 DOFs

The anthropometric data of the skeletal model are given in Table 3.2. The data are generated from GEBOD™ software with experimentally measured height, weight, and stature data. The strength percentile is retrieved from symmetric maximum weight lifting (Xiang et al., 2019).

Table 3.2: Link length, mass, and moment of inertia of 2D model

Link name	**Segment**	**Link length (m)**	**Link mass (kg)**	**Moment of inertia, I_{zz} ($kg \cdot m^2$)**
Link 1 (L_1)	Sacrum (S1 to S5)	0.056	2.32	0.033
Link 2 (L_2)	L1 to C7	0.415	20.96	1.188
Link 3 (L_3)	C7 to Shoulder (Y-axis)	0.035	Included in Link 8	
Link 4 (L_4)	C7 to Shoulder (X-axis)	0.113	6.78	0.072
Link 5 (L_5)	Shoulder to Elbow (Right)	0.334	1.9	0.067
Link 6 (L_6)	Elbow to Wrist (Right)	0.247	1.34	0.040
Link 7 (L_7)	Wrist to Finger (Right)	0.107	0.5	0.007
Link 8 (L_8)	C7 to Back Head center	0.212	5.8	0.066
Link 9 (L_9)	Sacrum to Hip (Right)	0.093	4.48	0.041
Link 10 (L_{10})	Hip to Knee (Right)	0.438	9.54	1.014
Link 11 (L_{11})	Knee to Ankle (Right)	0.442	3.74	0.317
Link 12 (L_{12})	Ankle to Subtalar joint (Right)	0.1	0.7	0.000889
Link 13 (L_{13})	Subtalar joint to Toe (Right)	0.165	0.23	0.000296

The major steps to develop a 3D skeletal model are: optimization formulations, 3D skeletal model setup, lifting prediction, and validation. The workflow of the 3D skeletal model development is shown in Figure 3.2.

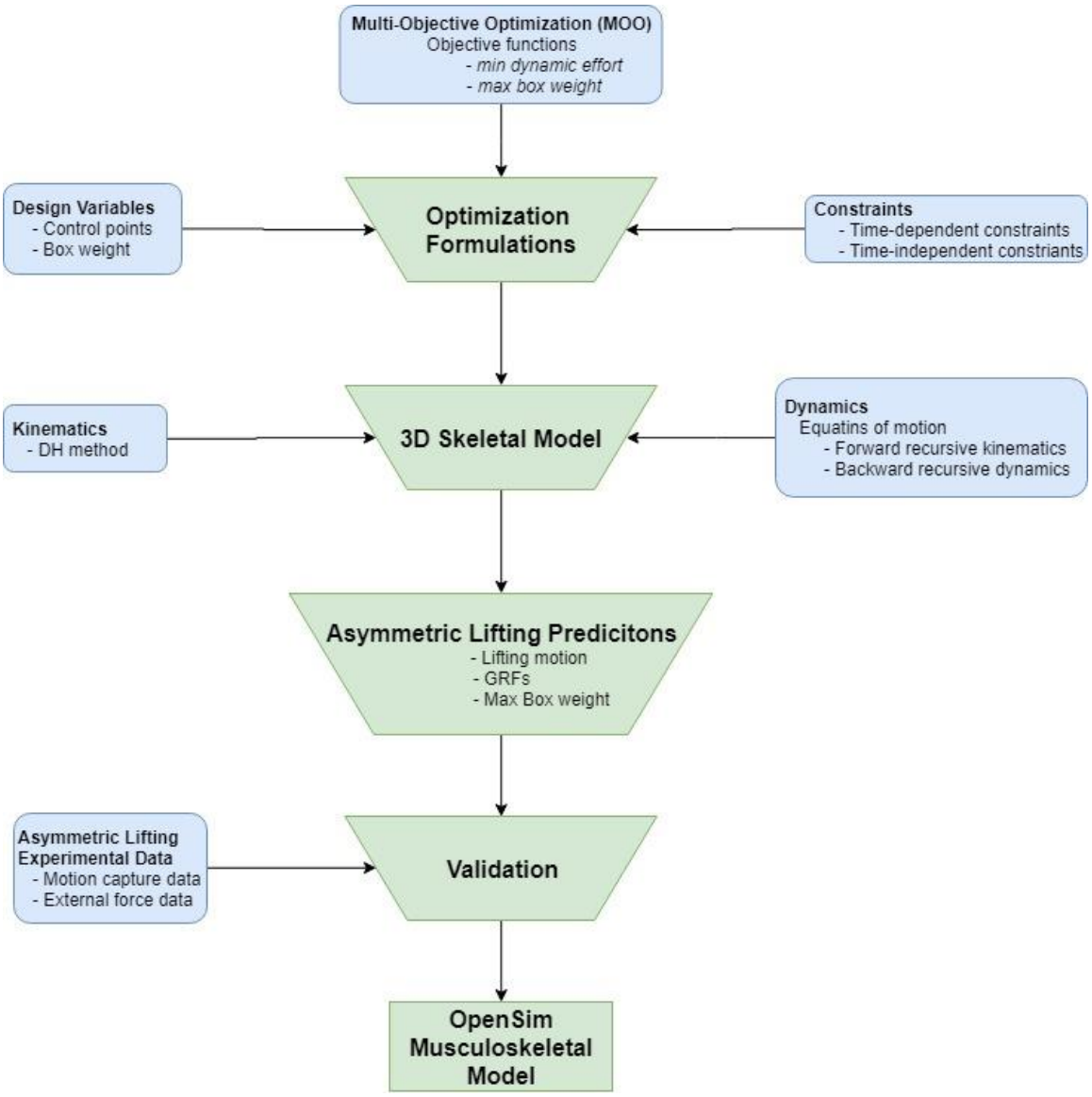

Figure 3.2: Development of the 3D skeletal model

3.2 Kinematics and dynamics

Denavit–Hartenberg method

The relationship among joints and links of the spatial skeletal model is expressed using DH representation and is given in Table 3.3.

Table 3.3: DH table for 3D human model

DOF	**θ**	**d**	**a**	**α**	**Segment**
Global Translations and Rotations					
z_1	$\pi/2$	0	0	$\pi/2$	Global translation
z_2	$\pi/2$	0	0	$\pi/2$	
z_3	$\pi/2$	L_{10}+L_{11}	0	$\pi/2$	
z_4	$\pi/2$	0	0	$\pi/2$	Global rotation
z_5	$\pi/2$	0	0	$\pi/2$	
z_6(to spine)	$\pi/2$	0	L_1	$\pi/2$	
z_6(to right leg)	$\pi/2$	0	L_9	$\pi/2$	
z_6 (to left leg)	$\pi/2$	0	L_9	$\pi/2$	
Spine					
z_7	$\pi/2$	0	L_4	$\pi/2$	Lower spine
z_8	$\pi/2$	0	L_5	$\pi/2$	
z_9	$\pi/2$	0	L_6	$\pi/2$	
z_{10}	$\pi/2$	0	L_7	0	Upper spine
z_{11}	$\pi/2$	0	0	0	
z_{12} (to right arm)	$-\pi/2$	L_3	L_4	$-\pi/2$	
z_{12} (to left arm)	$\pi/2$	L_3	L_4	$\pi/2$	
z_{12} (to neck)	0	L_8	0	0	
Right Arm					
z_{13}	$\pi/2$	0	0	$\pi/2$	Right shoulder
z_{14}	$\pi/2$	0	0	$\pi/2$	
z_{15}	0	L_5	0	$\pi/2$	
z_{16}	0	0	0	$-\pi/2$	Right knee
z_{17}	$\pi/2$	6	0	$\pi/2$	
z_{18}	$\pi/2$	0	0	$\pi/2$	Right wrist
z_{19}	0	0	L_7	0	
Left Arm					
z_{20}	$\pi/2$	0	0	$-\pi/2$	Left shoulder
z_{21}	$-\pi/2$	0	0	$\pi/2$	
z_{22}	0	0	0	$\pi/2$	
z_{23}	0	-L_5	0	$-\pi/2$	Left knee

z_{24}	$\pi/2$	-L_6	0	$\pi/2$	
z_{25}	-$\pi/2$	0	0	$-\pi/2$	Left wrist
z_{26}	0	0	L_7	0	
Right Leg					
z_{27}	$\pi/2$	0	0	$-\pi/2$	
z_{28}	$-\pi/2$	0	0	$\pi/2$	Right hip
z_{29}	0	-L_{10}	0	$-\pi/2$	
z_{30}	$\pi/2$	0	L_{11}	0	Right knee
z_{31}	0	0	0	$\pi/2$	
z_{32}	0	L_{12}	0	$-\pi/2$	Right foot
z_{33}	-$\pi/2$	0	L_{13}	0	
Left Leg					
z_{34}	$-\pi/2$	0	0	$-\pi/2$	
z_{35}	$-\pi/2$	0	0	$\pi/2$	Left hip
z_{36}	0	L_{10}	0	$-\pi/2$	
z_{37}	$\pi/2$	0	-L_{11}	0	Left knee
z_{38}	0	0	0	$\pi/2$	
z_{39}	0	-L_{12}	0	$-\pi/2$	Left foot
z_{40}	$\pi/2$	0	L_{13}	0	

Equations of motions

The general EOM of the 3D skeletal model can be expressed using the recursive Lagrangian formulation in matrix forms which contain forward recursive kinematics and backward recursive dynamics (Xiang et al., 2009b). The forward recursive kinematics and backward recursive dynamics will be the same as the 2D skeletal model in chapter 2.

Forward recursive kinematics

$$\mathbf{A}_i = \mathbf{A}_{i-1}\mathbf{T}_i \tag{3.1}$$

$$\mathbf{B}_i = \dot{\mathbf{A}}_i = \mathbf{B}_{i-1}\mathbf{T}_i + \mathbf{A}_{i-1}\frac{\partial \mathbf{T}_i}{\partial q_i}\dot{q}_i \tag{3.2}$$

$$\mathbf{C}_i = \dot{\mathbf{B}}_i = \mathbf{C}_{i-1}\mathbf{T}_i + 2\mathbf{B}_{i-1}\frac{\partial \mathbf{T}_i}{\partial q_i}\dot{q}_i + \mathbf{A}_{i-1}\frac{\partial^2 \mathbf{T}_i}{\partial q_i^2}\dot{q}_i^2 + \mathbf{A}_{i-1}\frac{\partial \mathbf{T}_i}{\partial q_i}\ddot{q}_i \tag{3.3}$$

Details can be found in chapter 2.

Backward recursive dynamics:

$$\tau_i = \mathrm{tr}\left(\frac{\partial \mathbf{A}_i}{\partial q_i}\mathbf{D}_i\right) - \mathbf{g}^{\mathrm{T}}\frac{\partial \mathbf{A}_i}{\partial q_i}\mathbf{E}_i - \mathbf{f}_k^{\mathrm{T}}\frac{\partial \mathbf{A}_i}{\partial q_i}\mathbf{F}_i - \mathbf{G}_i^{\mathrm{T}}\mathbf{A}_{i-1}\mathbf{z}_0 \tag{3.4}$$

$$\mathbf{D}_i = \mathbf{I}_i\mathbf{C}_i^{\mathrm{T}} + \mathbf{T}_{i+1}\mathbf{D}_{i+1} \tag{3.5}$$

$$\mathbf{E}_i = m_i\mathbf{r}_i + \mathbf{T}_{i+1}\mathbf{E}_{i+1} \tag{3.6}$$

$$\mathbf{F}_i = \mathbf{r}_k\delta_{ik} + \mathbf{T}_{i+1}\mathbf{F}_{i+1} \tag{3.7}$$

$$\mathbf{G}_i = \mathbf{h}_k\delta_{ik} + \mathbf{G}_{i+1} \tag{3.8}$$

$\mathbf{f}_k = [f_{kx} \quad f_{ky} \quad f_{kz} \quad 0]^{\mathrm{T}}$ is the external force applied on link *k*, $\mathbf{r}_k$ is the position of the external force in the local frame *k*, $\mathbf{h}_k = [h_x \quad h_y \quad h_z \quad 0]^{\mathrm{T}}$ is the external moment applied on link *k*. Details can be found in chapter 2.

3.3 Optimization formulation

The asymmetric lifting task is formulated as a general NLP: find the optimal design variable **x** by minimizing the human performance $f(\mathbf{x})$ considering physical constraints.

Objective functions

We used MOO to predict asymmetric maximum lifting weight similar to the 2D symmetric maximum lifting weight formulation in chapter 2. The objective functions are maximization of box weight (W) and minimization of dynamic effort. The combined objective function J can be expressed as:

$$J = w_1 \mathrm{N}\left[\int_0^T \sum_{i=7}^{n} \left(\frac{\tau_i(\mathbf{x},t)}{\tau_i^U - \tau_i^L}\right)^2 dt\right] - w_2 \mathrm{N}[\log(W+10)] \quad (3.9)$$

Details are explained in chapter 2.

Design variables

In the current optimization formulation, the design variables are the control points (**c**) of cubic B-spline interpolation of joint angle profiles for lifting motion, box weight W, and total time T as $\mathbf{x} = [\mathbf{c}^{\mathrm{T}} \quad W \quad T]^{\mathrm{T}}$. The joint torques $\boldsymbol{\tau}(t)$ are directly calculated from EOM using inverse dynamics, instead of integrating the differential equations.

Constraints

The constraints imposed on the lifting motion can be divided into two types: time-dependent constraints and time-independent constraints. The asymmetric lifting formulation shares some time-dependent constraints with the symmetric lifting formulation. The three new time-dependent constraints of asymmetric lifting are – box collision avoidance, the distance between the two hands, and the box parallel to the ground. These constraints are imposed throughout the lifting time interval T. Time-independent constraints include initial and final hand positions, initial and final static conditions, initial, mid-time, and final key joint values, and initial, intermediate, and final GRF values from the experiment. These constraints are imposed only at specific time points of lifting motion.

<u>Time-dependent constraints</u>

Joint angle limits, dynamic joint strength, feet-contacting position, and dynamic stability- these time-dependent constraints will be similar to the 2D symmetric maximum lifting

weight formulation in chapter 2. We will discuss the three new time-dependent constraints here:

(1) Box collision avoidance is used in the current formulation to avoid penetration of the box into the body. The thickness of the human body is represented by filling up the model with spheres on the ankle, shank, knee, thing, hip, lower spine, and higher spine. The distance (*d*) between the box center and sphere center is used to impose the box collision avoidance.

$$d(\mathbf{x}, t) \geq r + \frac{dep}{2} \tag{3.10}$$

where *r* is the radius of a sphere to represent body thickness, and *dep* is the box depth.

(2) The distance between the two hands in 3D space is a constant and equals to the width of the box. This constraint is expressed as,

$$\left\| \mathbf{p}_{right\_hand}(\mathbf{x}, t) - \mathbf{p}_{left\_hand}(\mathbf{x}, t) \right\|_2 = wid \tag{3.11}$$

where $\mathbf{p}_{right\_hand}$ and $\mathbf{p}_{left\_hand}$ are the right and left hand locations, respectively, and *wid* is the width of the box.

(3) To keep the box parallel to the ground during the lifting process, the height of both hands should be same.

$$h_{right\_hand}(\mathbf{x}, t) = h_{left\_hand}(\mathbf{x}, t) \tag{3.12}$$

where h_{right_hand} and h_{left_hand} are the right and left hand heights, respectively.

Time-independent constraints

(1) The initial and final hand (box) locations are given from experiments,

$$\mathbf{p}_{hand}(\mathbf{x}, t) = \mathbf{p}_{box}^{S}(t), \qquad t = 0, T \tag{3.13}$$

where $\boldsymbol{p}_{hand}$ is the calculated hand position, and $\boldsymbol{p}_{box}^{S}$ is the specified box position from the experiment.

(2) The whole body will be at rest at the initial and final time points.

$$\dot{\mathbf{q}}(\mathbf{x}, t) = \mathbf{0}, \qquad t = 0, T \tag{3.14}$$

(3) Initial, mid-time, and final key joint angles are given from experimental data.

$$\left|q_i(\mathbf{x}, t) - q_i^E(t)\right| \leq \varepsilon; \qquad i = 7, \ldots, n; \qquad t = 0, \frac{T}{2}, T \tag{3.15}$$

Where, n is the number of DOFs, q_i^E is the experimental joint angle for *i*th joint including right and left ankle flexion, right and left knee flexion, right and left hip flexion, right and left elbow flexion, spine flexion and rotation, $\varepsilon = 10$ degree at boundaries and $\varepsilon = 5$ degree at the mid-time point.

(4) Initial, intermediate, and final vertical GRFs are given from experimental data.

$$\left|GRF_{left}(\mathbf{x}, t) - GRF_{left}^{E}(t)\right| \leq 40, \quad t = 0, \frac{T}{3}, \frac{T}{2}, \frac{2T}{3}, T \tag{3.16a}$$

$$\left|GRF_{right}(\mathbf{x}, t) - GRF_{right}^{E}(t)\right| \leq 40, \quad t = 0, \frac{T}{3}, \frac{T}{2}, \frac{2T}{3}, T \tag{3.16b}$$

where GRF_{left}^{E}, GRF_{right}^{E} are the experimental vertical GRF for the left and right foot, respectively.

3.4 Experimental data collection

Participants

The experimental protocol was approved by the Texas Tech University Institutional Review Board, and all subjects signed an informed consent form. 12 subjects were used for the asymmetric lifting study (sex: male; age: 25.42±7.72 years; height: 182.2±3.6 cm; body mass: 84.16±10.16 kg, where ± indicates standard deviation), and all 12 subjects were using a squat-lifting strategy for maximum weight lifting. The subjects were selected based on the criterion that they should: (1) be physically and mentally sound, (2) be able to perform the scripted task, and (3) not be on any medication that might hamper their performance during the box-lifting task.

Experimental protocol

The participant performed three repetitions of the lifting task which involved the subject lifting the box from the weight disk and setting it down on a 1-meter-tall table to their right (asymmetric lifting), as seen in Figure 3.3. Each participant was asked to psychophysically determine their maximum weight-lifting capability by gradually increasing the load on the box (65 cm × 35 cm × 15 cm) until the subject felt the load was too heavy to carry safely. It is important to note that the true maximum lifting capacity was not used so that subjects could avoid injury during the experiment. Therefore, the maximum weight in this study refers to the maximum weight a participant can safely carry. Once the weight was determined, the lifting study was initiated. The rest of the experimental protocols are similar to the symmetric lifting mentioned in chapter 2.

Data processing

The data were processed in Vicon® software. All markers were labeled, and the data were smoothed and converted into a C3D file, which was then imported into Visual 3D® (C-Motion, Inc., Germantown, MD, USA). In Visual 3D, each subject's raw kinematic data and measured anthropometries were used to create hybrid models which included the following 15 segments: pelvis, trunk, thigh (bilateral), shank (bilateral), foot (bilateral), head, upper arm (bilateral), forearm (bilateral), and hand (bilateral). The kinematic and kinetic data were filtered using a Butterworth filter with cutoff frequencies of 6 Hz and 25 Hz, respectively. The following variables were extracted from the processed kinematic and kinetic data: bilateral ankle flexion, bilateral knee flexion, bilateral hip flexion, spine flexion and rotation, bilateral elbow flexion, and bilateral vertical GRFs.

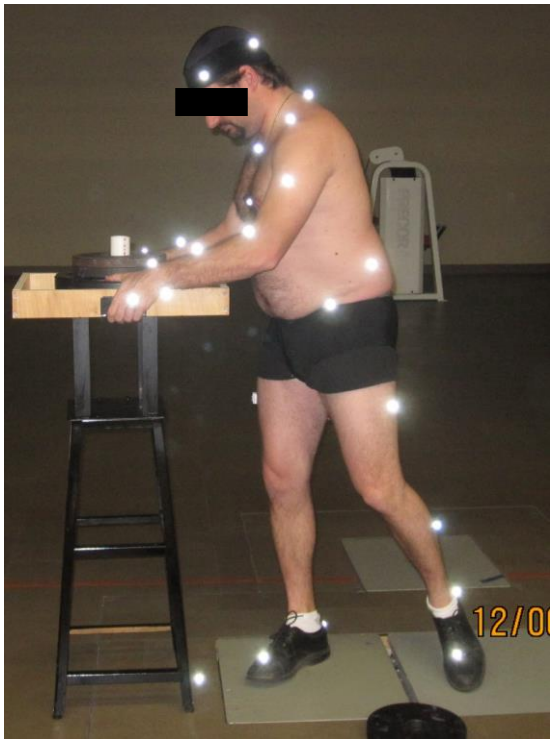

Figure 3.3: 3D asymmetric lifting experiment

3.5 Results and validation

The asymmetric lifting problem was solved using a sequential-quadratic-programming (SQP)-based optimizer SNOPT (Gill et al., 2005). It took about 72.77 seconds of CPU time to solve the problem on a desktop computer with an Intel (R) Xeon (R) E-2186G CPU @ 3.80GHz processor. The maximum lifted weight during the experiment was 245.37 N (25.01 kg). The predicted maximum lifted weights on the right hand and left hand were 124.92N and 120.45 N, respectively. The predicted total lifted weight was 256.78 N that is 8.9% larger than the maximum lifted weight during experiment. The optimal lifting time is 1.32 seconds. The strength (z_{score}) for the simulated model was retrieved from symmetric maximum weight lifting as 1.05 (Xiang et al., 2019). Figure 3.4 depicts the predicted joint angle and vertical GRF profiles. The snapshots of the optimal asymmetric lifting motion are shown in Figure 3.5.

The predicted joint angles agree well with the experimental data. Although the predicted right ankle at the beginning of lifting (Figure 3.4B) and right knee at the last portion of lifting motion (Figure 3.4D) are outside of one standard deviation, the pattern and timing of phase change are consistent with the experimental data. The predicted hip flexions, elbow flexions, spine flexion, and spine rotation are within one standard deviation of experimental joint angle profiles. However, for the simulation, the 3D human model started to straighten and rotate its spine earlier than the experimental subject did (Figure 3.4 G and H). Figure 3.4 (K and L) shows the comparisons of vertical GRFs on both feet during lifting. The predicted GRFs are within one standard deviation of experimental data, except the right GRF during 20%-35% of the task.

The predicted maximum lifting weight is 8.9% higher than the experimental maximum lifting weight. As mentioned in section 3.4, the maximum lifting weight determined during the experiment was a safe maximum weight. The true maximum lifting weight should be higher than the experimentally determined maximum lifting weight. The proposed MOO asymmetric maximum weight lifting prediction reveals this insight.

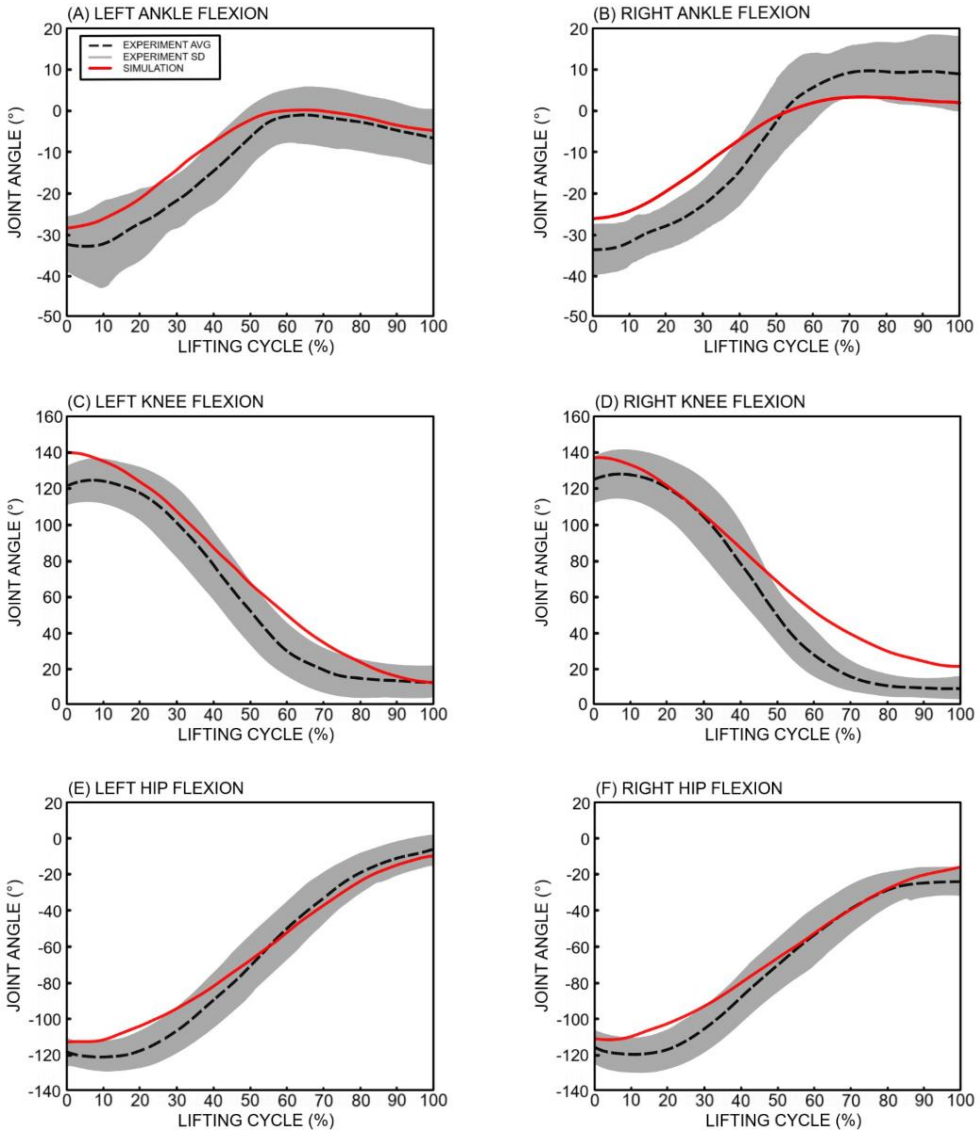
(A) LEFT ANKLE FLEXION
EXPERIMENT AVG
EXPERIMENT SD
SIMULATION
JOINT ANGLE (°)
LIFTING CYCLE (%)
(B) RIGHT ANKLE FLEXION
JOINT ANGLE (°)
LIFTING CYCLE (%)
(C) LEFT KNEE FLEXION
JOINT ANGLE (°)
LIFTING CYCLE (%)
(D) RIGHT KNEE FLEXION
JOINT ANGLE (°)
LIFTING CYCLE (%)
(E) LEFT HIP FLEXION
JOINT ANGLE (°)
LIFTING CYCLE (%)
(F) RIGHT HIP FLEXION
JOINT ANGLE (°)
LIFTING CYCLE (%)

(continued)

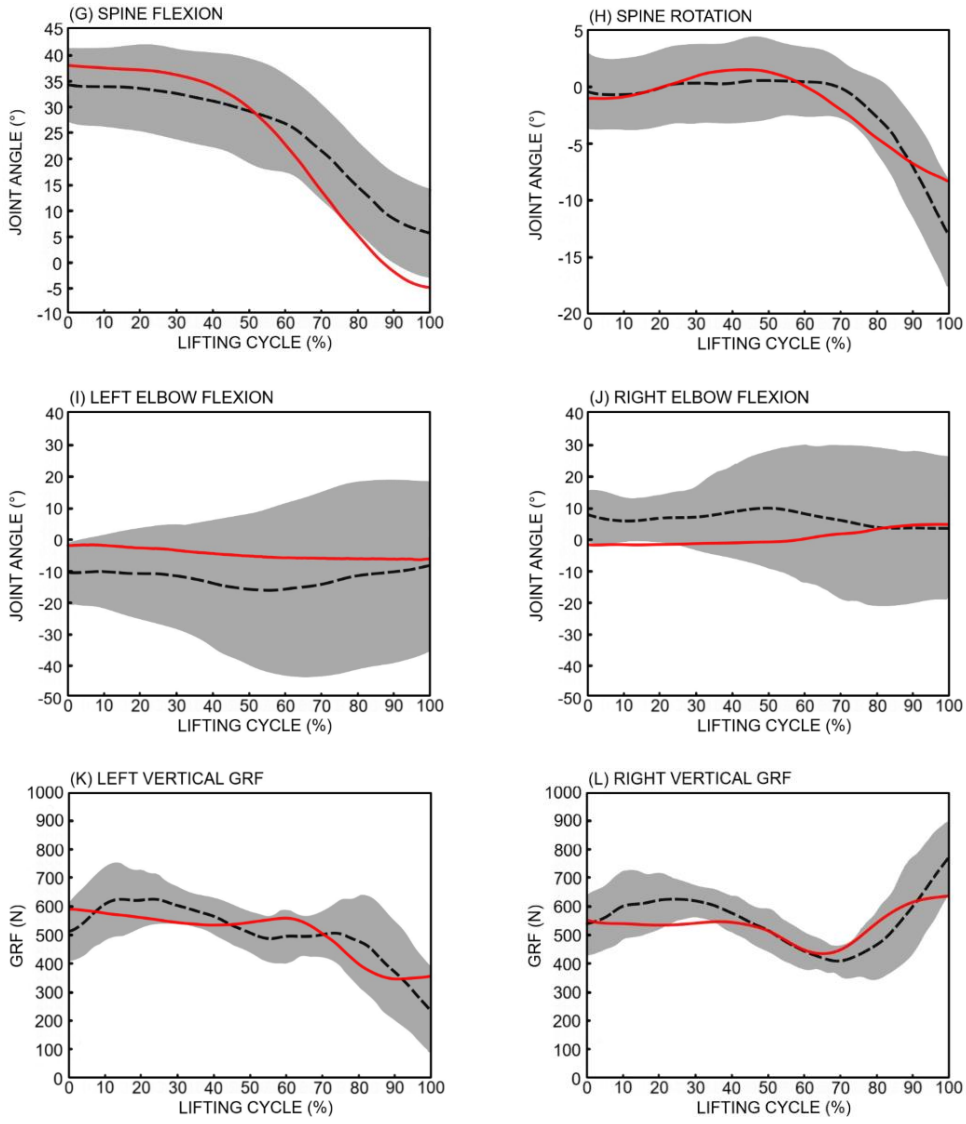

Figure 3.4: Joint angle and vertical GRF profiles during lifting

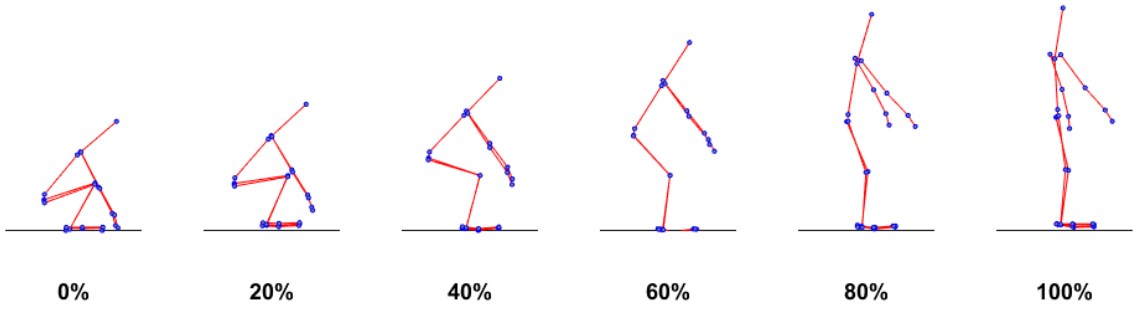

Figure 3.5: Snapshots of 3D asymmetric maximum weight lifting

There are some minor discrepancies between the simulated and experimental joint angle profiles. One noticeable difference between the prediction and experimental data was the time lag of phase change for a small portion of the vertical GRF profiles (Figure 3.4 K and L). The reason for this discrepancy might be early phase changes of spinal flexion and rotation compared to experimental data (Figure 3.4 G and H). Early extension of the spine worked as a catalyst to give the model early upright standing stability and to start the rotation. That early upright standing is also the reason for the flat profile after 90% of the task for both GRFs. On the other hand, the experimental lifting strategy extended the spine later than the simulation model and rotated the body faster to place the box at the desired position on the right side. As a result, after the second peak (85% of the task), the subjects created higher GRF on the right side and lower GRF on the left side than the simulation did. Although there are some deviations of phase change for GRFs, the simulated profiles were almost within one standard deviation of the experimental data.

Although some experimental data are used in the optimization formulation (Eqs 3.15 and 3.16) to guide the prediction, they are necessary to predict accurate results because of the complexity of the 3D asymmetric lifting motion. The previous studies showed that mid-time postures or key joint values could improve the accuracy of lifting prediction (Chang

et al., 2010, Xiang et al., 2021). In this study, we tried to use minimal experimental data in the optimization formulation. It was found that three experimental intermediate GRF constraints (Eqs. 3.16a, b) were necessary to capture the history of GRF profiles due to the fluctuating nature of asymmetric GRFs and the effects of spine flexion and rotation. Compared to the regression models (Mital et al., 1997), the proposed predictive model uses much less experimental data and has more powerful predictive capability. However, the model's predictive ability is compromised by the amount of experimental data used in the optimization formulation.

It is noted that we used symmetric maximum weight lifting strength for asymmetric maximum weight lifting prediction for subject #8. Here we assume that symmetric and asymmetric lifting strength percentiles are similar for this subject. This assumption is reasonably proved through simulation and experiments. The simulation results predict accurate asymmetric lifting motion, box weight, and time duration compared to experimental data by using symmetric lifting strength. In case the symmetric and asymmetric strength percentiles are very different for a subject, the optimization-based enumeration retrieval approach (Xiang et al., 2019) can be used to approximate the subject's strength percentile for the asymmetric lifting based on experimental data.

This is the first study using MOO to predict 3D asymmetric maximum weight lifting motion considering the dynamic joint strength in the literature. Based on the comparisons with experimental data for both kinematics and kinetics, it is clear that, except for some minor discrepancies, the results of the predictive model demonstrated the ability to predict realistic 3D asymmetric lifting motion, accurate maximum lifting weight, and lifting time duration. This model also provides some insight view of 3D asymmetric maximum weight

lifting considering the dynamic joint strength, which can be helpful when analyzing ergonomic safety problems involving lifting.

3.6 Summary

In this study, a 3D 40-DOF skeletal model was used to predict asymmetric human lifting motion and maximum lifting weight. The lifting task was formulated as a MOO problem with two cost functions: minimizing the dynamic effort and maximizing the box weight. The lifting motion prediction problem was solved by an SQP based optimizer SNOPT considering the dynamic joint strength as one of the constraints. The development of a predictive human model that can predict human kinematics and kinetics accurately is a big challenge. It is necessary to include a dynamic strength constraint to predict maximum lifting weight, optimal lifting motion, and lifting time duration. In addition, MOO can generate more accurate simulation than single objective optimization (Xiang et al., 2020). The validated dynamic-joint-strength-based 3D asymmetric lifting model will give researchers a robust tool to work on subject-specific motion analysis, which is helpful for designing workplace and ergonomic tools to avoid injury for lifting. In the next chapter, we will develop a hybrid model by integrating the skeletal motion prediction with an OpenSim model to study muscle activities (Zaman et al., 2019).

CHAPTER IV

HYBRID MODEL FOR SYMMETRIC LIFTING PREDICTION

A skeletal human model can predict the lifting motion efficiently, but it cannot evaluate potential musculoskeletal injuries. The prediction results generated from the 2D skeletal module will be inserted into the OpenSim musculoskeletal module to analyze muscle activities for symmetric lifting motion. The purpose of the musculoskeletal modeule is to predict muscle activation, forces, joint reaction forces, and other biomechanical properties. Biomechanical evaluation based on the musculoskeletal model can reveal the reasons for lifting-related musculoskeletal disorders. The combined package is called the hybrid predictive model, which can assess injury risk for symmetric lifting by combining the skeleton motion prediction with OpenSim musculoskeletal analysis.

The purposes of this chapter are 1) integration of skeletal models with the OpenSim musculoskeletal model to develop a novel hybrid predictive model, 2) validation of the hybrid predictive model for maximum lifting weight. In this chapter, the static optimization tool in OpenSim will be used to obtain the muscle activations, and the joint reaction analysis tool to evaluate the spine joint reaction forces.

4.1 Hybrid model

The hybrid model has two modules, as shown in Figure 4.1. The first module consists of the predictive skeletal model, where the kinematics and kinetics of the symmetric lifting motion are predicted. The second module consists of the OpenSim musculoskeletal model, where the muscle activations, forces, and joint reaction loads are estimated.

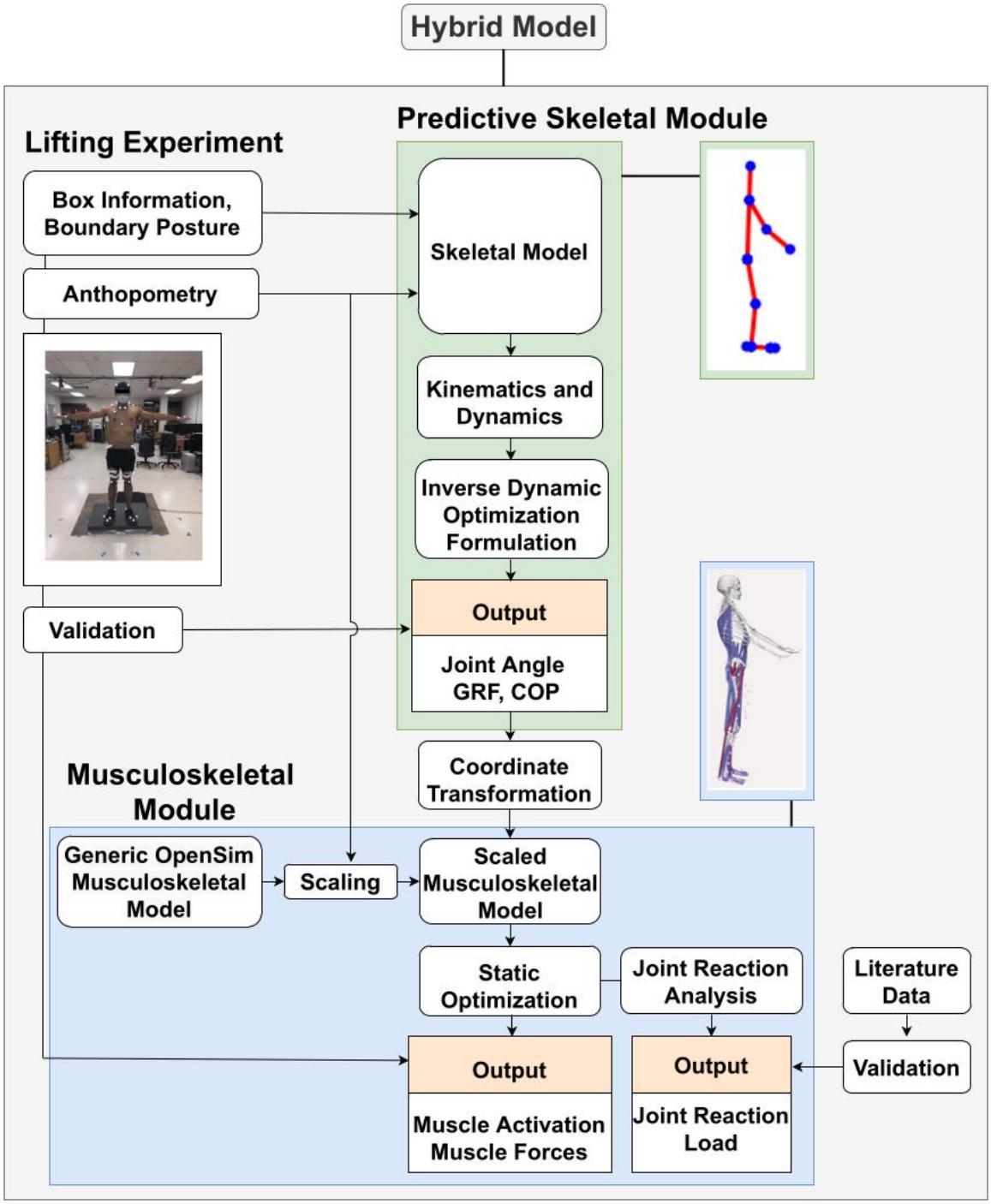

Figure 4.1: Development of hybrid OpenSim musculoskeletal model

4.1.1 Predictive skeletal module

A 2D skeletal model is used to predict the lifting motion using an inverse dynamic optimization formulation. This 2D skeletal model has 10 DOFs, as shown in Figure 4.2. 3 DOFs are used for global translation and rotation. 7 DOFs are used for body joints. The anthropometric data for the experimental subject, a 72nd percentile male, is generated by GEBOD software.

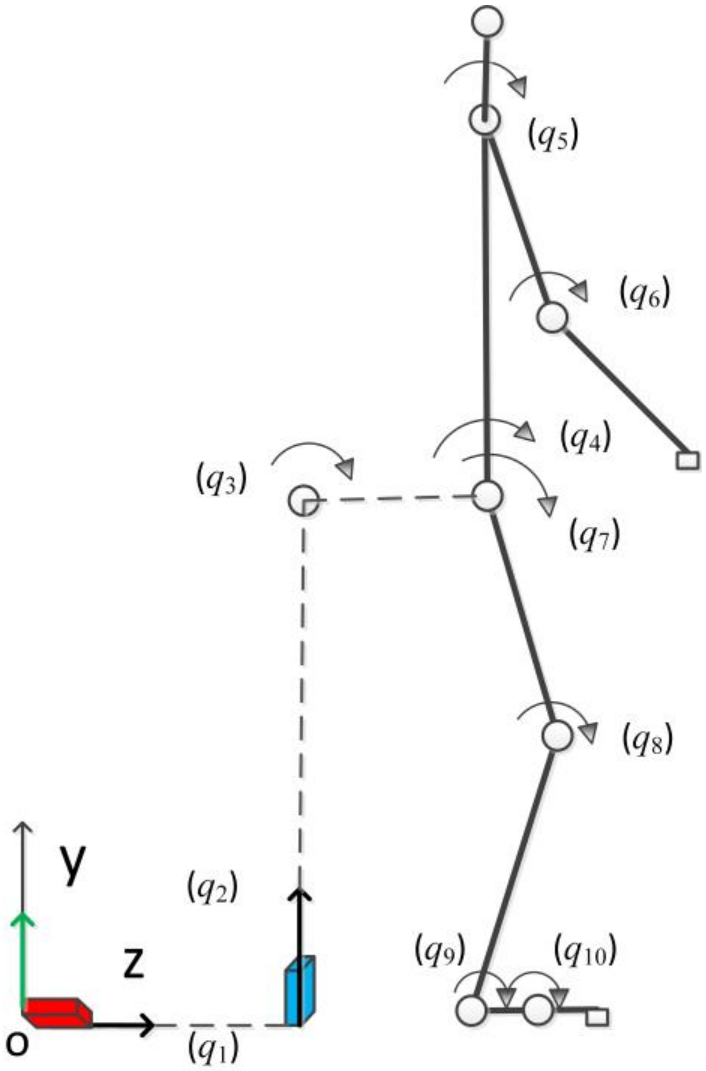

Figure 4.2: 10-DOF 2D skeletal model

4.1.1.1 Kinematics and dynamics

The kinematics and dynamics are similar to Section 2.2

4.1.1.2 Optimization formulation

The design variables ($\mathbf{x}$) are cubic B-spline control points of joint angle profiles. The objective function $f(\mathbf{x})$ is the summation of normalized joint torque squares. The lifting task is formulated as a general nonlinear programming (NLP) problem: find the optimal design variables $\mathbf{x}$ to minimize a human performance measurement, $f(\mathbf{x})$, subject to physical and task constraints including joint angle limits, dynamic joint torque limits, balance condition, foot contacting position, collision avoidance, initial and final hand positions, initial and final static conditions, and initial, mid-time, and final postures.

1. Joint angle limits,

$$\mathbf{q}^L \leq \mathbf{q}(\mathbf{x}, t) \leq \mathbf{q}^U \tag{4.1}$$

where $\mathbf{q}^L$ and $\mathbf{q}^U$ are the joint angle lower and upper bounds.

2. Joint torque limits,

$$\boldsymbol{\tau}^L \leq \boldsymbol{\tau}(\mathbf{x}, t) \leq \boldsymbol{\tau}^U \tag{4.2}$$

where $\boldsymbol{\tau}^L$ and $\boldsymbol{\tau}^U$ are the joint torque lower and upper bounds.

3. Balance condition,

$$p_{ZMP}(\mathbf{x}, t) \in \text{FSR} \tag{4.3}$$

where p_{ZMP} is the zero-moment-point (ZMP) location, and FSR represents the foot support region.

4. Foot contacting position,

$$p_{foot}(\mathbf{x}, t) = p_{foot}^{E} \tag{4.4}$$

where p_{foot} is the calculated foot position and p_{foot}^{E} is the measured experimental foot position.

5. Collision avoidance,

$$d(\mathbf{x}, t) \geq r_1 + r_2 \tag{4.5}$$

where d is the calculated distance between box center and circle center on body segment representing body thickness, r_1 is the radius of the circle on a body segment and r_2 is half of the box depth.

6. Initial and final hand (box) locations,

$$p_{hand}(\mathbf{x}, t) = p_{box}^{E}(t); \qquad t = 0, T \tag{4.6}$$

where p_{hand} is the calculated hand position, p_{box}^{E} is the experimental box position, and T is total time.

7. Initial and final static conditions,

$$\dot{\mathbf{q}}(\mathbf{x}, t) = \mathbf{0}; \qquad t = 0, T \tag{4.7}$$

8. Posture constraints from experiment,

$$|\mathbf{q}(\mathbf{x}, t) - \mathbf{q}^{E}(t)| \leq \varepsilon; \qquad t = 0, \frac{T}{2}, T \tag{4.8}$$

where $\mathbf{q}^{E}$ is the experimental joint angle, $\varepsilon = 0.15$ rad.

The total lifting time is uniformly discretized into twelve segments. There are a total of 50 design variables (5 control points for each DOF) and 523 nonlinear constraints for the symmetric lifting motion optimization. The sequential quadratic programming-based

optimizer SNOPT (Gill et al., 2005) is used to solve the optimization problem and to find the optimal lifting motion. Details about the constraints and the optimization formulation are described in Xiang et al. (2019, 2021), Zaman et al. (2022), Rakshit et al. (2020).

The optimization solutions (joint angle control points) are used to calculate the joint angle profiles, GRFs, and COP. These resultants and external forces will be transferred to OpenSim as a function of time to analyze muscle activation and joint reaction loads. This is in contrast to the traditional method wherein the input parameters for OpenSim are obtained from a motion capture system that inherently lacks a predictive capability.

4.1.2. Musculoskeletal analysis module

The musculoskeletal analysis is done in OpenSim, an open-source biomechanical software package that can be used to build, exchange, and analyze computer models of the musculoskeletal system and dynamic simulations of movement. The static optimization tool of OpenSim is used to estimate the muscle activations and forces. The joint reaction analysis tool is used to estimate the lumbar spine and knee joint reaction loads.

4.1.2.1 Musculoskeletal model

A full-body lumbar spine (FBLS) model is used as the musculoskeletal model for the hybrid method. The model is shown in Figure 4.3. The model has 30 DOFs, 21 segments, and 324 musculotendon actuators. The model is the combination of three other OpenSim models - Hamner's full-body model (Hamner et al., 2010) is used as the base model, Christophy's lumbar spine model (Christophy et al., 2012) is used for the torso, and

Arnold's model (Arnold et al., 2010) is used for the patella. The model has five lumbar vertebrae connected to each other by 6-DOF joints. The eight major muscle groups of the lumbar spine are modeled—erector spinae (ES), rectus abdominis (RA), external obliques (EO), internal obliques (IO), multifidus (MF), quadratus lumborum (QL), psoas major (PS), and latissimus dorsi (LD). The model was validated by comparing the model parameters and simulation to experimental data. The FBLS model was validated in three phases: model parameters, muscle function, and model simulations. The model parameters were validated by comparing them to experimental data. The muscle function was validated by comparing moment generation capacity to experimental results from seven healthy adult males. The model simulations were validated by comparing estimated muscle activation to experimentally measured surface EMG. Details about this model can be found in Raabe and Chaudhari (2016). Since the spine muscles of this model are relatively weak, their maximum isometric force, optimal fiber length, and tendon slack length are modified according to Beaucage-Gauvreau et al. (2019) to make the model suitable for lifting tasks.

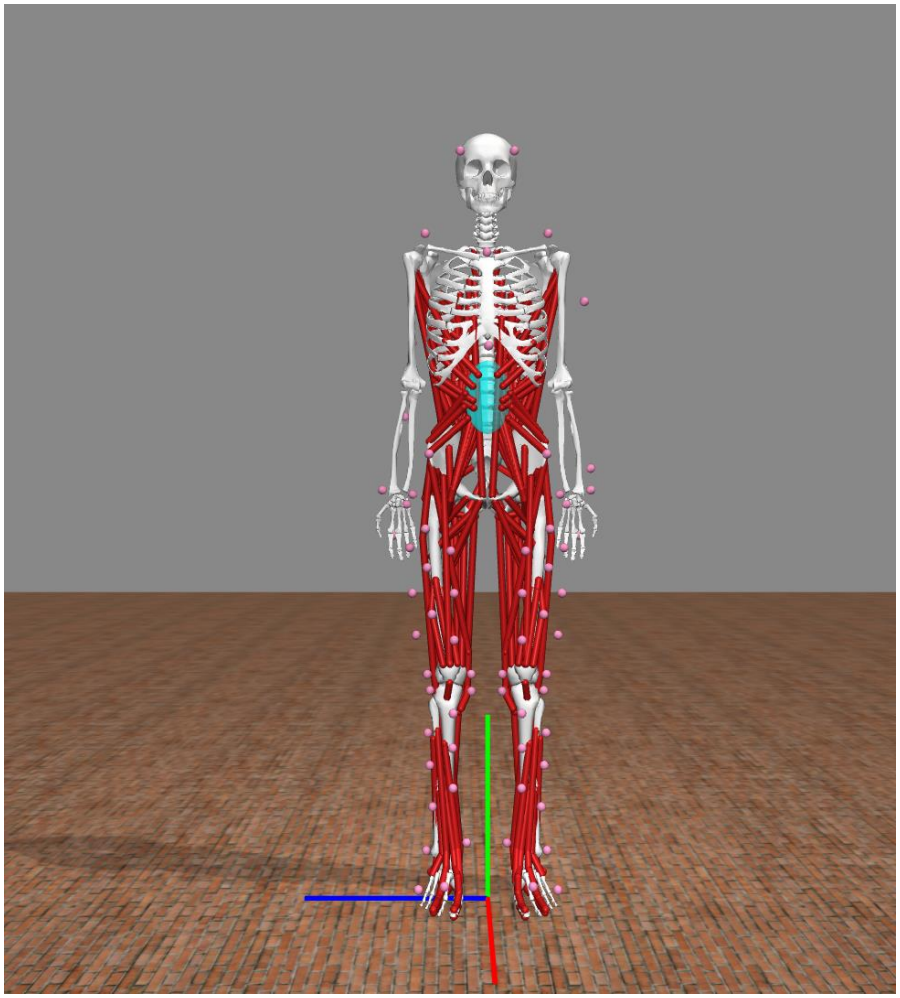

Figure 4.3: Musculoskeletal model in OpenSim (Raabe and Chaudhari, 2016)

4.1.2.2. Integration of predictive skeleton module with musculoskeletal module

The traditional experimental input data for OpenSim includes marker positions from motion capture, GRFs from force plates, and given external loads. In contrast, the predictive simulation model makes available the predicted state variables ($q, \dot{q}, \ddot{q}$), GRFs, COP, and external forces (F_{ex}). Muscle activations, muscle forces, and joint reaction forces can be found by importing these data into the OpenSim.

Step 1: Scaling

The first step to interface OpenSim with the predictive model is scaling, wherein the dimensions of the musculoskeletal model are programmatically adjusted to match the anthropometry of the human subject. The FBLS model was scaled according to the anthropometry generated for each body segment from Visual3D (C-Motion Inc., Germantown, Maryland, USA).

Step 2: Coordinate transformation

Next, before importing the kinematics and kinetics data into the musculoskeletal model, the coordinate systems for both must match. For both the predictive simulation model and OpenSim model, the center of the coordinate system is halfway between the feet. For both models, the Y axes are coincident, But the Z and X axes of the OpenSim model are different from the predictive model, as shown in Figure 4.4. Therefore, the data for the X and Z axes of the predictive model are transformed for the OpenSim environment based on the right-hand rule.

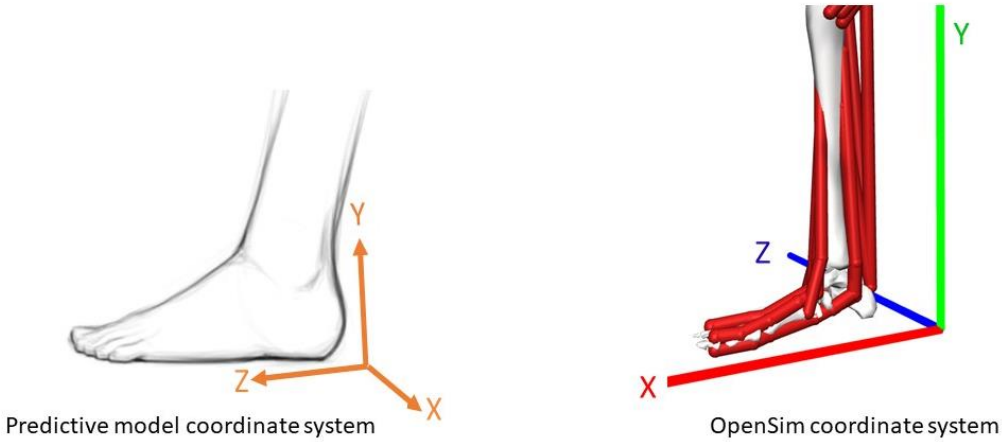

Figure 4.4: Comparison of coordinate systems between the predictive model and the OpenSim model

After the coordinate transformation, the input kinematics and kinetics are transferred to the OpenSim musculoskeletal model from the predictive skeletal model in a specific format using a motion (.mot) file. The joint angle name in both the motion file and in the OpenSim model should be identical to extract the kinematic data. GRFs and the external load on the hands are transcribed in the following sequence: magnitude of force, COP, and finally the ground reaction moment vector. Both GRFs, the external force, and the COP are expressed in the ground (laboratory) frame. GRFs are considered point forces applied to the calcaneus.

4.1.2.3. Inverse dynamics-based static optimization

Inverse dynamics-based static optimization is a widely popular method to estimate muscle forces. At first, in the inverse dynamics section, joint torques are calculated from the predicted kinematics and GRFs by solving the EOM (Eq. 4.9) of the body segment (Erdemir et al., 2007, Pandy, 2001).

$$\boldsymbol{\tau} = \mathbf{M}(\mathbf{q})\ddot{\mathbf{q}} + \mathbf{C}(\mathbf{q})\dot{\mathbf{q}} + \mathbf{G}(\mathbf{q}) + \mathbf{E}(\mathbf{q}, \dot{\mathbf{q}}) \tag{4.9}$$

Here, $\boldsymbol{\tau}$ is the muscular joint torque vector, $\mathbf{q}, \dot{\mathbf{q}}, \ddot{\mathbf{q}}$ are the joint angle, velocity, and acceleration vectors, respectively, $\mathbf{M}(\mathbf{q})$ is the system mass matrix, $\mathbf{C}(\mathbf{q})$ is the centrifugal and Coriolis force vector, $\mathbf{G}(\mathbf{q})$ is the gravitational loading vector, and $\mathbf{E}(\mathbf{q}, \dot{\mathbf{q}})$ is the external force vector. At this stage, muscle forces are not included. This redundant system is then solved at each time instant by minimizing an objective function subject to an equilibrium constraint where the sum of the individual muscle moments is equal to the calculated joint torques from inverse dynamics.

The static optimization tool in OpenSim is used to find individual muscle activations at each time instant. To find the optimal muscle activation, static optimization considers minimization of muscle activations as the objective function, and subject to muscle-torque equilibrium constraint. The joint torques are obtained from EOM by plugging in the given input data from the skeletal model.

$$\begin{aligned} &\boldsymbol{Find}: \ a_m \\ &\boldsymbol{minimize} \ \ J = \sum_{m=1}^{n} (a_m)^p \\ &\boldsymbol{subject\ to}: \ \sum_{m=1}^{n} [a_m f(F_m^0, l_m, v_m)] r_{m,j} = \tau_j \end{aligned} \tag{4.10}$$

where n is the number of muscles in the model, a_m is the activation level of muscle m at a discrete time step, F_m^0 is the maximum isometric force, l_m is muscle length, v_m is velocity, $f(F_m^0, l_m, v_m)$ is the muscle force-length-velocity surface, $r_{m,j}$ is its moment arm about the jth joint axis, τ_j is the generalized force acting about the jth joint axis, and p is a user-defined constant. Here, p is 2.

4.1.2.4. Joint reaction force analysis

The joint reaction load (force and moment) represents the sum of contact forces between two consecutive bodies. It is calculated by solving the Newton-Euler equations where all the translational and rotational dynamics of a body are presented. The Newton-Euler equation for estimating the lumbosacral (L5-S1) joint reaction load is

$$\mathbf{R_{SL}} = [\mathbf{M}]_5(\mathbf{q_5})\,\ddot{\mathbf{q}}_5 - [\sum \mathbf{F_m} + \mathbf{F_g}(\mathbf{q_5}) + \mathbf{R_{45}}] \quad (4.11)$$

where $[\mathbf{M}]_5(\mathbf{q_5})$ is the 6×6 mass matrix of L5 vertebra, $\mathbf{q_5}$ is the vector of linear and angular displacement of the L5 vertebra, $\ddot{\mathbf{q}}_5$ is the vector of the linear and angular accelerations of the L5 vertebra, $\mathbf{F_m}$ are the required muscle forces and moments to follow the given kinematics, $\mathbf{F_g}(\mathbf{q_5})$ is the gravitational loading, $\mathbf{R_{45}}$ is the L4-L5 vertebral joint reaction force and moment which can be found from similar step for upper bodies, and $\mathbf{R_{SL}}$ is the lumbosacral (L5-S1) joint reaction force and moment. $\mathbf{R_c}$ and $\mathbf{R_s}$ are the compressive and shear forces on the lumbosacral (L5-S1) joint in Figure 4.5.

The compressive and shear forces of the lumbosacral (L5-S1) joint are calculated using the joint reaction analysis tool in OpenSim. Joint reaction analysis is a post-processing procedure that uses the muscle forces generated from static optimization, and joint

kinematics from the skeletal model to calculate the joint reaction forces and moments. Details of the OpenSim joint reaction analysis tool are discussed in Steele et al. (2012).

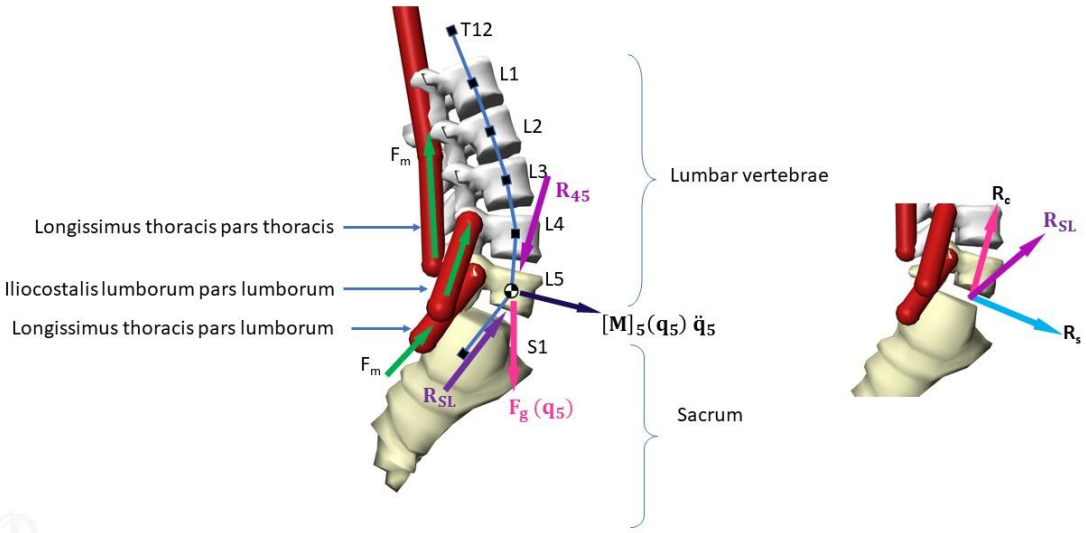

Figure 4.5: Joint reaction force analysis (simplified L5-S1 joint reaction force calculation)

4.2. Injury analysis:

As *in-vivo injury* assessment is not a feasible solution to manual material handling, simulation-based injury assessment has become popular for the last few decades. We will assess the injury based on three criteria.

1. Joint torque injury analysis
2. Muscle activation injury analysis
3. Spine joint injury analysis based on joint reaction forces.

4.2.1 Joint torque injury analysis

Joint torques show the combined effect of internal body forces such as ligaments, joint constraints, and muscle-tendon forces. As joint torque is the output of multiple physiological parameters, it can be an effective measurement for injury analysis. For joint space injury analysis, we are using the ratio of joint torque and dynamic joint strength limit, which is defined as the Joint torque injury index (I^{τ}).

$$I_i^{\tau} = \frac{\tau_i}{\tau_i^D} \tag{4.12}$$

where I_i^{τ} is the joint-torque-injury index of i-th joint, τ_i is the predicted joint torque of the i-th joint, and τ_i^D is the dynamic joint strength which has upper bound and lower bound. Details about dynamic joint strength are discussed in Section 2.3. τ_i^D is equal to its lower bound when τ_i is negative and τ_i^D is equal to its upper bound when τ_i is positive.

4.2.2 Muscle activation injury analysis

The relation between the rate of change of muscle activation and muscle excitation can be expressed using first-order differential equation-

$$\frac{da}{dt} = \frac{u-a}{\tau(a,u)} \tag{4.13}$$

where a is the muscle activations, u is the muscle excitations, $\tau(a,u)$ is a time constant that varies with activation level (Thelen et al.,2003). The muscle activation and excitation signal are allowed to vary from 0 (no contraction/excitation) to 1 (full contraction/excitation). The minimum activation level is set to 0.0 in OpenSim to avoid

any singularity. The risk of muscle activation injury increases as the activation of a muscle goes closer to 1 for a period of time.

4.2.3 Spine joint injury analysis based on joint reaction forces

Moderate joint reaction forces may improve joint health (Roos and Dahlberg,2005), but overuse and disuse can result in cartilage degradation which leads to Osteoarthritis (OA) (Sun, 2010). According to the Center for Disease Control and Prevention (CDC), over 32.5 million US adults are affected by OA during 2013-2015 (Barbour et al., 2017, CDC, 2018), and by 2040, about 78 million US adults are projected to have doctor-diagnosed arthritis (Hootman et al., 2016).

Spine osteoarthritic is a significant source of chronic back pain (Lindsey and Dydyk, 2020). To avoid spine injury, the NIOSH recommended action limit is 3400 N (350 kg), and the maximum permissible limit is 6400 N (650 kg) for compressive force on L5-S1 (NIOSH Technical report, 1981). The recommended shear force limit for occasional lifting task (≤100 loading/day) is 1000 N and for repetitive lifting task (100-1000 loadings/day) is 700 N (Gallagher and Marras, 2012, McGill et al., 1998).

According to NIOSH guidelines (NIOSH Technical report, 1981), if the compression force is below the action limit (3400 N), it represents nominal risk. If the compressive force is between the action limit (3400 N) and the maximum permissible limit (6400 N), the lifting is not acceptable without administrative or engineering controls. For compression force above the maximum permission limit (6400 N), the lifting task is not acceptable and has a high risk of injury, and it requires engineering controls.

4.3 Lifting experiment

The sole test subject was a healthy 31-year-old male, 1.69 m tall, with a mass of 63.5 kg. The experimental procedure was approved by the Institutional Review Board of Texas Tech University, and the subject gave written informed consent. A motion capture system consisting of 8 overhead Eagle-4 cameras (Motion Analysis Corp., Santa Rosa, California, USA) tracked 58 ¾-inch-diameter retroreflective markers attached to anatomical landmarks on the subject's person at 100 Hz. A pair of Bertec force plates (Bertec, Columbus, Ohio, USA) were used to record ground reaction forces and moments at 2,500 Hz. 14 Delsys Trigno sensors (Delsys Inc., Natick, Massachusetts, USA) attached to the subject (Criswell, 2011) measured the EMG activity of 6 muscles (vastus lateralis, vastus medialis, biceps femoris, gluteus medius, gluteus maximus, and latissimus dorsi) bilaterally, also at 2,500 Hz. First, EMG activities corresponding to maximum-voluntary-contractions (MVCs) for all 12 muscles were obtained by having the subject perform three 3-second maximal contractions (Criswell, 2011) for each muscle separated by 60-second rest periods. The lifting tasks were started 30 minutes after the last MVC. The objective for each lifting task was to lift one of two wooden boxes from the floor in front of the subject onto a platform of a fixed height. The subject was instructed to adopt a semi-squat lifting strategy in which they would enter a partial squat, grab the box and switch to back lifting, and then rise from the squat while lifting the box. This would avoid using either the lower back muscles or the knee extensors at the extremes of their ranges of motion. Both boxes were identical, measured 0.305 m × 0.238 m × 0.127 m, and had cutouts on the smallest sides for gripping securely. One was loaded to bring its total mass to 7 kg, and the other was loaded to a total mass of 12 kg. The box to be lifted would be positioned 0.033

m away from the forward edge of the force plates each time. The platform onto which it would be lifted was 0.9 m above the top of the force plates, and 0.305 m in front of them. Figure 4.6 shows a T-pose in the experimental setup for symmetric lifting.

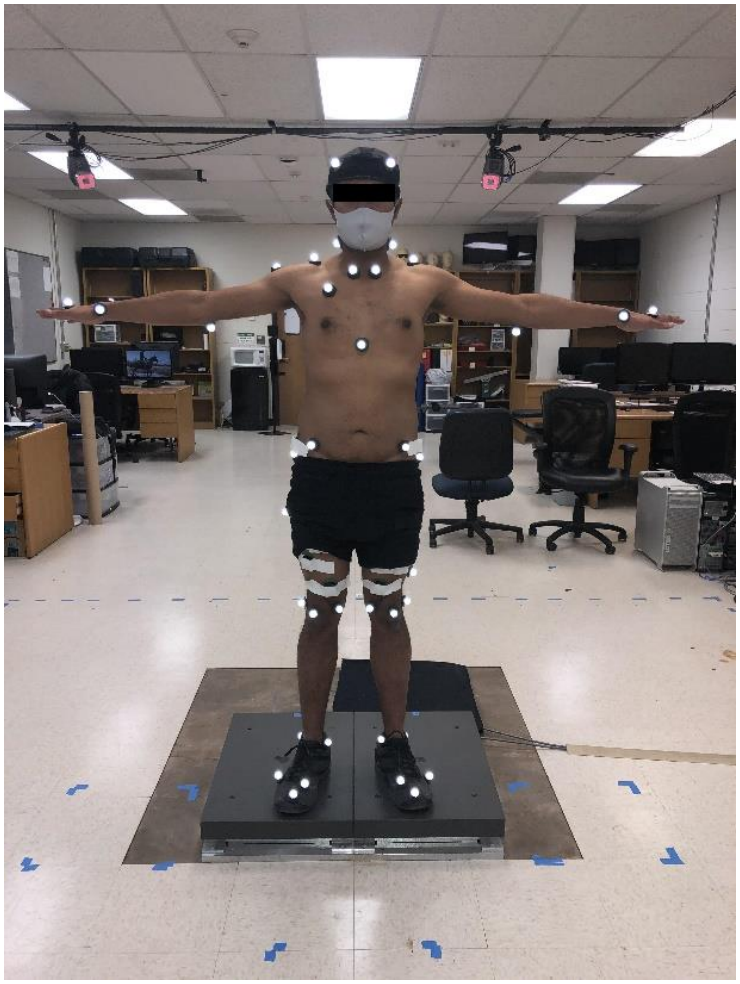

Figure 4.6: Experimental setup

We collected EMG data for five muscles from the lower extremity and one muscle from the upper extremity. For the lower extremity, we took one muscle from the hamstring, two muscles from the quadriceps femoris, and two muscles from the gluteal muscles. The hamstring muscle is biceps femoris, the quadriceps femoris muscles are vastus lateralis and

vastus medialis, the gluteal muscles are gluteus maximus and gluteus medius (Figure 4.7). For the upper extremity, we took latissimi dorsi, the largest muscle in the upper body (Figure 4.8).

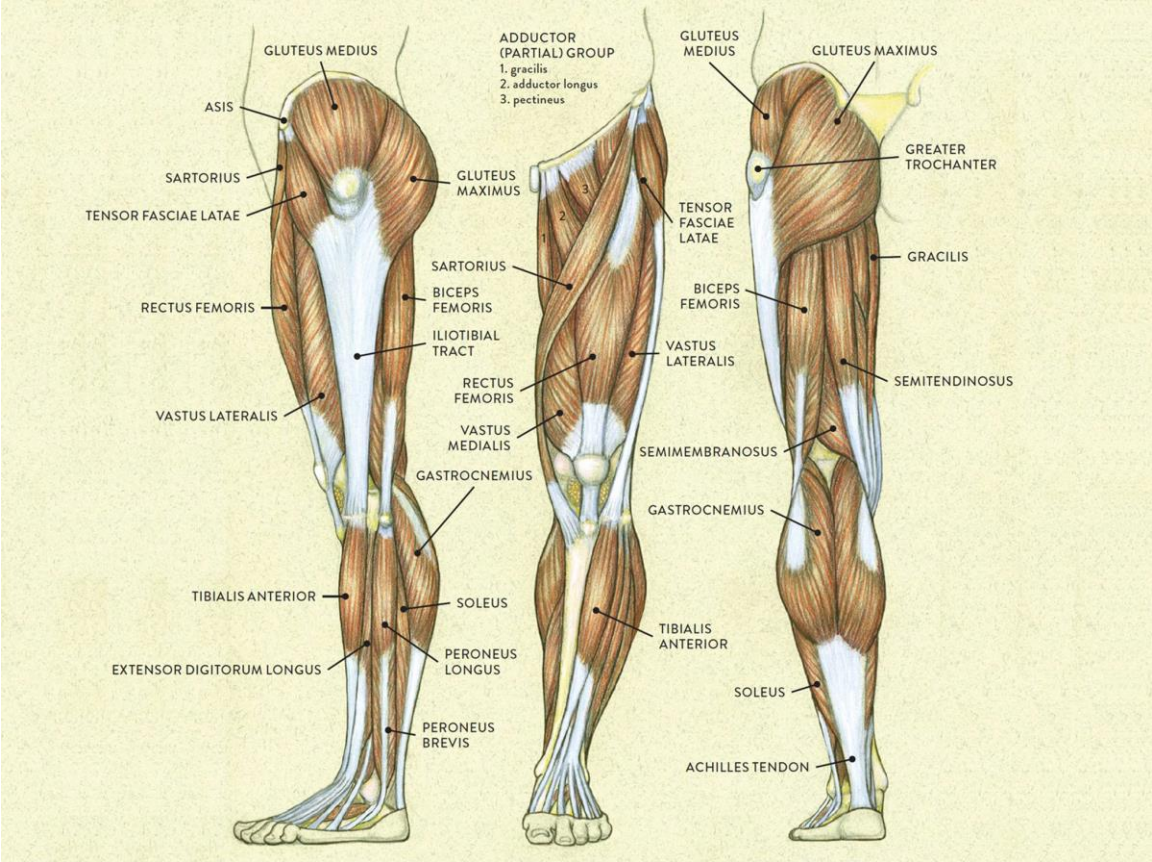

Figure 4.7: Leg muscles (“Classic Human Anatomy in Motion”, n.d.)

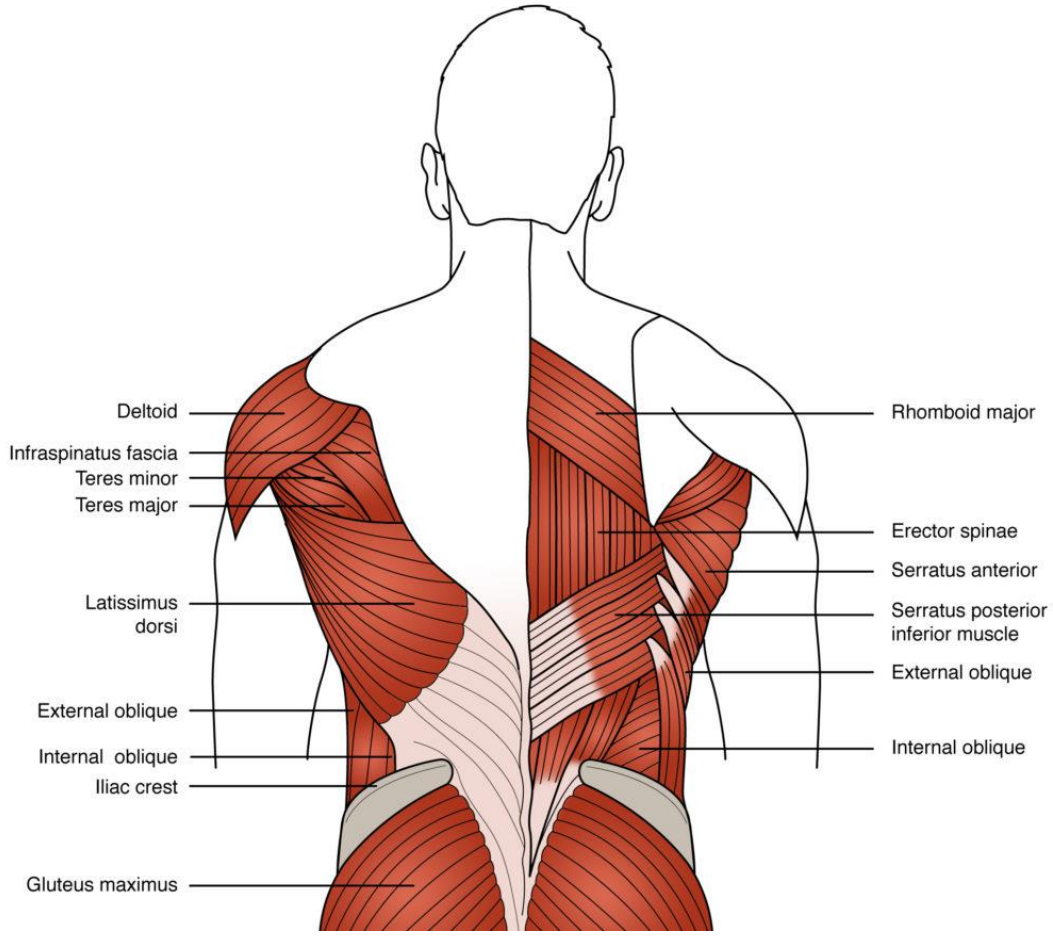

Figure 4.8: Spine muscles (Filley, 2020)

After all data collection was done, data analysis was carried out. Motion capture data was labeled, cleaned up, and smoothed in Cortex 6.2 (Motion Analysis Corp., Santa Rosa, California, USA) and further processed along with EMG and force plate data in Visual3D v6. EMG data for the lifting tasks was bandpass filtered with a passband of 10 Hz-450 Hz, rectified, and then lowpass filtered with a cutoff frequency of 5 Hz before being normalized by the respective MVC EMG readings. Force plate data were lowpass filtered with a cutoff frequency of 6 Hz. The start of the data was marked by the first frame in which the velocity of the box increased from rest in the upward direction, and the end was marked by the

frame in which the box vertical position reached its first local maximum after lifting started. Joint angles projected onto the sagittal plane for joints on the left and right sides of the body were averaged, and contributions to ground reaction forces and moments from each side were summed.

4.4. Results

We solved the nonlinear optimization problem for the predictive skeletal model. The computational platform was an Intel Xeon E-2186G 3.80 GHz CPU desktop computer. The given experimental box weights for symmetric lifting were 7 kg and 12 kg. It took 0.48 seconds and 0.62 seconds of CPU time using SNOPT (Gill et al., 2005) to solve, respectively, the 7 kg box and 12 kg box lifting problems. Snapshots of the two box lifting motions are shown in Figure 4.9, and the joint angle predictions are contrasted with the experimental data for the 7 kg lifting and the 12 kg lifting in Figure 4.10 and Figure 4.11, respectively. Comparisons of vertical GRF for the two liftings are shown in Figure 4.12. Comparisons of joint torques with dynamic joint strength limits and static joint strength limits for 12 kg box lifting are shown in Figure 4.13. The comparisons of muscle activation with EMG are shown in Figure 4.14 and Figure 4.15 for the 7 kg box and 12 kg box, respectively. Generated forces for two spinal muscles (multifidus spinous process and right longissimus thoracis) for the two lifting motions are shown in Figure 4.16. The lumbosacral (L5-S1) joint reaction forces for both lifting trials are presented in Figure 4.17. The joint torque injury index throughout the lifting task is shown in Figure 4.18.

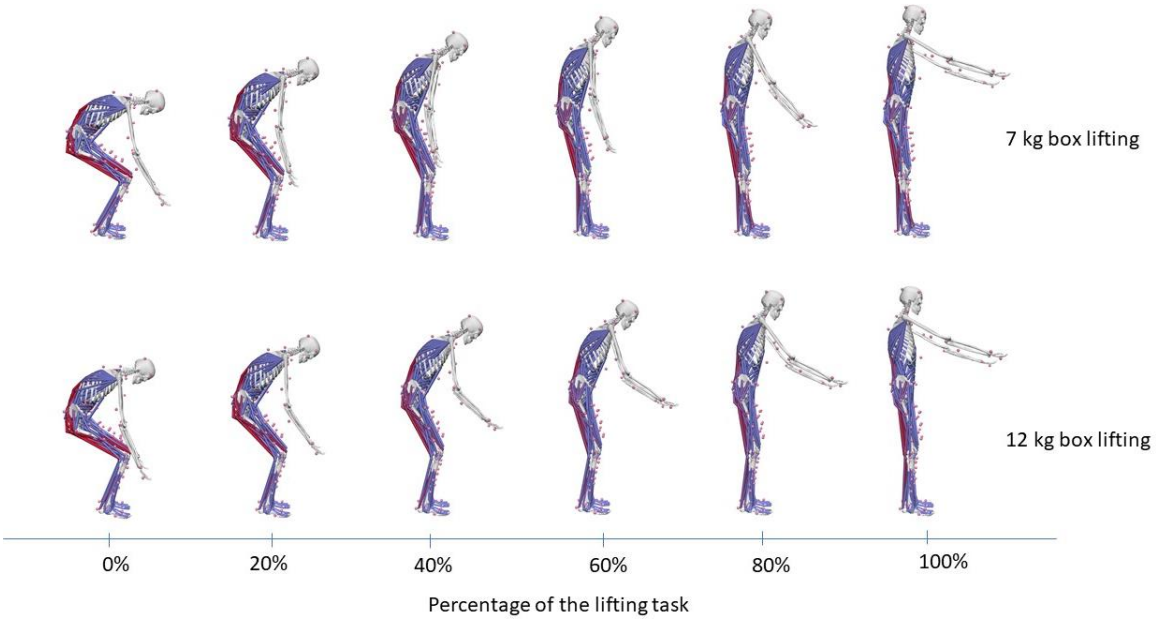

Figure 4.9: Snapshot of OpenSim lifting for 7 kg and 12 kg boxes

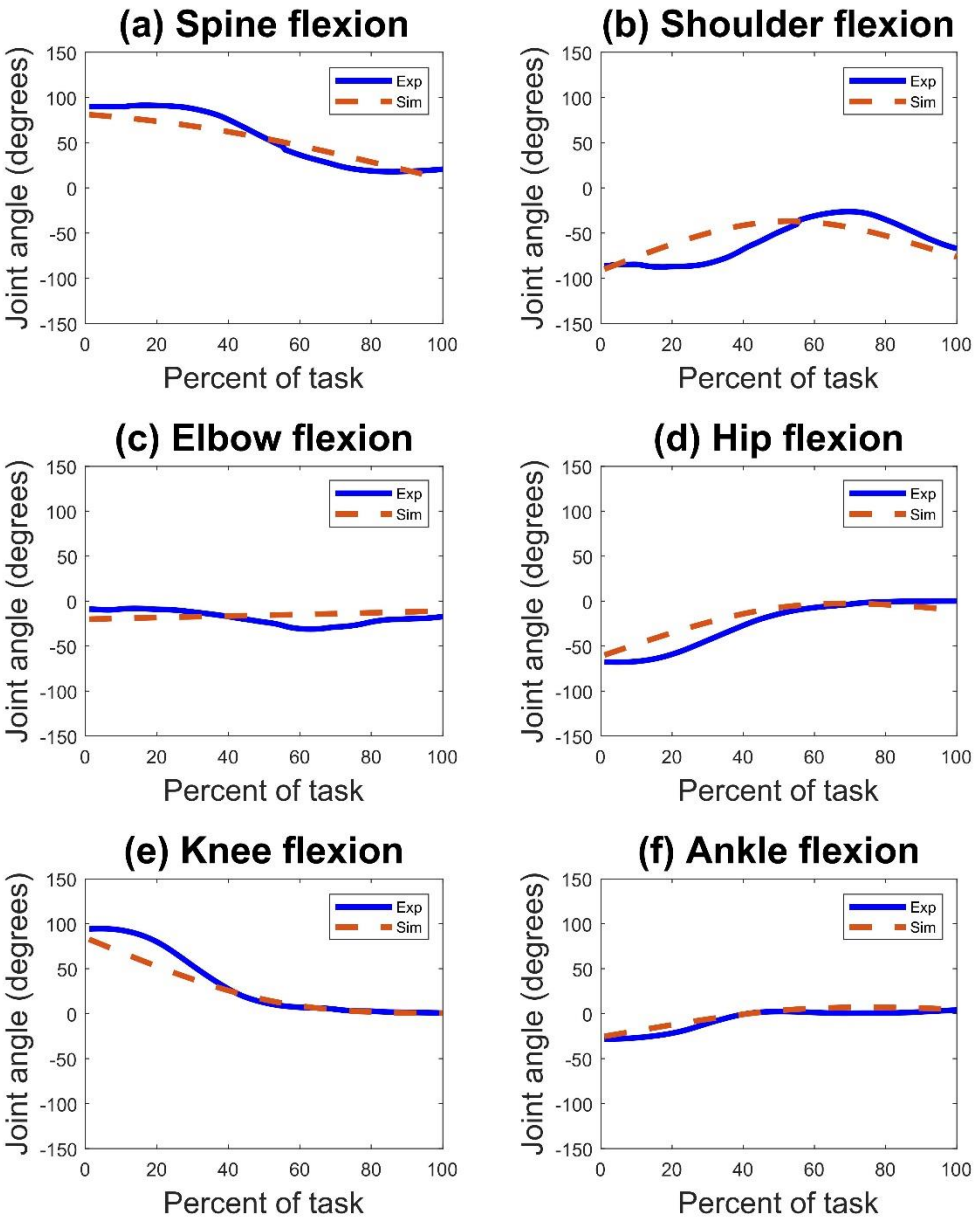

Figure 4.10: Comparison of experimental and predicted joint angles for 7 kg box

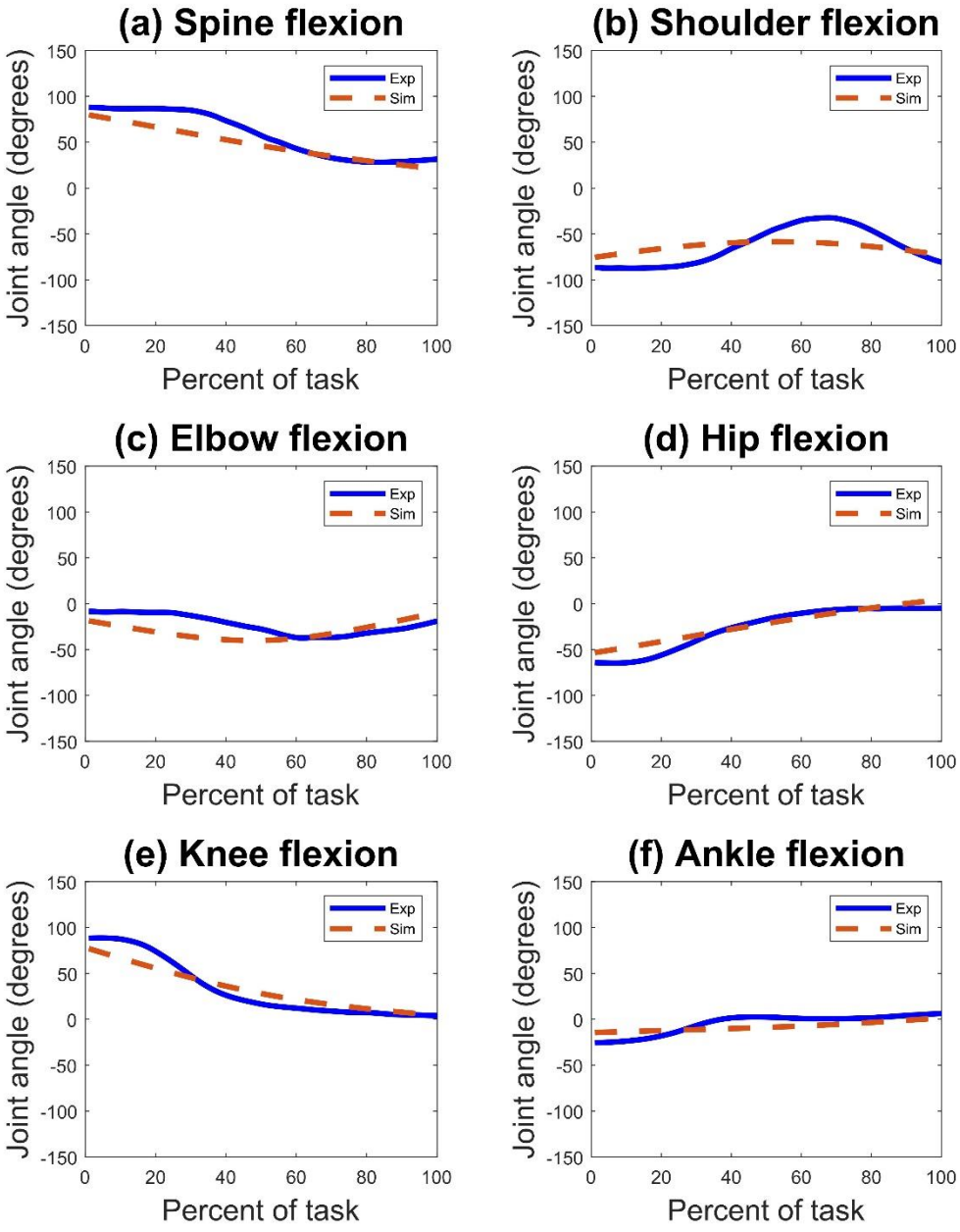

Figure 4.11. Comparison of experimental and predicted joint angles for 12 kg box

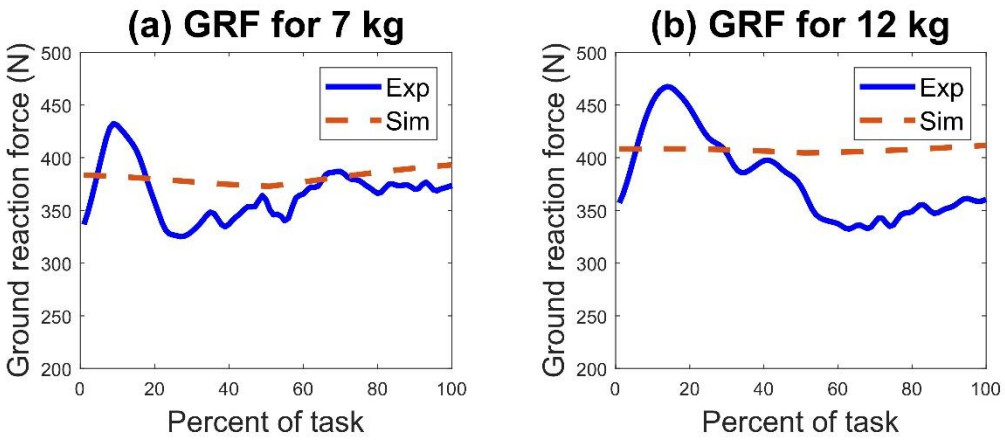

Figure 4.12: Comparison of experimental and predicted GRFs for 7 kg and 12 kg boxes

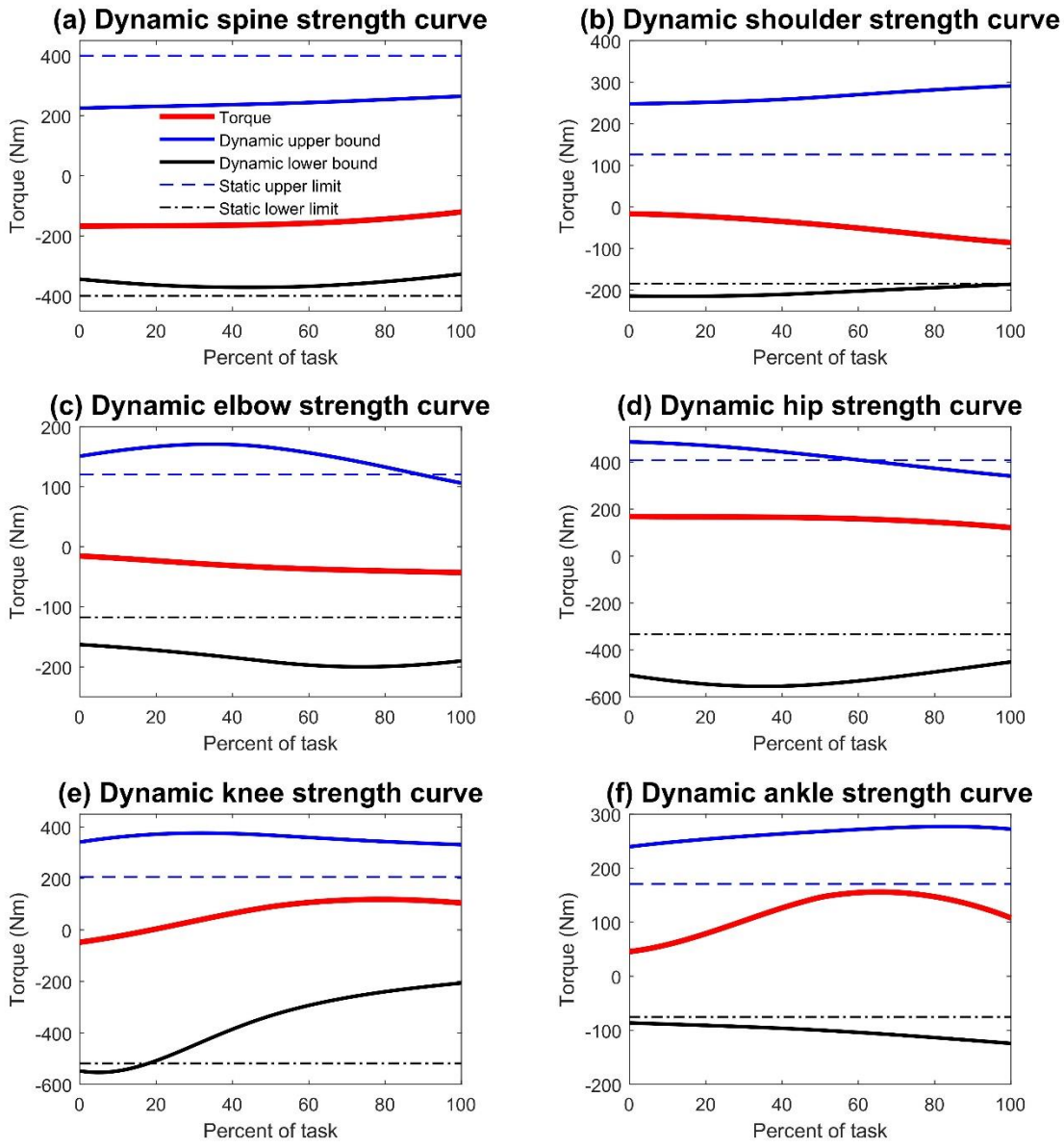

Figure 4.13: Comparison of joint torque profiles with dynamic joint strength limits and static joint strength limits for 12 kg box

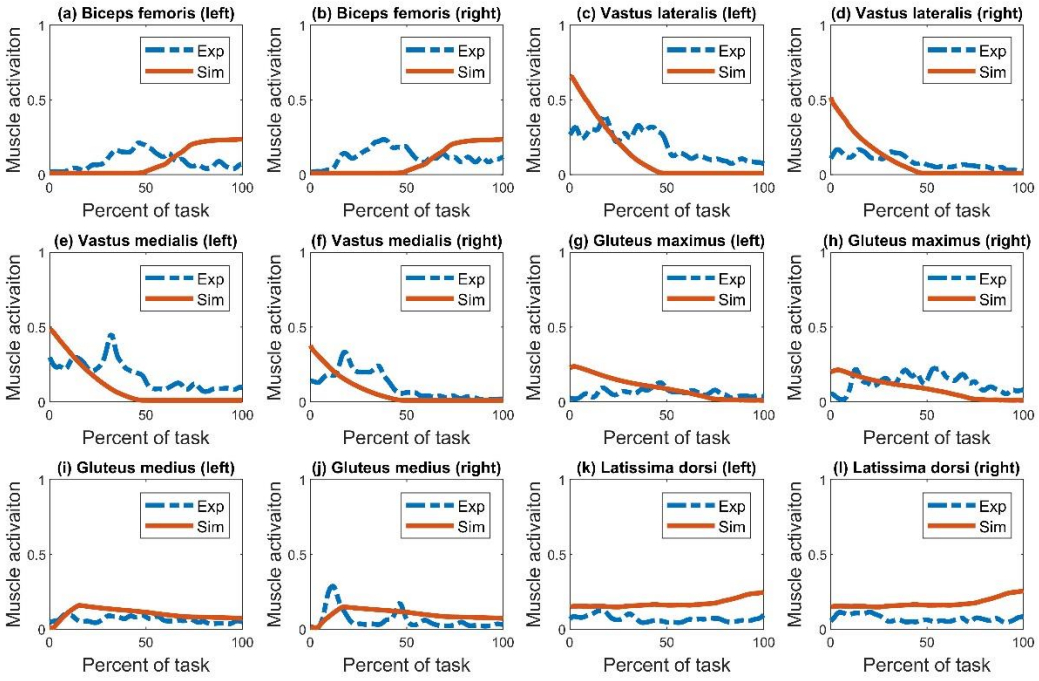

Figure 4.14: Comparison of EMG and muscle activations for 7 kg box

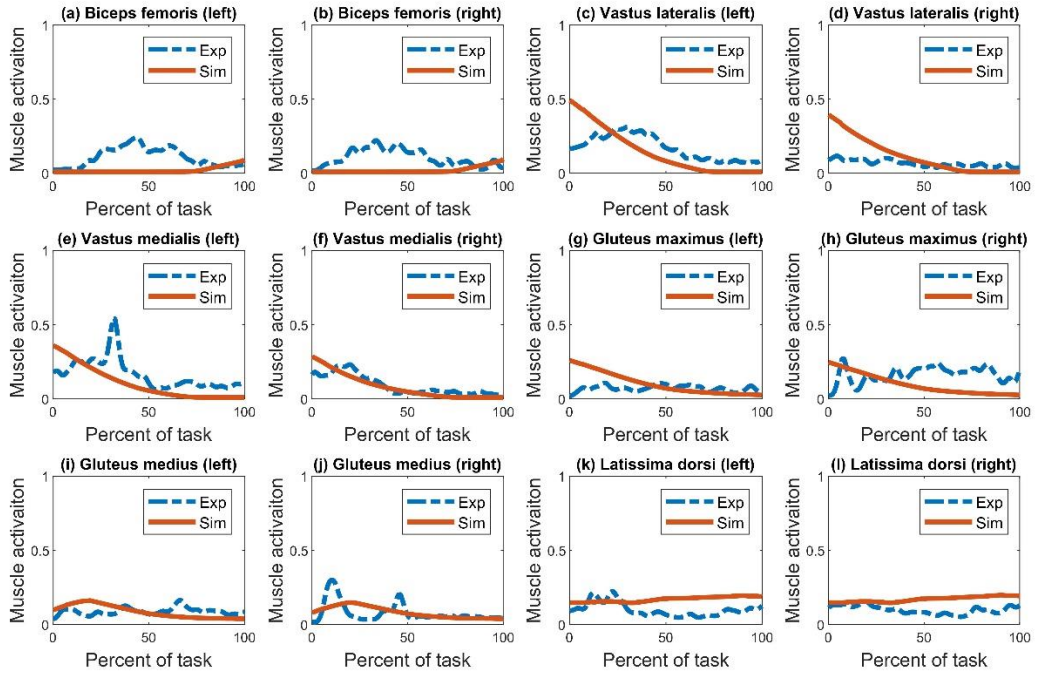

Figure 4.15: Comparison of EMG and muscle activations for 12 kg box

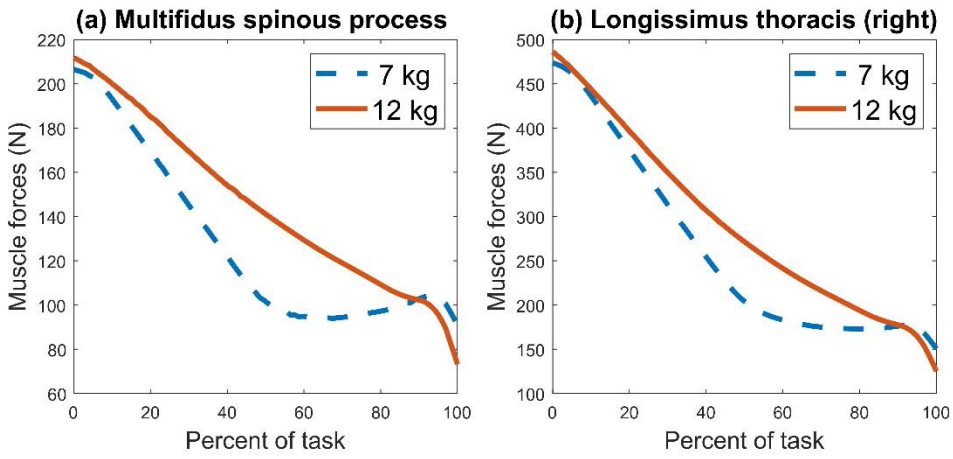

Figure 4.16. Spine muscle forces for 7 kg and 12 kg boxes

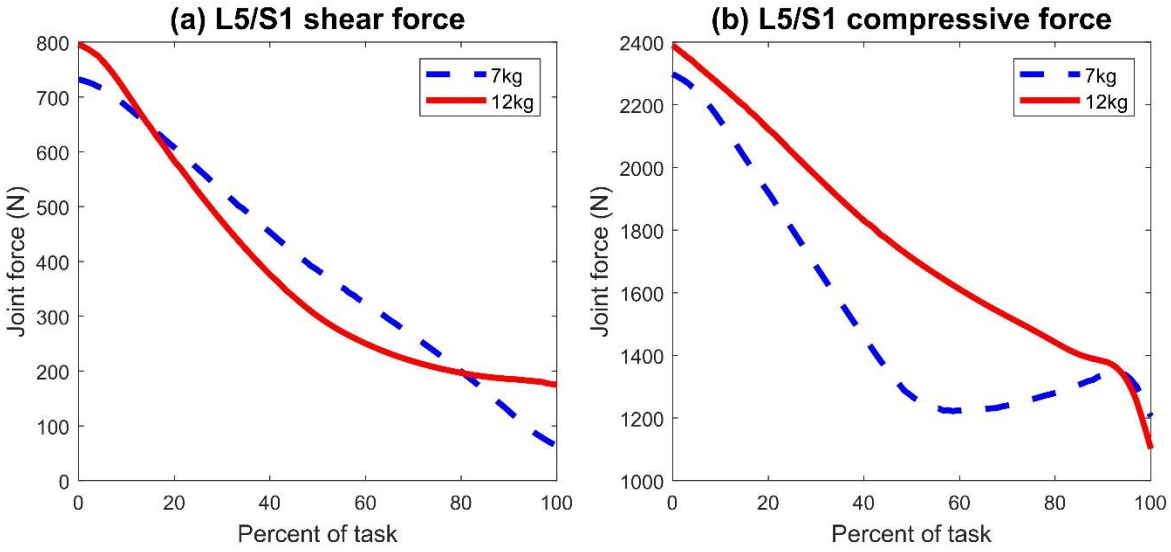

Figure 4.17: Lumbosacral (L5-S1) joint shear and compression forces

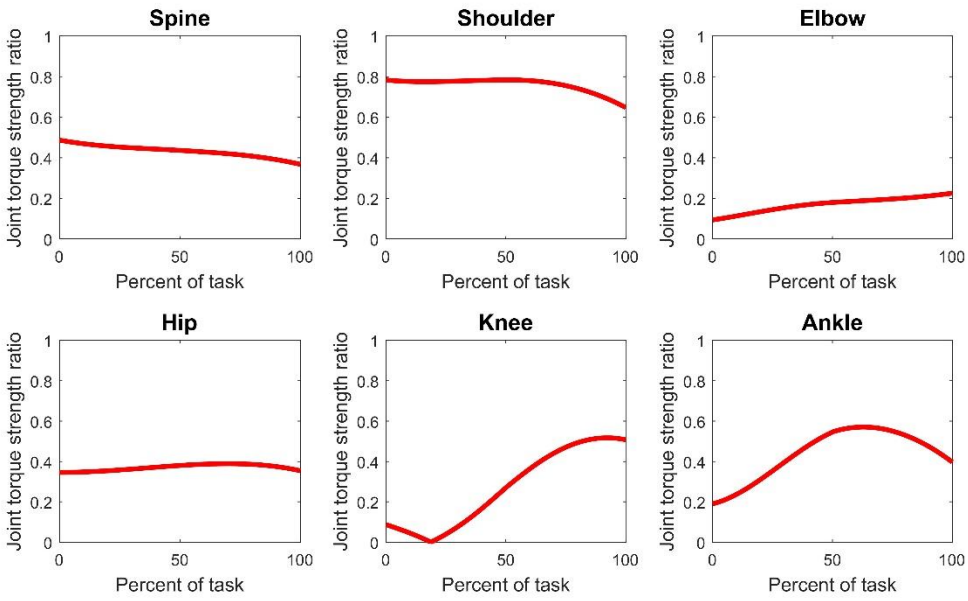

Figure 4.18: Joint torque injury index throughout the lifting task

4.5. Discussions

Six predicted joint angle profiles (spine, shoulder, elbow, hip, knee, and ankle) are compared with experimental data in Figure 4.10 and Figure 4.11. The pattern and phase change of the predicted joint angle profiles agree well with the experimental joint angle profiles. In Figure 4.12, there are some discrepancies between the predicted and experimental GRFs. The experimental GRF is higher than the predicted GRF for more than 50 N at 10% of the lifting task, for both 7 kg and 12 kg boxes. Except that, the predicted GRFs were within 15% of the experimental GRF profile. All the predicted joint torque profiles are within the dynamic joint strength limits for 12 kg box load (Figure 4.13). From Figure 4.18, we can see that the joint torques injury index was between 0.4 to 0.5 for the spine joint from the beginning of the lifting to 80% of the lifting task. The joint torque injury index for the shoulder joint was 0.6 to 0.8 throughout the lifting task. The joint torque

injury index was higher than 0.4 after 60% of the lifting task for the knee, and after 30% of the lifting task for the ankle.

For muscle activation comparison (Figure 4.14 and Figure 4.15), we compare five muscles from the lower extremity and one muscle from the upper extremity. There are some discrepancies between the predicted muscle activation and EMG data for the biceps femoris (Figure 4.14a, b, and Figure 4.15a, b). For the left and right biceps femoris, the timings of the phase changes are different. For both 7 kg box and 12 kg box liftings, the peak muscle activations of left and right biceps femoris are around 80-100% of the lifting task, whereas the peak values are around 30-50% of the lifting task for EMG data (Figure 4.14a, b, and Figure 4.15a, b). The initial predicted muscle activations for the vastus lateralis are higher than the experimental activations, but the trends of the predicted muscle activations are similar to those of the experimental EMG data (Figure 4.14c, d, and Figure 4.15c, d). For the rest of the muscles, the predicted activations agree well with the experimental activation for both 7 kg box and 12 kg box liftings.

The peak muscle force for multifidus spinous process is 212 N for 12 kg box at 88-degree spine joint angle and 206 N for 7 kg at 81-degree spine joint angle (Figure 4.16a). The peak muscle force for longissimus thoracis pars thoracis is 486 N for 12 kg and 473 N for 7 kg (Figure 4.16b). The peak positions for 12 kg and 7 kg are similar to multifidus spinous peak muscle force positions.

The peak forward shear force for L5-S1 is 796 N (12.6 N/kg: force/subject-weight) for 12 kg and 732 N (11.6 N/kg) for 7 kg box (Figure 4.17a). The peak compression force for L5-S1 is 2390 N (38 N/kg) for 12 kg and 2298 N (36.5 N/kg) for 7 kg (Figure 4.17b). The joint

angle positions for peak forces for forward shear and compression forces are similar to multifidus peak muscle force positions.

Table 4. 1: Studies of L5-S1 compression and forward shear forces for squat lifting

Reference	Subject weight (kg)	Lifting load (kg)	Peak compressive force (N) & (N/kg)	Peak forward shear force (N)
Kim and Zhang (2017)	73.1±8.7 kg	7 kg	3600 N (44-56 N/kg) *	730 N (8.9-11.3 N/kg) *
		12 kg	4200 N (51.3-64.2 N/kg) *	900 N (11-14 N /kg) *
Beaucage-Gauvreau et al. (2019)	81.6±3.8 kg	15 kg	4190-4700 N * (55-65 N/kg)	12-26 N/kg
Kingma et al. (2006)	68.7 kg	20 kg	3900 -6700 N (56.7-97.5 N/kg) **	1200-1700 N (17.5- 24.7 N/kg) *
Kingma et al. (2016)	70.9 kg	0 kg	2800 N (39.5 N/kg)	800 N (11.2 N/kg)
		15 kg	3600 N (50.8 N/kg)	1300 N (18.3 N/kg)
Rajaee et al. (2015)	68.4 kg	19.8 kg	2348- 3245N (34.32- 47.44 N/kg) *	308-1171 N (4.5 -17.12 N/kg) *
Bazrgari et al. (2007)	74±11 kg	0 kg	1900 N (22 - 30 N/kg) *	800 N (9.4 - 12.7 N/kg)
		18.3 kg	3600 N (42.3 -57.14 N/kg) *	1300 N (15.3 – 20.6 N/kg)
Hybrid model	63 kg	7 kg	2300 N (36.5 N/kg)	720 N (11.4 N/kg)
		12 kg	2400 N (38.1 N/kg)	800 N (12.6 N/kg)

N.B.: Normalized to body mass (N/kg), * = approximate, ** = depending on box size

From Figure 4.17 and Table 4.1, we can see that the predicted compressive and forward shear forces of L5-S1 agree well with (Bazrgari et al., 2007) and (Rajaee et al., 2015) but are lower than (Beaucage-Gauvreau et al., 2019, Kim and Zhang, 2017, Kingma et al., 2006, Kingma et al., 2016). It was reported that the compressive and shear forces varied with the height and weight of the subject, box weight and size, distance between the box and L5-S1 (Kingma et al., 2006), lifting techniques, lifting analysis tools (Rajaee et al., 2015), lifting speed (Bazrgari et al., 2007), etc. As the hybrid model tries to find the optimal lifting strategy by reducing the square of the joint torque, the simulated joint reaction forces

are lower than some experimental lifting motions (Beaucage-Gauvreau et al., 2019, Kim and Zhang, 2017). This hybrid model will help find the best lifting practice to avoid low back injuries.

Considering the subject's height, weight, box size, and distance between the box and body, the predicted L5-S1 joint compression forces for both 7 kg and 12 kg are within the expected limit and below the NIOSH action limit, as discussed in Section 4.2.3. The predicted L5-S1 joint shear forces for both the 7 kg box and 12 kg box are above the repetitive task limit but below the occasional lifting shear force limit. For a different lifting weight and box size, the lifting strategy, as well as compression and shear forces, may be changed for the same subject. Therefore, we should update the anthropometry of the subject, the lifting task, and box size along with other parameters in the simulation to get accurate results for low back injury analysis.

There are some limitations to this study. First, we did not consider the stance width in this work since our skeletal model is 2D. It has been observed that there are no significant differences in quadriceps muscles between the narrow and wide stance (Escamilla et al., 2001). There may be some changes for the gluteus medius muscles if the stance distance is changed. Secondly, due to the 2D skeletal model, we assume the left and right-side joint angle and strengths are symmetric, but they may not be symmetric even in symmetric lifting tasks. Thirdly, we did not consider any motion within the coronal plane like abduction and adduction movements or any medial or lateral rotations. We also did not consider any inversion-eversion movements of the foot. Finally, there is the possibility of errors arising during scaling of the model from the subject in OpenSim, which may lead to

the previously mentioned discrepancies for GRFs, muscle activations, and joint reaction forces.

4.6. Summary

In this study, we developed a novel hybrid model which gives us access to three-step injury analysis. First, it predicts human motion and joint torque using a skeletal model, which can be used to evaluate any potential injury in joint space for the lifting task. Then, it can assess the muscle activations/forces to determine which muscles, if any, are at risk. Finally, it can evaluate joint reaction forces to check the pressure on the intervertebral disc or load-bearing joints like the hip and the knee. The proposed hybrid model is both computationally efficient and generic, and it can be readily applied to other motions as well. The hybrid predictive musculoskeletal model has wide applications for workers' injury prevention to reduce the risk of musculoskeletal disorders.

CHAPTER V

HYBRID MODEL FOR ASYMMETRIC LIFTING PREDICTION

In an industrial setup, the combination of symmetric and asymmetric lifting tasks is common. Asymmetric lifting task requires spinal rotation and moment and the ZMP moves away from the sagittal plane. With the rotation of the spine, the upper extremity loads shifted from the large erector spinae muscles to the less capable oblique muscles. These varying loads play a crucial role in the investigation of low back injuries. It is important to carefully analyze the asymmetric lifting tasks for injury prevention.

The purposes of this chapter are to 1) deploy the hybrid model to predict asymmetric lifting motion and muscle activations, 2) study asymmetric lifting injuries using the hybrid predictive model, 3) compare symmetric and asymmetric lifting motions, muscle activations, and lumbar joint loads using the hybrid model.

5.1 Hybrid model for asymmetric lifting

The hybrid model for asymmetric lifting includes a 3D skeletal model and a 3D OpenSim musculoskeletal model. The 3D skeletal model predicts the joint torques, lifting motion,

and GRFs. The OpenSim musculoskeletal model estimates the muscle activations and joint reaction loads. Combining these data, the hybrid predictive model is able to predict asymmetric lifting injuries by following steps.

5.1.1 Predictive skeletal model

We used a 40-DOF 3D skeletal model for asymmetric lifting motion prediction. The model has six global DOFs including three global translations and three global rotations. In addition, the model has six DOFs for the spine, seven DOFs for each arm, and seven DOFs for each leg. The details of the 3D skeletal model are presented in chapter 3.1.

The relationships among the joints and links of the 3D model are expressed using the DH representation. The general EOM of the skeletal model is expressed using recursive Lagrangian formulation in matrix forms. It contains forward recursive kinematics and backward recursive dynamics. Details about the kinematics and dynamics equations of the 3D skeletal model can be found in chapter 3.2.

For 3D skeletal asymmetric lifting prediction, the design variables ($\mathbf{x}$) are cubic B-spline control points of joint angle profiles. The objective function $f(\mathbf{x})$ is the summation of normalized joint torque squares. The lifting task is formulated as a general nonlinear programming problem: find the optimal design variables $\mathbf{x}$ to minimize a human performance measurement, $f(\mathbf{x})$, subject to physical and task constraints including joint angle limits, dynamic joint torque limits, balance condition, foot contacting position, collision avoidance, initial and final hand positions, initial and final static conditions, initial, mid-time, and final postures, and GRF constraints. These constraints are same as

the 3D asymmetric lifting prediction in chapter 3.3 except for the GRF constraints which are defined as:

GRF constraints: Initial, intermediate, and final vertical GRFs are given from experimental data.

$$\left|GRF_{left}(\mathbf{x},t) - GRF^{E}_{left}(t)\right| \leq 50, \quad t = 0, \frac{T}{2}, T \tag{5.1a}$$

$$\left|GRF_{right}(\mathbf{x},t) - GRF^{E}_{right}(t)\right| \leq 50, \quad t = 0, \frac{T}{2}, T \tag{5.1b}$$

where GRF^{E}_{left}, GRF^{E}_{right} are the experimental vertical GRFs for left foot and right foot, respectively.

5.1.2 Musculoskeletal analysis module

The musculoskeletal analysis for asymmetric lifting is carried out in OpenSim. A modified full body-lumbar spine (FLBS) musculoskeletal model is used to analyze the asymmetric lifting motion using the hybrid predictive model. The musculoskeletal model has 30 DOFs, 21 segments, and 324 musculoskeletal actuators. The model was scaled according to the subject's anthropometry data. Details about the musculoskeletal module can be found in chapter 4.1.2.1: Musculoskeletal model.

Before importing the predicted joint angles, GRFs, and COP into the OpenSim, the coordinate system was transformed to match with each other's coordinate system. The static optimization tool in OpenSim is used to generate muscle activations and forces. The static optimization minimizes the muscle activations, subject to the muscle-torque

equilibrium constraints. The joint reaction analysis tool in OpenSim is used to calculate the compressive and shear joint reaction forces of the lumbosacral (L5-S1) spine joint.

5.1.3 Injury analysis

First, muscle activations are analyzed. The risk of muscle injury increases as the activation of a muscle is close to 1 for a long period. Secondly, the hybrid model assesses the lumbar spine compressive and shear forces by comparing them with the recommended data provided by NIOSH and literature.

5.2 Lifting experiment:

The subject for the lifting experiment was a 31-year-old male, 1.69m tall, and with a body mass of 63.5 kg. The experiment was approved by the IRB of Texas Tech University. The motion capture data was collected by 8 overhead cameras. The GRF data was collected using two force plates. The EMG activities were recorded using 14 EMG sensors. The procedure of the lifting experiment is similar to chapter 4.3 with the following changes:

1. The box weight is 7 kg
2. The subject was instructed to lift the box and put it on a table placed at the left side of the subject (Figure 5.1).

Figure 5.1: Asymmetric lifting experimental setup

5.3 Results

The nonlinear optimization problem is solved using an Intel(R) Core (TM) i7-8650U CPU @ 1.90GHz and 16 GB RAM laptop computer. It took 42.01 seconds CPU time for the SNOPT to find the optimal solution.

The snapshot of the predicted asymmetric lifting motion is presented in Figure 5.2(a). The snapshot of musculoskeletal lifting motion in OpenSim is presented in Figure 5.2(b). Figures 5.3 and 5.4 compare asymmetric lifting joint angle profiles between simulation and

experiment. Figure 5.5 compares asymmetric lifting vertical GRFs between simulation and experiment. The predicted left and right GRFs agree well with the experimental data.

Figure 5.6 compares simulated muscle activations with the experimental EMG data for asymmetric lifting. The blue dotted line represents the experimental EMG data for asymmetric lifting. The solid red line represents the predicted muscle activations for asymmetric lifting. The yellow dashed-dotted line represents the predicted muscle activations for symmetric lifting.

Figure 5.7 compares lumbar spine compressive and shear forces between symmetric and asymmetric liftings.

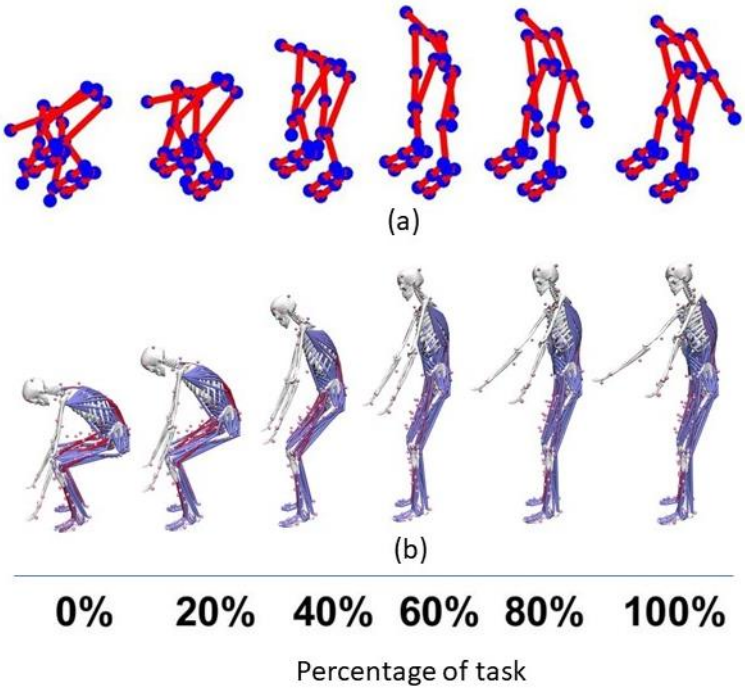

Figure 5.2: Snapshots of 7 kg asymmetric weight lifting motion (a) predictive skeletal lifting motion, (b) musculoskeletal lifting motion in OpenSim

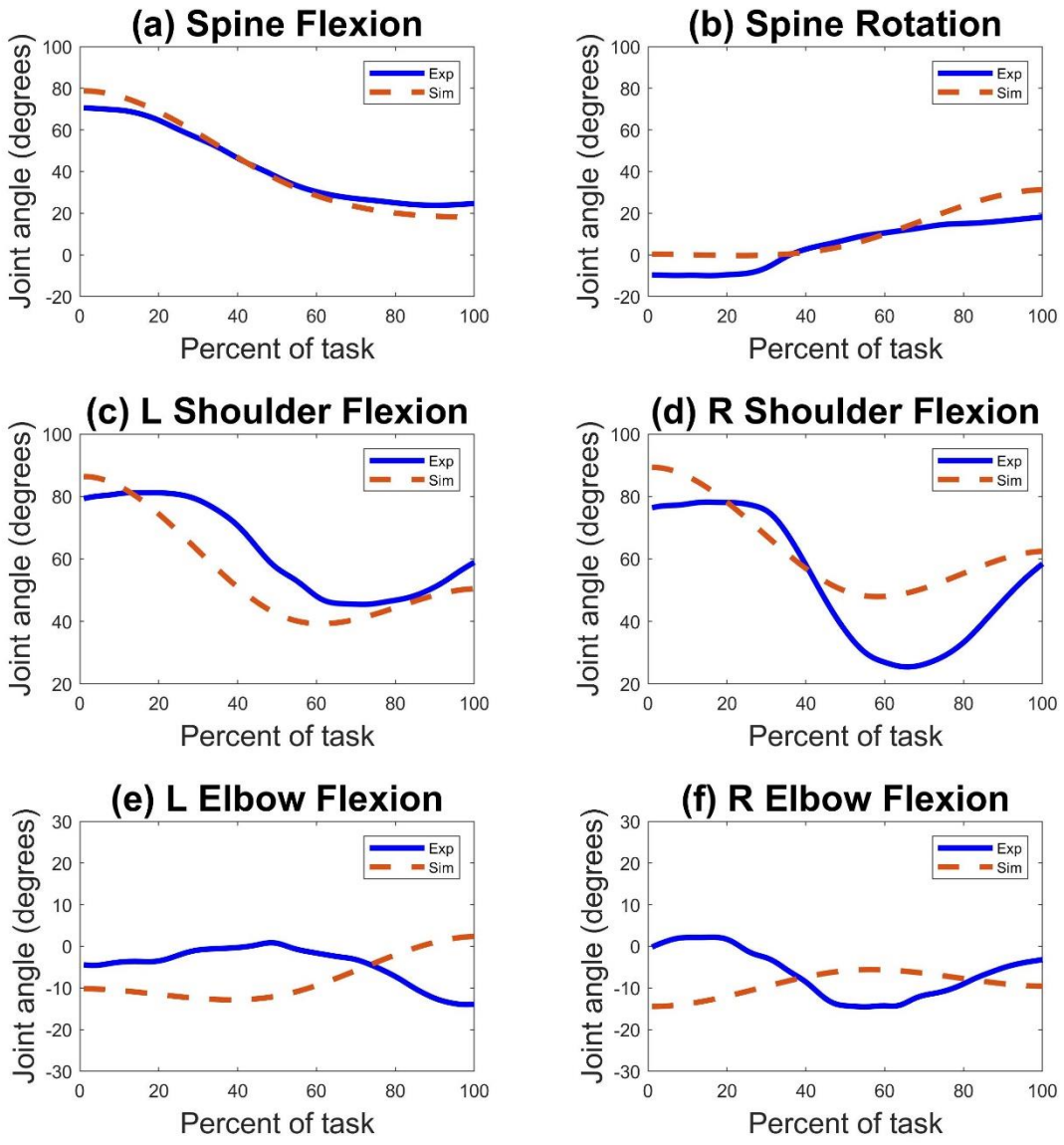

Figure 5.3: Upper body joint angles prediction and validation for asymmetric lifting

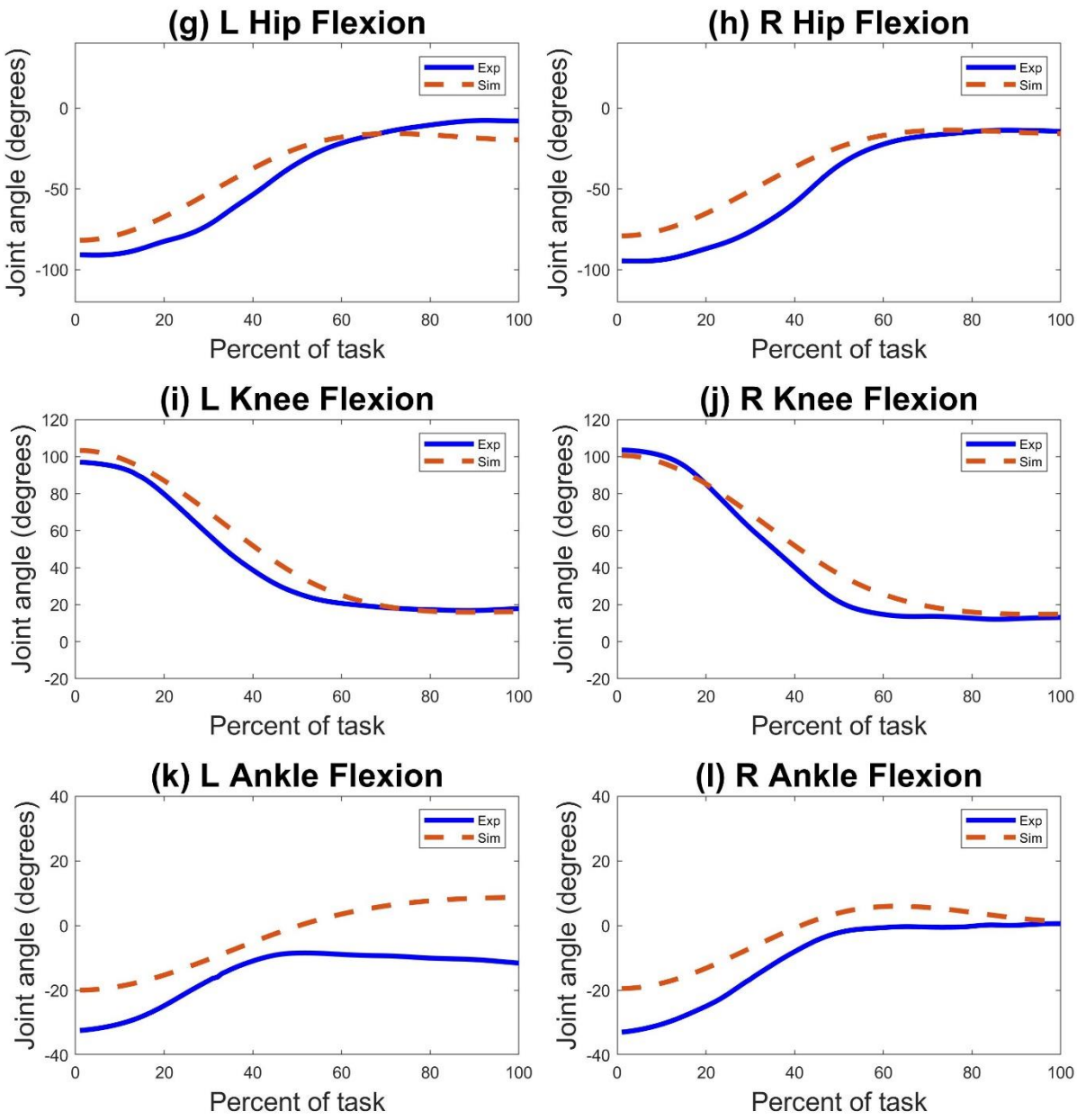

Figure 5.4: Lower body joint angles prediction and validation for asymmetric lifting

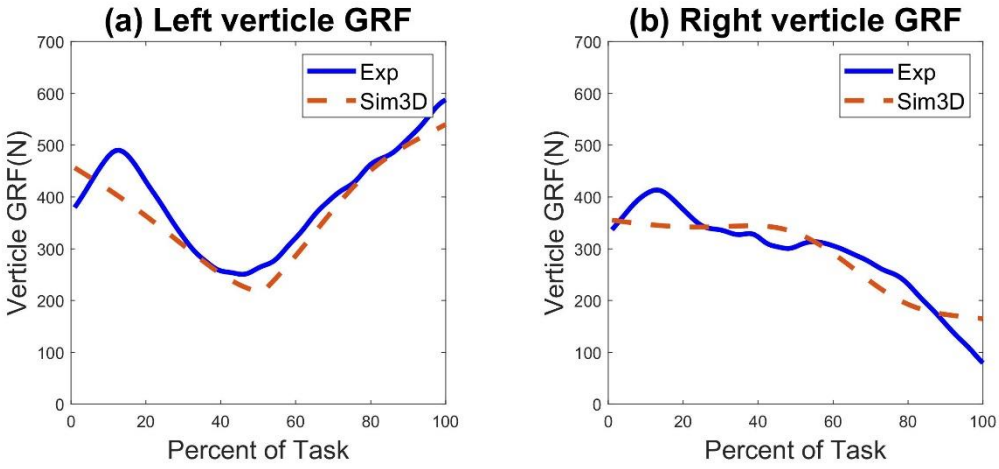

Figure 5.5: GRFs prediction and validation for asymmetric lifting

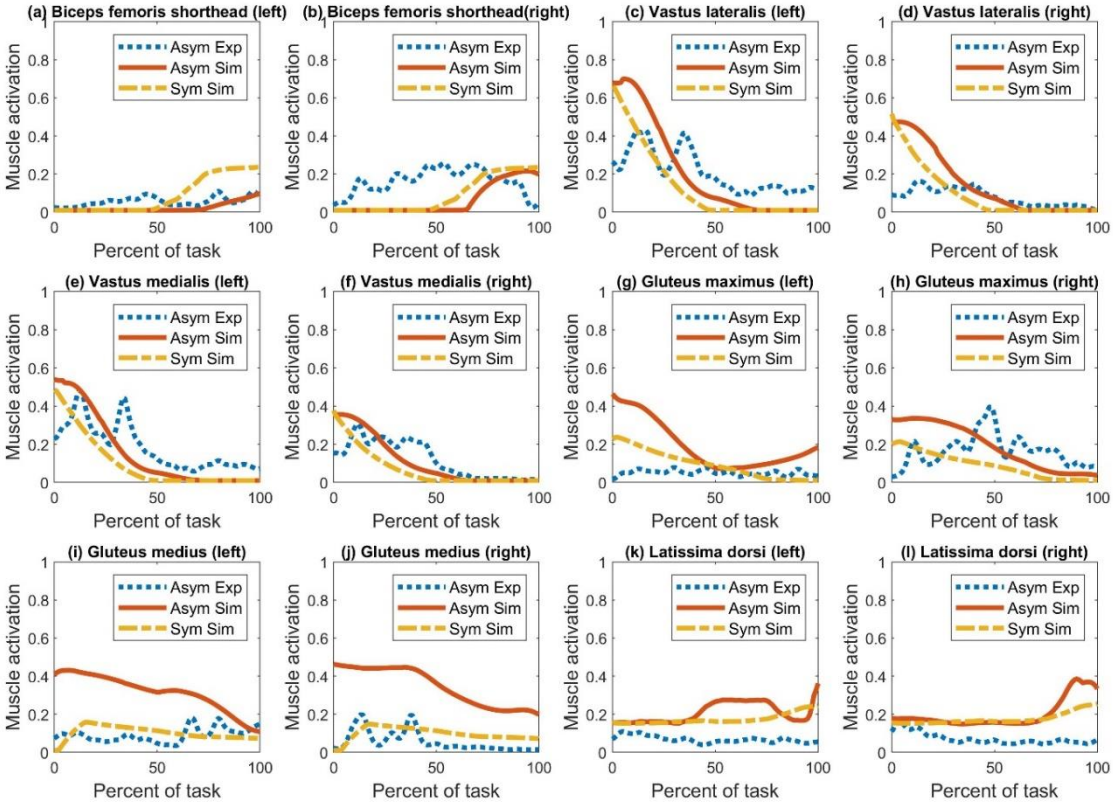

Figure 5.6: Muscle activations validation and comparisons between symmetric and asymmetric liftings

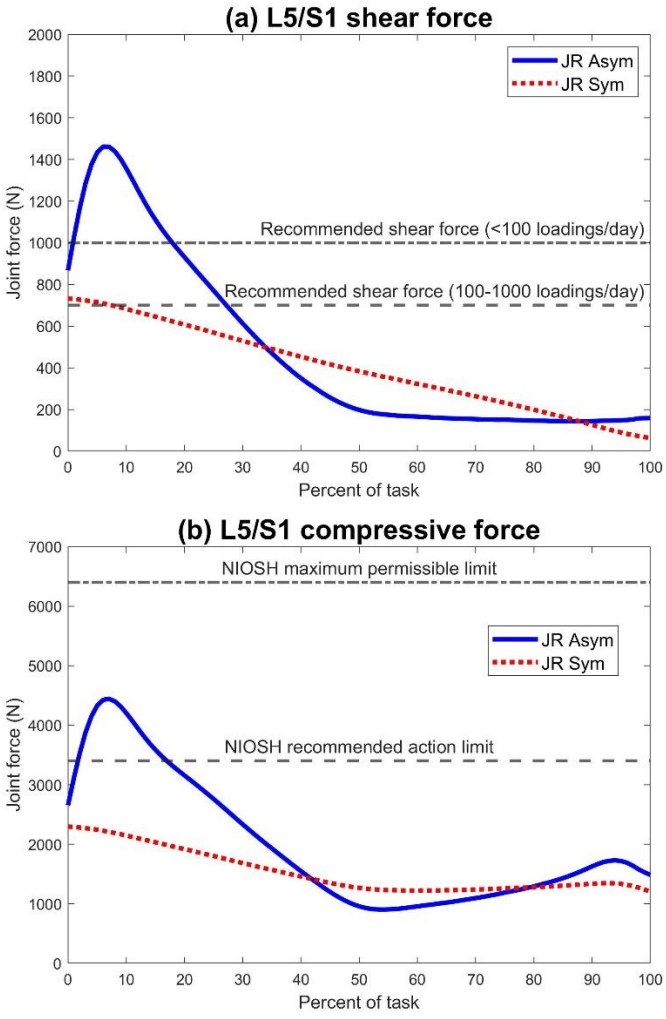

Figure 5.7: Lumbosacral (L5-S1) joint shear and compression forces comparisons between symmetric and asymmetric liftings

5.4 Discussion

Six upper-extremity and six lower-extremity, in total twelve joint angle profiles, are compared with experimental data for asymmetric lifting in Figures 5.3 and 5.4. The predicted joint angle profiles of spine flexion, spine rotation, hip flexions, and knee flexions agree well with the experimental data for asymmetric lifting. There are some

deviations for shoulder flexions and elbow flexions joint angle profiles, but most of the time the predicted joint profiles were within the 10 degrees deviation of the experimental data.

For the 7 kg box asymmetric lifting task (turning left) in Figure 5.5, the maximum vertical GRF on the left-side GRF is around 530 N. The left-side GRF starts to increase after around 50% of the lifting task. The reason is that, the subject starts to rotate the spine more than 20 degrees (-10 degrees to +10 degrees) at the left side (Figure 5.3 b) from the 40% of the lifting task and puts the box on the table at the end of the lifting task. As a result, the ZMP gradually moves to the left foot resulting in the maximum left GRF at the end of the lifting motion (Figure 5.5 a). In contrast, the right GRF starts to decline from around 60% of the lifting task (Figure 5.5 b).

The predicted muscle activations for asymmetric lifting agreed well with EMG data for the vastus lateralis (Figure 5.6 c and d), vastus medialis (Figure 5.6 e and f), right gluteus maximus (Figure 5.6 h), right gluteus medius (Figure 5.6 j). There are some discrepancies for bicep femoris shorthead (Figure 5.6 a and b), left gluteus maximus (Figure 5.6 g), gluteus medius (Figure 5.6 i and j), and latissimi dorsi (Figure 5.6 k and l), but most of the time the magnitude, pattern and phase changes of the predicted muscle activations agree well with the EMG data. The muscle activations for asymmetric lifting are higher than the symmetric lifting in most of the cases except the bicep femoris (Figure 5.6 a and b). Especially, vastus and gluteus muscles take more load during asymmetric lifting than symmetric lifting. Also, we can see that the predicted left vastus and gluteus muscle activations are higher than the predicted right vastus and gleutus muscles. One reason is,

for the symmetric task, the ZMP stays on the sagittal plane. The asymmetric lifting task requires spinal rotation which moves the ZMP away from the sagittal towards the left side of the coronal plane. As a result, the vertical GRF on the left side is higher than the right side, as we discussed earlier. Another reason is, there are spine and hip rotations during asymmetric lifting. To stabilize the movement while putting the box on the left side table, it requires extra forces from muscle and tendon, resulting in high left vastus and gluteus muscle activations, and joint reaction forces than symmetric lifting tasks.

For the symmetric lifting, the shear forces cross the recommended shear force only at the beginning of the lifting task. It stays below the recommended shear force limit after 10% of the lifting task (Figure 5.7 a). For the asymmetric lifting, the shear force stays above the recommended shear force limit (100-1000 loadings/day) from the beginning to 35% of the lifting task. It stays above the recommended shear force limit (<100 loadings/day) from the beginning to about 20% of the lifting task. The compressive forces are higher than the NIOSH recommended action limit from 5% of the lifting task to around 18% of the lifting task (Figure 5.7 b) but remain below the NIOSH maximum permissible limit.

The initial high shear and compressive forces for the asymmetric lifting task are expected as sometimes the subject stays inclined forward to lift a box and create a higher moment with respect to the ZMP. The subject should avoid such kind of motion as much as possible to avoid any potential lower back injury. NIOSH recommended limits do not consider the dynamic effects, and they are all static situations. Also, the NIOSH lifting equation considers at least one lift in every five minutes (12 loading/ hour) for the action limit and maximum permissible limit. In this study, we considered only single and one time lifting.

This also explains why the predicted 3D asymmetric lifting has higher spine loads than the NIOSH recommended action limit.

The rotation of the spine and varying compressive and shear loads on the spine joint make asymmetric lifting tasks more injury-prone than symmetric lifting tasks. It is necessary to reduce the allowable hand load during asymmetric lifting tasks. This suggestion depends on the individuals. Heavier individuals may have higher spinal compressive and shear forces at low box weight on hand (Han et al. 2013).

There are some limitations in this study.

1. Only one subject is considered in this study for symmetric and asymmetric lifting comparisons. It ignores the inter- and intra-individual difference.

2. The findings of this study are limited to squat lifting activities where knees are bent during lifting. Different participants may choose different lifting techniques, such as squat, stoop, and semi-squat. The spinal compression and shear forces vary with the lifting techniques. But, the proposed optimization formulation of the predictive skeletal model is general and can predict different lifting techniques by imposing initial and final experimental postures constraints.

3. Static optimization does not accurately consider the co-contraction of antagonistic muscles (Koelewijn et al., 2020). That may affect the spinal compressive and shear force results. Also, static optimization does not consider the deformation of bones for joint reaction force calculations.

4. The predictive model requires some motion capture and force plate data to improve the accuracy of the optimization.

5. The comparison in this study does not consider the age effect. Older adults generally have decreased muscle strength. It was reported that the strength and total muscle cross-sectional area reduced by about 20-40% between the ages of 20 and 60 (Dohetry, 2003). The percentile of dynamic joint strength in the skeletal model can be adjusted for older people. Also, the musculoskeletal model's muscle strength needs to be adjusted to make the model suitable for older people.

6. This predictive model is only for one-time lifting. Fatigue is not considered in the model.

Although the hybrid predictive model has some limitations, it gives us a lot of internal information such as joint torques, muscle activations, and joint reaction forces for symmetric and asymmetric liftings. This information is crucial for injury analysis but not feasible to get from in-vivo experiments.

Summary

In this study, we have studied the asymmetric lifting task using the hybrid model and compared the symmetric and asymmetric lifting tasks for injury analysis. The hybrid model predicted the 3D asymmetric lifting motion, GRFs, muscle activations, and joint reaction forces. It is clear that the asymmetric task is riskier than the symmetric lifting task with the same weight box. Asymmetric lifting tasks involve spinal rotation and moment. Also, they require extra muscle activation to balance the body, which creates higher joint reaction

forces. For this reason, asymmetric lifting tasks should be analyzed carefully for injury prevention.

CHAPTER VI

CONCLUSIONS AND FUTURE RESEARCH

6.1 Conclusions

In this study, a hybrid predictive model is developed to predict lifting motion and assess potential musculoskeletal injuries. The hybrid predictive model consists of two modules: 1) predictive skeletal module and 2) musculoskeletal analysis module. The predictive skeletal module consists of a 2D model and a 3D model. The 2D model is for symmetric lifting motion prediction and the 3D model for asymmetric lifting motion prediction. The 2D model is more computationally efficient than the 3D model, but the 3D model is required for asymmetric lifting tasks for considering the spinal rotation and kinetic differences on both sides of the human body. Both skeletal models are based on dynamic joint strength. The skeletal models can predict both symmetric and asymmetric lifting motions, joint torques, GRFs, and COP trajectories. For the maximum weight lifting task, we combine two objective functions: maximization of box weight and minimization of dynamic effort. For the fixed weight lifting task, the dynamic effort is used as the objective function. Using an inverse-dynamics-based optimization, the skeletal model successfully predicts maximum lifting weight and motion for both symmetric and asymmetric lifting

tasks. The musculoskeletal analysis module consists of an OpenSim full-body lumbar spine model. The musculoskeletal analysis module can estimate muscle activations and joint reaction forces using the data from the predictive skeletal module. The muscle activations are generated using the static optimization tool in OpenSim. The static optimization minimizes muscle activation as an objective function considering the muscle-torque as equilibrium constraints. The joint reaction analysis tool in OpenSim estimates the joint reaction loads (force and moments) of each joint by solving the Newton-Euler equations, where all the translational and rotational dynamics of a body are presented. We employed the hybrid predictive model to analyze the lower back injuries for symmetric and asymmetric lifting tasks. The results of the hybrid predictive models were validated by experimental data. The hybrid predictive model showed promising results when compared to experimental data. Also, it gave a lot of insight information related to joint and musculoskeletal injuries which are difficult to get from *in-vivo* experiments. The proposed hybrid model is both computationally efficient and generic, and it can be readily applied to other motions as well. The hybrid predictive musculoskeletal model has wide applications for workers' injury prevention to reduce the risk of musculoskeletal disorders.

6.2 Contributions and publications

The research contributions of this work are summarized as follows:

(1) A optimization-based skeletal model is developed to predict the lifting motion considering the dynamic joint strength.

(2) Maximum lifting weight is predicted for both symmetric and asymmetric lifting tasks using 2D and 3D models, respectively.

(3) A novel hybrid predictive model is developed by integrating the predictive skeletal model with OpenSim musculoskeletal model for muscle forces/activations and joint reaction loads calculations.

(4) The hybrid predictive model is deployed to study lower back injuries for symmetric and asymmetric lifting tasks.

I have following publications on this work.

Peer-reviewed journal publications:

1. Zaman, R., Arefeen, A., Quarnstrom, J., Barman, S., Yang, J., and Xiang, Y., 2022, Optimization-based biomechanical lifting models for manual material handling: A comprehensive review. *Proceedings of the Institution of Mechanical Engineers, Part H: Journal of Engineering in Medicine*, (under review).
2. Zaman, R., Xiang, Y., Rakshit, R., and Yang, J., 2022, Hybrid predictive model for lifting by integrating skeletal motion prediction with an OpenSim musculoskeletal model, *IEEE Transactions on Biomedical Engineering*., 69(3): p. 1111-1122, DOI: 10.1109/TBME.2021.3114374.
3. Zaman, R., Xiang, Y., Cruz, J., and Yang, J., 2021, Two-dimensional versus three-dimensional symmetric lifting motion prediction models: A case study. ASME *Journal of Computing and Information Science in Engineering*, 21(4), 044501.

4. Xiang, Y., Cruz, J., Zaman, R., and Yang, J., 2021, Multi-objective optimization for two-dimensional maximum weight lifting prediction considering dynamic strength. *Engineering Optimization*, 53(2), 206-220.
5. Zaman, R., Xiang, Y., Cruz, J., and Yang, J., 2021, Three-dimensional asymmetric maximum weight lifting prediction considering dynamic joint strength, Proceedings of the Institution of Mechanical Engineers, Part H: Journal of *Engineering in Medicine*, 235(4), 437-446.
6. Xiang, Y., Zaman, R., Rakshit, R., and Yang, J., 2019, Subject-specific strength percentile determination for two-dimensional symmetric lifting considering dynamic joint strength. *Multibody System Dynamics*, 46, 63-76.

Peer-reviewed conference papers:

1. Zaman, R., Quarnstrom, J., Xiang, Y., Rakshit, R., and, Yang, J., 2022, Hybrid predictive model for assessing spinal loads for 3D asymmetric lifting. in Proceedings of ASME 2022 International Design Engineering Technical Conferences and Computers and Information in Engineering Conference (IDETC/CIE 2022). August 14-17, 2022, St. Louis, Missouri, (under review).
2. Zaman, R., Xiang, Y., Cruz, J., and Yang, J., 2020, Three-dimensional symmetric maximum weight lifting prediction. Proceedings of ASME 2020 International Design Engineering Technical Conferences and Computers and Information in Engineering Conference, Volume 9: 40th Computers and Information in Engineering Conference (CIE), August 16-19, Virtual online.

3. Zaman, R., Xiang, Y., Rakshit, R., and Yang, J., 2019, Muscle force prediction in OpenSim using skeleton motion optimization results as input data. Proceedings of ASME 2019 International Design Engineering Technical Conferences and Computers and Information in Engineering Conference, August 26-29, 2019, Anaheim, CA.

6.3 Future Research

Besides the foregoing work, the following issues will be studied in the future.

1. Fatigue

Muscle fatigue is one of the main reasons for musculoskeletal disorders. For repetitive liftings, it is necessary to include fatigue in the hybrid predictive model to assess injuries. But, fatigue is a complex biochemical process. Fatigue-based injury prediction is a computationally heavy and time-consuming process which makes it difficult to implement. In the next step, I will improve the hybrid predictive model by including the fatigue to make the process faster and computationally efficient. A graduate student in Dr. Xiang's lab is working on the muscle fatigue research. I will improve the hybrid predictive model by including the muscle fatigue model developed by my colleagues in the lab.

2. Finite element spine model

The static optimization in the OpenSim considers the muscle and bones as rigid bodies. It ignores passive muscle forces. But, muscle and bones deformed under loads in real life. When we analyze lower back injury analysis, it is important to consider the deformation of

the vertebral column, especially the lumbar spine. The OpenSim joint reaction forces data will be transformed into a spine model to analyze the deformation and stress of the lumbar spine. This will give us stress and strain information about spine injuries.

3. Physics-based computational neuromusculoskeletal model with AI

Real-time injury analysis and performance measurement is a requirement for future translation to clinical or in-field conditions, where clinicians/coaches/commanders and their patients/athletes/soldiers expect immediate feedback about behavioral choices that influence their performance. The Artificial Neural Network (ANN) has vast potential to aid neuromusculoskeletal modeling in several key domains like feature extraction, synthesizing missing data, model generation, and data digitization. To make a subject-specific real-time prediction of different motions, ANN will be trained using the results from experimental data (for fast motions), hybrid predictive model (for heavy weight tasks), and OpenSim Moco. If successful, the model can be used to evaluate sports performance and injury risks in real-time.

REFERENCES

Ackermann, M., and Van den Bogert, A. J., 2010, Optimality principles for model-based prediction of human gait. *Journal of Biomechanics*, 43, 1055-1060.

Anderson, F. C., and Pandy, M. G., 1999, A dynamic optimization solution for vertical jumping in three dimensions. *Computer methods in biomechanics and biomedical engineering*, 2, 201-231.

Arnold, E. M., Ward, S. R., Lieber, R. L., and Delp, S. L., 2010, A model of the lower limb for analysis of human movement. *Annals of biomedical engineering*, 38, 269-279.

Ausavanonkulporn, A., Areekul, K., Senavongse, W., and Sukjamsri, C., 2019, Lumbar Spinal Loading during Stoop, Squat, and Kneeling Lifting: A Musculoskeletal Modeling Analysis. *Proceedings of the 2019 9th International Conference on Biomedical Engineering and Technology*, 51-55.

Azghani, M., Farahmand, F., Meghdari, A., Vossoughi, G., and Parnianpour, M., 2009, Design and evaluation of a novel triaxial isometric trunk muscle strength measurement system. *Proceedings of the Institution of Mechanical Engineers, Part H: Journal of Engineering in Medicine*, 223, 755-766.

Barbour, K. E., Helmick, C. G., Boring, M., and Brady, T. J., 2017, Vital signs: prevalence of doctor-diagnosed arthritis and arthritis-attributable activity limitation—United States, 2013–2015. *MMWR. Morbidity and mortality weekly report*, 66, 246.

Bazrgari, B., Shirazi-Adl, A., and Arjmand, N., 2007, Analysis of squat and stoop dynamic liftings: muscle forces and internal spinal loads. *European Spine Journal*, 16, 687-699.

Beaucage-Gauvreau, E., Robertson, W. S., Brandon, S. C., Fraser, R., Freeman, B. J., Graham, R. B., Thewlis, D., and Jones, C. F., 2019, Validation of an OpenSim full-body model with detailed lumbar spine for estimating lower lumbar spine loads during symmetric and asymmetric lifting tasks. *Computer methods in biomechanics and biomedical engineering*, 22, 451-464.

Bergmann, G., Bender, A., Graichen, F., Dymke, J., Rohlmann, A., Trepczynski, A., Heller, M. O., and Kutzner, I., 2014, Standardized loads acting in knee implants. *PLoS One*, 9, e86035.

Blache, Y., Desmoulins, L., Allard, P., Plamondon, A., and Begon, M., 2015a, Effects of height and load weight on shoulder muscle work during overhead lifting task. *Ergonomics*, 58, 748-761.

Blache, Y., Dal Maso, F., Desmoulins, L., Plamondon, A., and Begon, M., 2015b, Superficial shoulder muscle co-activations during lifting tasks: Influence of lifting height, weight and phase. *Journal of Electromyography and Kinesiology*, 25, 355-362.

Centers for disease control and prevention (CDC), 2018, *Arthritis data and statistics-National statistics* [Online]. Available: https://www.cdc.gov/arthritis/data_statistics/national-statistics.html [Accessed March 30 2021].

Chang, C.-C., Brown, D. R., Bloswick, D. S., and Hsiang, S. M., 2001, Biomechanical simulation of manual lifting using spacetime optimization. *Journal of Biomechanics*, 34, 527-532.

Chang, C. C., McGorry, R. W., Lin, J. h., Xu, X., and Hsiang, S. M., 2010, Prediction accuracy in estimating joint angle trajectories using a video posture coding method for sagittal lifting tasks. *Ergonomics*, 53, 1039-1047.

Cheng, H., Obergefell, L., and Rizer, A., 1994, Generator of Body Data (GEBOD) Manual. Systems research laboratories Inc., Dayton, OH.

Childs, J. D., Wu, S. S., Teyhen, D. S., Robinson, M. E., and George, S. Z., 2014, Prevention of low back pain in the military cluster randomized trial: effects of brief psychosocial education on total and low back pain–related health care costs. *The spine journal*, 14, 571-583.

Christophy, M., Senan, N. A. F., Lotz, J. C., and O'Reilly, O. M., 2012, A musculoskeletal model for the lumbar spine. *Biomechanics and modeling in mechanobiology*, 11, 19-34.

Cloutier, A., Boothby, R., and Yang, J. J., 2011, Motion capture experiments for validating optimization-based human models. *International Conference on Digital Human Modeling*, 2011, 59-68.

Cohen, S. P., Brown, C., Kurihara, C., Plunkett, A., Nguyen, C., and Strassels, S. A., 2010, Diagnoses and factors associated with medical evacuation and return to duty for service members participating in Operation Iraqi Freedom or Operation Enduring Freedom: a prospective cohort study. *The Lancet,* 375, 301-309.

Criswell, E., 2010. *Cram's introduction to surface electromyography*, Jones & Bartlett Publishers.

De Groote, F., Kinney, A. L., Rao, A. V., and Fregly, B. J., 2016, Evaluation of direct collocation optimal control problem formulations for solving the muscle redundancy problem. *Annals of biomedical engineering,* 44, 2922-2936.

Dembia, C. L., Bianco, N. A., Falisse, A., Hicks, J. L., and Delp, S. L., 2019, OpenSim Moco: Musculoskeletal optimal control. *BioRxiv*, 839381.

Dempsey, P. G., and Hashemi, L., 1999, Analysis of workers' compensation claims associated with manual materials handling. *Ergonomics,* 42, 183-195.

Denavit, J., and Hartenberg, R. S., 1955, A kinematic notation for low pair mechanisms based on matrices. *ASME Journal of Applied Mechanics,* 22, 215-221.

Doherty, T. J., 2003, Invited review: aging and sarcopenia. *Journal of applied physiology*.

Dysart, M. J., and Woldstad, J. C., 1996, Posture prediction for static sagittal-plane lifting. *Journal of Biomechanics,* 29, 1393-1397.

Erdemir, A., McLean, S., Herzog, W., and van den Bogert, A. J., 2007, Model-based estimation of muscle forces exerted during movements. *Clinical biomechanics,* 22, 131-154.

Escamilla, R. F., Fleisig, G. S., Zheng, N., Lander, J. E., Barrentine, S. W., Andrews, J. R., Bergemann, B. W., and Moorman Iii, C. T., 2001, Effects of technique variations on knee biomechanics during the squat and leg press. *Medicine & Science in Sports & Exercise,* 33, 1552-1566.

Freburger, J. K., Holmes, G. M., Agans, R. P., Jackman, A. M., Darter, J. D., Wallace, A. S., Castel, L. D., Kalsbeek, W. D., and Carey, T. S., 2009, The rising prevalence of chronic low back pain. *Archives of internal medicine,* 169, 251-258.

Frey-Law, L. A., Laake, A., Avin, K. G., Heitsman, J., Marler, T., and Abdel-Malek, K., 2012, Knee and elbow 3D strength surfaces: peak torque-angle-velocity relationships. *Journal of applied biomechanics,* 28, 726-737.

Gallagher, S., and Marras, W. S., 2012, Tolerance of the lumbar spine to shear: a review and recommended exposure limits. *Clinical biomechanics,* 27, 973-978.

Garg, A., and Moore, J. S., 1992, Prevention strategies and the low back in industry. *Occup Med,* 7, 629-40.

Ghiasi, M. S., Arjmand, N., Boroushaki, M., and Farahmand, F., 2016, Investigation of trunk muscle activities during lifting using a multi-objective optimization-based model and intelligent optimization algorithms. *Medical & biological engineering & computing,* 54, 431-440.

Gill, P. E., Murray, W., and Saunders, M. A., 2005, SNOPT: An SQP algorithm for large-scale constrained optimization. *SIAM review,* 47, 99-131.

Gunantara, N., 2018, A review of multi-objective optimization: Methods and its applications. *Cogent Engineering,* 5, 1502242.

Gundogdu, O., Anderson, K. S., and Parnianpour, M., 2005, Simulation of manual materials handling: Biomechanial assessment under different lifting conditions. *Technology and Health Care-European Society for Engineering and Medicine,* 13, 57-66.

Hamner, S. R., Seth, A., and Delp, S. L., 2010, Muscle contributions to propulsion and support during running. *Journal of Biomechanics,* 43, 2709-2716.

Han, K.-S., Rohlmann, A., Zander, T., and Taylor, W. R., 2013, Lumbar spinal loads vary with body height and weight. *Medical engineering & physics,* 35(7), 969-977.

Hartvigsen, J., Hancock, M. J., Kongsted, A., Louw, Q., Ferreira, M. L., Genevay, S., Hoy, D., Karppinen, J., Pransky, G., and Sieper, J., 2018, What low back pain is and why we need to pay attention. *The Lancet,* 391, 2356-2367.

Hootman, J. M., Helmick, C. G., Barbour, K. E., Theis, K. A., and Boring, M. A., 2016, Updated projected prevalence of self-reported doctor-diagnosed arthritis and arthritis-attributable activity limitation among US adults, 2015–2040. *Arthritis & rheumatology,* 68, 1582-1587.

Hussain, S. J., and Frey-Law, L., 2016, 3D strength surfaces for ankle plantar-and dorsi-flexion in healthy adults: an isometric and isokinetic dynamometry study. *Journal of foot and ankle research,* 9, 43.

Katz, J. N., 2006, Lumbar disc disorders and low-back pain: socioeconomic factors and consequences. *Journal of Bone and Joint Surgery*, 88 Suppl 2, 21-4.

Kim, H. K., and Zhang, Y., 2017, Estimation of lumbar spinal loading and trunk muscle forces during asymmetric lifting tasks: application of whole-body musculoskeletal modelling in OpenSim. *Ergonomics*, 60, 563-576.

Kingma, I., Faber, G. S., Bakker, A. J., and Van Dieen, J. H., 2006, Can low back loading during lifting be reduced by placing one leg beside the object to be lifted? *Physical therapy*, 86, 1091-1105.

Kingma, I., Faber, G. S., and van Dieën, J. H., 2016, Supporting the upper body with the hand on the thigh reduces back loading during lifting. *Journal of Biomechanics*, 49, 881-889.

Koelewijn, A. D., and van den Bogert, A. J., 2020, Antagonistic Co-contraction Can Minimise Muscular Effort in Systems with Uncertainty. *bioRxiv*.

Liberty Mutual Insurance, 2019, *Liberty mutual workplace safety index* [Online]. Available: https://viewpoint.libertymutualgroup.com/article/top-10-causes-disabling-injuries-at-work-2019/?extcmp=NI_PR_VP_Content_WC [Accessed March 3 2020].

Lin, C., Ayoub, M., and Bernard, T., 1999, Computer motion simulation for sagittal plane lifting activities. *International Journal of Industrial Ergonomics*, 24, 141-155.

Lindsey, T., and Dydyk, A. M., 2020, Spinal osteoarthritis. *StatPearls [Internet]*.

Lloyd, D. G., and Besier, T. F., 2003, An EMG-driven musculoskeletal model to estimate muscle forces and knee joint moments in vivo. *Journal of Biomechanics*, 36, 765-776.

Looft, J. M., 2014, *Adaptation and validation of an analytical localized muscle fatigue model for workplace tasks.* Ph.D. thesis, The University of Iowa, Iowa City, IA.

Ma, L., Zhang, W., Chablat, D., Bennis, F., and Guillaume, F., 2009, Multi-objective optimisation method for posture prediction and analysis with consideration of fatigue effect and its application case. *Computers & Industrial Engineering*, 57, 1235-1246.

Marler, R. T., and Arora, J. S., 2004, Survey of multi-objective optimization methods for engineering. *Structural and Multidisciplinary Optimization*, 26, 369-395.

Marler, R. T., and Arora, J. S., 2005, Function-transformation methods for multi-objective optimization. *Engineering Optimization,* 37, 551-570.

Marler, T., Knake, L., and Johnson, R., 2011, Optimization-based posture prediction for analysis of box lifting tasks. *International Conference on Digital Human Modeling*, 2011, 151-160.

McGill, S., Norman, R., Yingling, V., Wells, R., and Neumann, P., 1998, Shear happens! Suggested guidelines for ergonomists to reduce the risk of low back injury from shear loading. *Proceedings of the 30th annual conference of the human factors association of Canada*, 1998, 157-161.

Mirakhorlo, M., Azghani, M. R., and Kahrizi, S., 2013, Validation of a musculoskeletal model of lifting and its application for biomechanical evaluation of lifting techniques. *Journal of research in health sciences,* 14, 23-28.

Mital, A., and Kromodihardjo, S., 1986, Kinetic analysis of manual lifting activities: Part II—Biomechanical analysis of task variables. *International Journal of Industrial Ergonomics,* 1, 91-101.

Mital, A., Nicholson, A. S., and Ayoub, M. M., 1997. *A Guide to manual materials handling* Washington DC, Taylor and Francis.

NIOSH Technical report, 1981, Work practices guide for manual lifting. US Department of Health and Human Services. 81-122.

Olney, S. J., and Winter, D. A., 1985, Predictions of knee and ankle moments of force in walking from EMG and kinematic data. *Journal of Biomechanics,* 18, 9-20.

Pandy, M. G., 2001, Computer modeling and simulation of human movement. *Annual review of biomedical engineering,* 3, 245-273.

Porsa, S., Lin, Y.-C., and Pandy, M. G., 2016, Direct methods for predicting movement biomechanics based upon optimal control theory with implementation in OpenSim. *Annals of biomedical engineering,* 44, 2542-2557.

Raabe, M. E., and Chaudhari, A. M., 2016, An investigation of jogging biomechanics using the full-body lumbar spine model: Model development and validation. *Journal of Biomechanics,* 49, 1238-1243.

Rajaee, M. A., Arjmand, N., Shirazi-Adl, A., Plamondon, A., and Schmidt, H., 2015, Comparative evaluation of six quantitative lifting tools to estimate spine loads during static activities. *Applied Ergonomics,* 48, 22-32.

Rakshit, R., Xiang, Y., and Yang, J., 2020, Dynamic-joint-strength-based two-dimensional symmetric maximum weight-lifting simulation: Model development and validation. *Proceedings of the Institution of Mechanical Engineers, Part H: Journal of Engineering in Medicine,* 234, 660-673.

Schultz, A., Andersson, G., Haderspeck, K., Örtengren, R., Nordin, M., and Björk, R., 1982, Analysis and measurement of lumbar trunk loads in tasks involving bends and twists. *Journal of Biomechanics,* 15, 669-675.

Shourijeh, M. S., McPhee, J. J., and Azad, N. L., 2014, Optimal control and forward dynamics of periodic forearm motions using fourier series for muscle excitations.

Shourijeh, M. S., Smale, K. B., Potvin, B. M., and Benoit, D. L., 2016, A forward-muscular inverse-skeletal dynamics framework for human musculoskeletal simulations. *Journal of Biomechanics,* 49, 1718-1723.

Song, J., Qu, X., and Chen, C.-H., 2016, Simulation of lifting motions using a novel multi-objective optimization approach. *International Journal of Industrial Ergonomics,* 53, 37-47.

Sreenivasa, M., Millard, M., Kingma, I., Van Dieen, J. H., and Mombaur, K., 2018, Predicting the influence of hip and lumbar flexibility on lifting motions using optimal control. *Journal of Biomechanics,* 78, 118-125.

Stambolian, D., Eltoukhy, M., and Asfour, S., 2016, Development and validation of a three dimensional dynamic biomechanical lifting model for lower back evaluation for careful box placement. *International Journal of Industrial Ergonomics,* 54, 10-18.

Steele, K. M., Demers, M. S., Schwartz, M. H., and Delp, S. L., 2012, Compressive tibiofemoral force during crouch gait. *Gait Posture,* 35, 556-60.

Stockdale, A. A., 2011, *Modeling three-dimensional hip and trunk peak torque as a function of joint angle and velocity.* Department of Biomedical Engineering Ph.D. thesis, The University of Iowa, Iowa City, IA.

Sun, H. B., 2010, Mechanical loading, cartilage degradation, and arthritis. *Annals of the New York Academy of Sciences,* 1211, 37-50.

Thelen, D. G., 2003, Adjustment of muscle mechanics model parameters to simulate dynamic contractions in older adults. *J. Biomech. Eng.,* 125, 70-77.

Thelen, D. G., and Anderson, F. C., 2006, Using computed muscle control to generate forward dynamic simulations of human walking from experimental data. *Journal of Biomechanics,* 39, 1107-1115.

U.S. Bureau of Labor Statistics, 2018, Employer reported workplace injuries and illness,. *In:* U.S. Department of Labor (ed.).

Van Dieen, J. H., Hoozemans, M. J., and Toussaint, H. M., 1999, Stoop or squat: a review of biomechanical studies on lifting technique. *Clinical biomechanics,* 14, 685-96.

Vukobratović, M., and Borovac, B., 2004, Zero-moment point—thirty five years of its life. *International journal of humanoid robotics,* 1, 157-173.

Waters, T. R., and Garg, A., 2010, Two-dimensional biomechanical model for estimating strength of youth and adolescents for manual material handling tasks. *Applied Ergonomics,* 41, 1-7.

Wilke, H.-J., Neef, P., Hinz, B., Seidel, H., and Claes, L., 2001, Intradiscal pressure together with anthropometric data–a data set for the validation of models. *Clinical biomechanics,* 16, S111-S126.

Xiang, Y., Rahmatalla, S., Chung, H.-J., Kim, J., Bhatt, R., Mathai, A., Beck, S., Marler, T., Yang, J., and Arora, J. S., 2008, Optimization-based dynamic human lifting prediction. SAE Technical Paper.

Xiang, Y., Arora, J. S., and Abdel-Malek, K., 2009a, Optimization-based motion prediction of mechanical systems: sensitivity analysis. *Structural and Multidisciplinary Optimization,* 37, 595.

Xiang, Y., Arora, J. S., Rahmatalla, S., and Abdel-Malek, K., 2009b, Optimization-based dynamic human walking prediction: One step formulation. *International Journal for Numerical Methods in Engineering,* 79, 667-695.

Xiang, Y., Arora, J. S., Rahmatalla, S., Marler, T., Bhatt, R., and Abdel-Malek, K., 2010, Human lifting simulation using a multi-objective optimization approach. *Multibody System Dynamics,* 23, 431-451.

Xiang, Y., Arora, J. S., and Abdel-Malek, K., 2011, Optimization-based prediction of asymmetric human gait. *Journal of Biomechanics,* 44, 683-693.

Xiang, Y., Arora, J. S., and Abdel-Malek, K., 2012a, 3D human lifting motion prediction with different performance measures. *International journal of humanoid robotics,* 9, 1250012.

Xiang, Y., Arora, J. S., and Abdel-Malek, K., 2012b, Hybrid predictive dynamics: a new approach to simulate human motion. *Multibody System Dynamics,* 28, 199-224.

Xiang, Y., Zaman, R., Rakshit, R., and Yang, J., 2019, Subject-specific strength percentile determination for two-dimensional symmetric lifting considering dynamic joint strength. *Multibody System Dynamics,* 46 (1), 63-76.

Xiang, Y., Cruz, J., Zaman, R., and Yang, J., 2021, Multi-objective optimization for two-dimensional maximum weight lifting prediction considering dynamic strength. *Engineering Optimization,* 53(2), 206-222.

Zaman, R., Xiang, Y., Rakshit, R., and Yang, J., 2019, Muscle force prediction in OpenSim using skeleton motion optimization results as input data. *ASME International Design Engineering Technical Conferences and Computers and Information in Engineering Conference*, August 26-29, 2019, Anaheim, CA.

Zaman, R., Xiang, Y., Cruz, J., and Yang, J., 2020, Three-dimensional symmetric maximum weight lifting prediction. *Proceedings of ASME 2020 International Design Engineering Technical Conferences and Computers and Information in Engineering Conference, Volume 9: 40th Computers and Information in Engineering Conference (CIE)*, August 16-19, Virtual online.

Zaman, R., Xiang, Y., Cruz, J., and Yang, J., 2021a, Three-dimensional asymmetric maximum weight lifting prediction considering dynamic joint strength. *Proceedings of the Institution of Mechanical Engineers, Part H: Journal of Engineering in Medicine,* 235 (4), 437-446.

Zaman, R., Xiang, Y., Cruz, J., and Yang, J., 2021b, Two-dimensional versus three-dimensional symmetric lifting motion prediction models: a case study. ASME Journal of Computing and Information Science in Engineering, 21(4), 044501.

Zaman, R., Xiang, Y., Rakshit, R., and Yang, J., 2022, Hybrid predictive model for lifting by integrating skeletal motion prediction with an Opensim musculoskeletal model. IEEE Transactions on Biomedical Engineering, 69(3): p. 1111-1122, DOI: 10.1109/TBME.2021.3114374.

VITA

Rahid Zaman

Candidate for the Degree of

Doctor of Philosophy

Dissertation: DEVELOPMENT OF A PREDICTIVE MUSCULOSKELETAL HYBRID MODEL BASED ON MAXIMUM WEIGHT LIFTING TASK

Major Field: Mechanical and Aerospace Engineering

Biographical:

Education:

Completed the requirements for the Doctor of Philosophy in Mechanical and Aerospace Engineering at Oklahoma State University, Stillwater, Oklahoma in May, 2022.

Completed the requirements for the Master of Science in Mechanical Engineering at University of Alaska Fairbanks, Fairbanks, Alaska in 2018.

Completed the requirements for the Bachelor of Science in Mechanical Engineering at Military Institute of Science and Technology, Dhaka, Bangladesh in 2014.

Experience:

Graduate Teaching and Research Assistant, Oklahoma State University, 2019-2022
Graduate Teaching and Research Assistant, University of Alaska Fairbanks, 2016-2018
Assistant Engineer, Bangladesh Power Development Board (BPDB), 2015-2016

Professional Memberships:

American Society of Mechanical Engineers (ASME)
American Society of Biomechanics (ASB)
Institute of Electrical and Electronics Engineers (IEEE)